AFRPL-TR-71-87

A STUDY OF THE EFFECTS OF ELECTRIC FIELDS ON SOLID PROPELLANT BURNING RATES

R.F. BESTGEN, CAPT, USAF

TECHNICAL REPORT AFRPL-TR-71-87

JULY 1971

AIR FORCE ROCKET PROPULSION LABORATORY
DIRECTOR OF LABORATORIES
AIR FORCE SYSTEMS COMMAND
UNITED STATES AIR FORCE
EDWARDS, CALIFORNIA

172

Unclassified

Security Classification

DOCUMENT CONTROL DATA - R & D

(Security classification of title, body of abstract and indexing annotation must be entered when the overall report is classified)

1. ORIGINATING ACTIVITY (Corporate author)	2a. REPORT SECURITY CLASSIFICATION
Air Force Institute of Technology (AFIT-SE) Wright-Patterson AFB, Ohio 45433	Unclassified
	2b. GROUP

3. REPORT TITLE

A Study of the Effects of Electric Fields on Solid Propellant Burning Rates

4. DESCRIPTIVE NOTES (Type of report and inclusive dates)

Research (October 1968 - June 1970)

5. AUTHOR(S) (First name, middle initial, last name)

Robert F. Bestgen
Captain USAF

6. REPORT DATE	7a. TOTAL NO. OF PAGES	7b. NO. OF REFS
July 1971	171	54

8a. CONTRACT OR GRANT NO.	9a. ORIGINATOR'S REPORT NUMBER(S)
b. PROJECT NO. 305901 ATB	AFRPL-TR-71-87
c.	9b. OTHER REPORT NO(S) (Any other numbers that may be assigned this report)
d.	

10. DISTRIBUTION STATEMENT

This document has been approved for public release and sale; its distribution is unlimited.

11. SUPPLEMENTARY NOTES	12. SPONSORING MILITARY ACTIVITY
	Air Force Rocket Propulsion Laboratory (AFRPL), Edwards, California 93523

13. ABSTRACT

An experimental study, guided by theoretical considerations, was made on the effects of electric fields on burning rates of two metallized composite propellants. Mechanisms causing observed burning rate changes were sought. Experimental data include flame electron number densities, electrical conductivities, electric field strengths, electric currents, combustion efficiencies, exhaust emissions spectra and concentrations, combustion temperatures, and continuous measurement of burning rates. Results show that burning rate increases are due to current heating of the nonburning propellant and that burning rate decreases involve flame electrons, causing inhibited combustion under proper voltage conditions. Non-collective reactional interference was inferred for this latter case.

DD FORM 1 NOV 68 1473

Unclassified

Security Classification

NOTICES

When U.S. Government drawings, specifications, or other data are used for any purpose other than a definitely related Government procurement operation, the Government thereby incurs no responsibility, nor any obligation whatsoever, and the fact that the Government may have formulated, furnished or in any way supplied that said drawings, specifications, or other data, is not to be regarded by implication or otherwise, or in any manner as licensing the holder or any other person or corporation, or conveying any rights or permission to manufacture, use, or sell any patented invention that may in any way be related thereto.

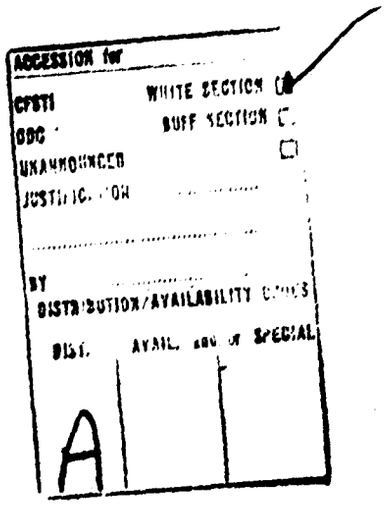

14. KEY WORDS	LINK A		LINK B		LINK C	
	ROLE	WT	ROLE	WY	ROLE	WT
Metallized Ammonium Perchlorate Solid Propellants						
Propellant Burning Rates						
Electric Fields						
Combustion Properties:						
(1) Metal additives combustion efficiency						
(2) Stable exhaust species						
Flame Electrical Properties:						
(1) Electron number density						
(2) DC electrical conductivity						

FOREWORD

This is a report on research conducted at the Air Force Rocket Propulsion Laboratory during the period of October 1968 to June 1970, under in-house Project No. 305901ATB. Captain Robert F. Bestgen was the investigator in charge of the research. The work was submitted to the School of Engineering, Air Force Institute of Technology, in October 1970, in partial fulfillment of the requirements for the Degree of Doctor of Philosophy.

Acknowledgment is made to Dr. Harold F. Wright, Professor at the Air Force Institute of Technology, who was the principal advisor for the research. His guidance assured the successful completion of the work.

This technical report has been reviewed and is approved.

A. D. BROWN, Jr., Lt Col, USAF
Chief, Technology Division
Air Force Rocket Propulsion Laboratory

ABSTRACT

An experimental study, guided by theoretical considerations, was made on the effects of imposed electric fields on solid propellant burning rates. Two composite metallized formulations, containing ammonium perchlorate, were extensively studied. A variety of electrical arrangements were used. Results from approximately 1000 tests are given. Included among experimental data are flame electron number densities, gas and solid-phase DC electrical conductivities, regional electric field strengths, combustion efficiencies, exhaust emission concentrations, and burning rates, all at various combustion pressures. Also discussed are measured electric currents, formulation impurities, two-color pyrometer combustion temperatures, camera data, and select results from a modified thermochemical computer program. Techniques included use of: (1) Langmuir probes, (2) high voltage rakes, (3) chemical analysis of combustion residue, (4) gas chromotography, (5) infrared spectroscopy, (6) continuous measurement of burning rate. Results show that electrically induced burning rate increases are due to breakdown current heating and that burning rate decreases involve flame electrons, causing inhibited combustion under certain voltage conditions. Voltage-induced non-collective reactional interference was inferred for this latter case. Typical burning rate increases and decreases of 25% and 20%, respectively, were observed under voltage conditions, although no attempt was made to seek the maximum change.

AFRPL-TR-71-87

A STUDY OF THE EFFECTS OF ELECTRIC FIELDS ON SOLID PROPELLANT BURNING RATES

ROBERT F. BESTGEN, CAPT, USAF

JULY 1971

AIR FORCE ROCKET PROPULSION LABORATORY
DIRECTOR OF LABORATORIES
AIR FORCE SYSTEMS COMMAND
UNITED STATES AIR FORCE
EDWARDS, CALIFORNIA

CONTENTS

LIST OF ILLUSTRATIONS

LIST OF TABLES

NOMENCLATURE

Arabic

A cross-sectional area, cm^2

A_b burning area, cm^2

A_p probe area, cm^2

B constant current density gradient, $(amperes/cm^2)/cm$

C_1, C_2, C_3, C_4 stoichiometric coefficients

c heat capacity, $cal/gm°K$

D diffusion coefficient, cm^2/sec

d_p probe diameter, cm

E electric field strength, KV/cm

e exponential or unit electronic charge, 1.6×10^{-19} coulombs

f force/unit volume, $dynes/cm^3$

$\dot{G}$ charge generation/unit volume, $charge/sec\ cm^3$

h distance between electrodes, cm

I current, amperes

J current density or flux, $amperes/cm^2$

K particle mobility, $cm^2/volt\ sec$

k Boltzmann constant, 1.38×10^{-16} erg/°K

L Optron working distance, cm

l_p probe length, cm

$\mathcal{M}$ molecular weight, gm/mole

m mass, gm

$\dot{M}$ total mass flow rate, gm/sec

$\dot{m}$ mass flow rate/unit burning area, gm/cm^2 sec

P_c combustion pressure, atmospheres

Q net heat of reaction, cal/gm

$\bar{q}$ heat flux vector, cal/cm^2 sec

$\mathcal{R}$ gas constant, 1.98 cal/mole °K

$\dot{R}$ charge recombination/unit volume, charge/sec cm^3

r linear burning rate, cm/sec

Re Reynolds number

Sc Schmidt number

Sh Sherwood number

T temperature, °K

t time, sec

V average speed, cm/sec

v_d drift velocity, cm/sec

W Optron calibration constant, 4.86×10^{-3} volts $^{-1}$

X reaction zone thickness, cm

x distance, cm

Y composition vector with i th component y_i

Greek

α thermoelectric coefficient, amperes/cm °K

β thermoelectric coefficient, amperes/cm

Γ reaction rate, $(gm/cm^3)^{1-\gamma}$ /sec

γ reaction order

$\dot{\varepsilon}$ source energy/unit length, cal/cm^3 sec

$\in$ Equation (9)

η particle number density, particles/cm^3

Λ thermal conductivity, cal/cm sec °K

λ mean free path, cm

μ viscosity, gm/cm sec

π_r temperature sensitivity of burning rate at constant pressure, %/°F

ρ density, gm/cm^3

σ DC electrical conductivity, (ohm cm)$^{-1}$

τ_e electron mean collision time, sec

ϕ voltage or electric potential, volts or KV

ϕ_p plasma potential, volts

Ω Equation (8), gm/cm^2 sec or resistance, ohms

ω_i burning rate variable

Subscripts

a impressed

b burning

c current

d drift

e electrons

f flame

g gas phase

i index to designate i th specie

m measured

o an arbitrary point designation

p probe, plasma

p propellant, ambient

r random, burning rate, reacting

s surface

x, y, z integers

$+, -$ positive or negative ions, respectively

Superscripts

$*$ burning rate designation under voltage, solid phase

$'$ burning rate designation under voltage, gas phase

A STUDY OF
THE EFFECTS OF ELECTRIC FIELDS ON
SOLID PROPELLANT BURNING RATES

I INTRODUCTION

The flexible nature of contemporary propulsion needs is such that a throttling capability is not only desirable but in many instances required. In this connection, controllable solid motors are under development. In addition, the control of small solid gas generators has been studied to complement the control of motors. Included among the various control schemes under present development are the mechanical driving of a pintle through a nozzle throat, injection of gas generated in one chamber into another chamber, and choking a nozzle outflow with an induced gas swirl. Without exception, the mechanics involved in these techniques only indirectly influence the burning process or the burning rate associated with the solid propellant. The burning rate of propellant is defined herein as the rate of linear regression of the solid-gas interface in the direction normal to the interface.

A more attractive alternative, in principle, would be to cause a direct modification to the burning process and ultimately the burning rate. If the nature of burning propellant can indeed be altered directly by some means, perhaps this means could be controlled by remote command. It might also be possible for such a method to present a suitable counter for adverse combustion phenomena. Some fairly

specific ideas to create a direct change to the burning rate of propellant have been outlined in recent literature along with some results of initial experiments (48). One concept, covered only briefly in this reference, envisions an electric field imposed upon the burning propellant system which acts to alter the burning rate. This research was concerned with studying the influence of an electric field, supplied by high voltage, on the burning rate of solid propellant.

Survey of Past Experiments

There is substantial literature dealing with the interactions of applied electric fields with either premixed or diffusion laboratory flames (c.f., 2,3,9,12,20,22,31,32,33). Other investigations have considered electric fields imposed upon combustion waves (6,13,17,35). A number of studies have also been reported on burning solid propellants subjected to electric fields (10,26,34, ,45,52,53).

Laboratory flames exposed to electric fields have responded in a variety of ways to the electric field and have, in general, resulted in marked effects. With proper electrode geometries, dramatic flame distortions and deflections have been created (2,33). Limits of flame stability and flame standoff distances have been changed (3,12). Depending upon experimental conditions, the flame speed has been variously increased, decreased, or even the flame extinguished by the electric field (12,22). Electric fields have also modified carbon formation from rich organic flames and have, additionally, altered flame spectra affecting such transient species as CH (37). Overall heat transfer rates have also been reported changed by a field (32,33,36). It is noted that the effects reported depend not only upon experimental

arrangements, but intimately upon the charged properties of the flame since an electric field fundamentally influences charged matter. Charged properties of a given flame are determined by its composition and controlling mechanism of ionization.

Combustion waves subjected to electric fields evidently respond in a manner similar to laboratory flames. In particular, an electric field caused either an increase or decrease in detonation wave velocity or even a wave quench (13).

In both the ideal flame and combustion wave cases, the effects due to the electric field have been largely explained on the basis that the imposed field creates a resultant Lorentz body force or a net space charge within the system. The gas is then induced to move in bulk constituting what has been termed the Chattock or ionic wind effect. The concept of the space charge or the Lorentz force embodies charged particles moving on a grand or macroscopic scale, resulting in a type of collective phenomena for an ionized gas (27).

With respect to solid propellants, References 10,34, ,45 and 53, represent the known literature on the influence of electric fields upon burning rate. Other works dealing with electric field effects upon the rate of flame spread along a propellant surface have also been completed (52,53). Turner (52), attributed flame spread rate increases to electrical energy added to the system preheating or preigniting the nonburning portion of the propellant. Table I outlines some comparative features from References 10,34, ,45 and 53. From Table I, it is seen that each study indicated some burning rate reduction with an imposed electric field, except for the work of Stones (45). Both Silla ( ) and Stones (45) conducted extensive studies.

The work of Silla focused upon electrode arrangements where the propellant served as part of the media between electrodes. The exception to this geometry occurred when the propellant contained an electrically conductive fuel. The propellant was then made one electrode and also served as a resistive component in the high voltage circuit. Variously, either AC or DC voltages were impressed across the electrodes with initial voltage values set below the value where repetitive arcing occurred. Average burning rates were measured by two photodiodes, responsive to incident light, set 1 inch apart. No-voltage burning rates were also measured over this same distance. Different propellant samples of each formulation were used for voltage and no-voltage conditions. Voltages recorded were initial values. Currents passing through the system were not recorded. Applied AC voltages were found to be effective in decreasing average burning rates while DC voltages produced flame deflections and flame extinction, regardless of polarity, but with little measurable change to the burning rate. Flame extinction occurred most frequently when the propellant passed by the top electrode. For the ammonium nitrate formulations used, burning rate reductions decreased with increasing combustion pressure and the reductions were greatest when the pressurizing gas was air rather than nitrogen. No explanations were offered for the effects noted beyond tentatively attributing their cause to a reduction of heat transfer from the combustion flame.

The experiments of Stones employed mainly an aluminized propellant as one electrode and a ring or wire gauze arrangement as the other electrode. The propellant served as a discrete electrical component as well as an electrode. An initial voltage of either 7KV or 13KV was

impressed across the electrodes. Average burning rates were deduced from a photomultiplier tube responding to flame light from ignition through burnout, knowing the total propellant length. Voltage and no-voltage burning rates were measured on different propellant samples of each formulation. Time traces of both applied voltage and current passing through the high voltage circuit were taken. From those traces published, it is seen that at some time during burning the high voltage supply shorted, decreasing the applied voltage to a value near zero. Resultant steady currents of approximately 5 mA were thus recorded. Extreme difficulty was reportedly encountered in viewing into the combustion vessel with voltages applied, as apparently a heavy opaque debris "coat" then covered the entire vessel. For the pressures tested, the total time of phototube response was reduced under voltage conditions implying average burning rate increases over no-voltage values. The published burning rate increases seem nearly independent of combustion pressure except at one test pressure where significantly shorter phototube response times resulted with applied voltage. Stones suggests that at this test pressure, the optimum burning rate increase existed for the power unit used and notes that such a condition is in agreement with theoretical consideration of breakdown field versus pressure. The implication was that ionic winds were involved in the burning rate increases.

Purpose of the Investigation

The purpose of this investigation was twofold. One purpose was to determine, for select experimental conditions, what effects applied high voltage has upon the burning of modern solid propellant

formulations, particularly the exacting effect on burning rate. The other purpose was to determine by experiment, guided by theoretical considerations, the mechanisms responsible for any observed modification to the burning rate. The ultimate goal of the study was to provide information in order to assess the practical control of propellant burning rates by electrical means.

II THEORETICAL CONSIDERATIONS

It is important to emphasize that, for the most part, theoretical considerations herein relate to the particular propellants selected for experiments. Also, aside from current interactions affecting the solid phase under certain conditions (later section and Chapter V), considerations are focused almost exclusively upon the gas phase. Even under this limitation the experimental portion of the study was not sufficiently extensive to examine all the factors mentioned in this chapter.

Reference Burning Rate

The steady state burning rate r of solid propellant can be functionally represented as

$$r = r(\omega_1, \omega_2, \cdots, \omega_i) \tag{1}$$

The ω_i can be determined either by experiment or theory. In the general case, it has been found by experiment that the burning rate depends at least upon the combustion pressure P_c and the propellant temperature T_p . From experiments using heterogeneous formulations, the oxidizer particle size and the fuel-oxidant ratio are also known to influence the burning rate.

For the case of a heterogeneous propellant burning without consideration of applied voltage, two basic theories treating composite

propellant combustion have been developed that are widely referenced. One theory is attributed to Summerfield (47), the other to Hermance (14). Collectively, these two models represent the present status of the theoretical understanding of composite propellant combustion.

The Summerfield model, commonly termed the granular diffusion flame model, was developed first. It has since been extended but not fundamentally revised (44). Summerfield treats the combustion process from a one-dimensional thermal model (Figure 1). An energy balance was performed using Figure 1 to yield a simple equation that includes the reaction zone thickness X . An average thermal gradient was assumed. Two distinct expressions were then written for the reaction zone thickness. One expression holds at low combustion pressures and was based on well known laminar flame theory (23,46), invoking a second order overall gas-phase reaction. At low pressures it is reasonable to assume that the burning process is reactionally controlled since the rate of diffusion in the gas phase greatly exceeds the chemical reaction rate Γ and the slowest process dominates. At high combustion pressures, the reaction zone thickness was contrived to be related to gas-phase diffusion involving small fuel vapor pockets entrained in the oxidizing environment. At high combustion pressures it is reasonable to assume that diffusional mechanisms control the burning process since reaction times are extremely short. Inserting the two distinct expressions for the reaction zone thickness into the energy balance equation, using mass conservation, yields unique closed form expressions for low and high pressure burning rates. An overall reciprocal burning rate is given by the sum of the reciprocal low and high pressure burning rates.

The Hermance model treats the combustion process from a chemical kinetics point of view. A set of physical-chemical processes were hypothesized that serve to provide the total mass flow rate $\dot{M}$ from the burning propellant surface. Complicated geometrical relationships were developed to account for the two-dimensional aspects of heterogeneous burning. The one-dimensional thermal model given in Figure 1 provides regional boundary conditions in the Hermance model. The final expression for burning rate is a transcendental function of more than 40 variables. Later extensions by Hermance (15) seem to be directed toward incorporating high combustion pressure gas-phase diffusion phenomena into the model, in a manner similar to that of Summerfield.

Comparing the two models, it was concluded that they actually serve different purposes. The Hermance model, on the one hand, is amenable to detailed combustion tailoring since the model features so many parametric relationships. Tradeoff studies, involving such as the effect of various sized oxidizer particle blends on burning rate, are obviously practical with the assistance of a computer ( ). On the other hand, the Summerfield model offers the advantage of simplicity. Thus, this model is of practical utility as an experimental guide to gather information about the combustion process. This was the use sought herein.

However, experimental evidence gathered (Chapter V) indicates that the range of impressed voltage effects, not simply explained, is restricted to modest combustion pressures. Thus, the physical artifice associated with the high pressure extreme used by Summerfield can be reasonably neglected here. Actually, there is sound theoretical

reason (discussed below) to believe that most gas-phase interactions conceivable under an imposed electric field would be non-existent (or a weak perturbation) at high combustion pressures if gas-phase diffusion phenomenon dominates the burning process there.

At all combustion pressures encountered herein, with high voltage impressed on the burning system, ambipolar diffusion (7,38) can be expected. This diffusion phenomenon acts to counterbalance space charge, precluding effective ionic winds (later section), and is involved when a characteristic length of a system greatly exceeds the Debye shielding length, the length over which significant departures from charge neutrality exist (38,43). By conservative calculation, using Figures 20,21,39 and 40 (discussed later), even a reaction zone thickness of 0.1 mm (47) is large compared to the Debye shielding length for electrons.

Based then upon the thermal model illustrated in Figure 1, the following expression is given for the purpose of serving as a reference (no-voltage) burning rate, controlled by gas-phase reactional processes:

$$r = \frac{1}{\rho_p}\sqrt{\frac{\Lambda_g (T_f - T_s) P (P_c)^{\gamma}}{\left[c_g (T_f - T_p) - Q\right]\left(\frac{\mathcal{R} T_g}{m_g}\right)^{\gamma}}} \qquad (2)$$

In Equation (2), Q represents the net heat of reaction of the combusting system, c_g the heat capacity, Λ_g the thermal conductivity, T the temperature, ρ_p the propellant density, γ the overall gas-phase reaction order, and m_g the molecular weight. Other symbols used have been previously noted. Subscripts used are given in Figure 1.

Summarizing the details of development, Equation (2) follows from either the simple energy balance used by Summerfield or from the one-dimensional differential form of the conservation of energy expression integrated across the reaction zone thickness (Appendix C). In either case, burning is assumed steady over a constant burning area A_b. Constant properties, except temperature, are assumed. Also, velocity gradients are ignored. The mechanism of energy exchange is by conduction alone where the Mallard - le - Chatelier assumption, that the local thermal gradient is the average gradient, is invoked. Additionally, the mass flux $\dot{m}$ and the reaction zone thickness (taken from laminar flame theory), are employed in the following forms:

$$\dot{m} = \rho_p r \tag{3}$$

$$X = \frac{\dot{m}}{\Gamma (\rho_g)^{\gamma}} \tag{4}$$

Lastly, the gas phase is taken to be ideal.

It is noted that there are similarities between Equation (2) and burning rate expressions developed in References 28 and 54. These references do not restrict analysis to the composite class of propellants. Here, of course, the heterogeneity of the system can be expected to be reflected through fluctuation of properties of the system. From Equation (2) it is seen that the burning rate depends upon the mechanical properties (P , ρ , η), thermal properties (T , Λ , c) and chemical properties (Γ , γ , Q) of the system.

Formulation variables, such as total volume fraction of oxidizer particles, are not involved in Equation (2). Unfortunately, of the properties noted in Equation (2), only the propellant properties and combustion pressure are readily determined or set by experiment. However, it might be possible to deduce, say, the approximate overall reaction order from the experimental pressure exponent. Thus, obvious experimental difficulty presents itself for the task of determining mechanisms responsible for voltage induced burning rate changes.

Macroscopic Considerations

Comparing Equations (1) and (2), it is seen that nine ω_i variables are displayed. The question naturally arises: are there any additional variables present when high voltage is supplied to the burning system. At present, there is no reason to expect that Equation (2) is valid. Before the result of a simple gas-phase thermoelectric coupling analysis is discussed, obvious factors associated with the solid phase under certain high voltage experimental conditions are given.

Consider a differential change to the total mass flow rate $\dot{M}$ from burning propellant of fixed density. From mass conservation,

$$d\dot{M} = \rho_p A_b \, dr + \rho_p r \, dA_b \quad . \tag{5}$$

It is important to note from Equation (5) that a mass flow rate change potentially involves changes to both burning rate and burning area. Many devices that supposedly measure burning rate actually measure the total mass flow rate (for example, timing wires or a photomultiplier responding to flame light). In the previous section it was assumed that the burning area was constant. In fact, under extremely high applied voltage the burning area is not constant (Chapter V). Thus, "apparent" burning rate changes need to be recognized for interpretation of experimental data.

Prolonged electric current passing through the solid phase can also alter the propellant temperature. Propellant preheating affects the burning rate through the temperature sensitivity of burning rate of the propellant π_r, and can be correlated with the relationship

$$\frac{r^*}{r} = e^{\pi_r (T_p^* - T_p)} \tag{6}$$

Equation (6) follows immediately from integration of the defining equation for temperature sensitivity of burning rate. The notation r^* denotes the burning rate associated with the current heated propellant at elevated temperature T_p^* and r denotes the reference burning rate at the reference propellant temperature. As will be seen, prolonged electric currents interacting with the solid phase do heat propellant and in concentration increase the burning rate (Chapter V).

Now, regarding the gas phase, an analysis consistent with the assumptions given to obtain Equation (2) was conducted for the case

where an electric field was imposed on the burning system. Appendix C contains the details of this elementary analysis. The work applies to an electric field imposed upon the gas phase in a direction parallel to the direction of regression and is based on phenomenological equations from irreversible thermodynamics.

In the interest of tractibility, the gas phase was regarded as a molecular gas upon which a dilute isolated electron cloud, in equilibrium with the gas, had been superimposed. This assumption appears essentially valid (next section, Chapter V, Appendix D), except that, naturally, electrons were then precluded from taking part in reactions that might influence the burning rate. Also, gas-phase current density gradients were ignored. This assumption also appears to be valid overall and restrains charge generation and recombination mechanisms from being collectively affected by the electric field (Appendix C). The resultant expression for the burning rate r' associated with combustion under an imposed electric field is placed below:

$$r' = \frac{\Omega}{2\rho_p} + \frac{1}{2\rho_p}\sqrt{\Omega^2 + \frac{4\epsilon\Lambda_g(T_f - T_s)\Gamma(P_e)^{\gamma}}{\left[c_g(T_f - T_p) - Q\right]\left(\frac{RT_g}{m_g}\right)^{\gamma}}} \quad . \quad (7)$$

Ω and ϵ are defined as follows:

$$\Omega = \frac{\frac{J^2}{\sigma_g} \pm \frac{\alpha_g}{\sigma_g} J(T_f - T_p)}{c_g(T_f - T_p) - Q} \quad (8)$$

$$\epsilon = 1 - \frac{\alpha_g \beta_g}{\lambda_g \sigma_g} \tag{9}$$

The electron current flux is given by J and σ_g, α_g and β_g represent the gas-phase DC electrical conductivity and thermoelectric coefficients, respectively. The $\pm$ signs noted in Equation (8) account for the direction of the imposed electric field (through the resulting direction of current flow).

Comparing Equations (2) and (7), it would appear that:

1. the imposition of an electric field alters the burning rate expression

2. if an electric field does not change basic system properties, the reference burning rate r is contained in the burning rate expression for r'.

Treating the first comment, the burning rate expression for r' includes the additional effect of electrical energy added to the gas phase, augmented or retarded by the direction of the imposed electric field through the current flux direction. The expression for r' also includes the thermoelectrically coupled reduction in thermal conductivity through ϵ. Thus, Ω essentially represents a burning rate augmentation term under applied field conditions. On the other hand, ϵ represents a burning rate reduction term under field conditions. Hence, based on this analysis, either the burning rate increases,

decreases, or, if Ω and ϵ effects counterbalance, remains constant under voltage conditions.

For the formulations used, Table II presents representative gas-phase properties. Computing Ω and ϵ given by Equations (8) and (9), using the values given in Table II, results in $\Omega \simeq 0$ and $\epsilon \simeq 1$ (see Table II). Thus, if the second statement above holds, $r' \simeq r$ and the burning rate remains unchanged when a properly oriented electric field is applied. Experimental evidence contradicts this deduction (Chapter V). The conclusions left are that either the analysis is invalid or not sufficiently extensive, or that, perhaps, Equation (2) suitably represents the burning rate with an electric field imposed but that some of the system properties noted in this expression are altered by the field. The latter possibility could not be ignored and was concluded for the purpose of providing experimental guidance. This conclusion may have been fortuitous.

Microscopic Inferences

For the formulations used, the question arises as to the identity of charged gas-phase species that would be expected to be influenced by an electric field. Also, how these charged species might relate to the burning rate needs to be considered. In response, the following statements can be made.

1. Microscopically, the gas phase consists of neutral species and charged species. Here, the gas phase contains both positive and negative ions of nearly equal number density as well as a slightly smaller number of electrons per unit volume (next section and Chapter V).

2. The gas phase represents a weakly ionized dense gas system where the DC electrical conductivity principally involves the migration of electrons (Appendices D and E, Chapter V).

3. The gas phase maintains the state of quasi-neutrality in bulk even when an electric field is imposed since the reaction zone thickness greatly exceeds the Debye shielding length.[1]

The second statement above suggests that an electric field imposed upon the burning systems used would only affect electrons to any extent. Since electrons are approximately a thousand times more mobile than either the positive or negative ions involved (next section), the electron drift velocity would be expected to greatly exceed the ion drift velocities.

The preceding also corroborates the earlier parenthetic remark that the convective (or collective) concept of ionic winds cannot be effective in influencing the burning rate. No appreciable net body force exists in the gas phase due to space charge. Experimental evidence and simple analysis completely confirm this statement (Chapter V and Appendix D).

Perhaps most significantly, the above statements and discussion taken collectively imply that, if the burning process is rate limited in the manner previously described, gas phase related electric field effects on burning rate would occur only at modest combustion pressures. Any influence that the field might exert would diminish as the combustion pressure increased to where diffusional phenomena completely dominate.

---

[1] Recall that this condition implies that ambipolar diffusion occurs, a stipulation where quasi-neutrality is automatically satisfied.

The essence is to suggest that electron-second body interactions are important to the burning process and high voltages impressed across the system affect these encounters. The phenomena involved would be classed as non-collective rather than collective (27).

There is evidence to indicate that flame electrons contribute to combustion inhibition. Recently, Mills (30), for instance, suggested that combustion inhibition of the type observed with the use of most halogenated hydrocarbon flames (like those used herein) is due to a two-step process: (1) negative ions and free radicals formed by dissociative electron attachment with inhibitor molecules, and then (2) these negative ions or free radicals react. Although the evidence was not conclusive, Mills concluded that serious consideration of this idea was justified. At any rate, the effective mechanism causing combustion inhibition does not evidently lower combustion temperatures appreciably (30). Mills points out that one objection to the suggestion that flame electrons play a role in combustion inhibition is the doubt that electron concentrations are large enough in hydrocarbon flames but concludes that an electron density of 10^{11} electrons/cm^3 is not too small to be important. As will be seen, electron number densities found herein are of the order of 10^{12} electrons/cm^3 (next section, Chapter V).

Thus, electron interactions, influenced by an electric field, provide a likely cause for an effect on the burning process. Of course, only burning rate reductions could follow from retarded combustion efficiency. An imposed electric field could also interfere with intimate oxidizing and reducing reactions involving electron encounters which could result in either enhanced or retarded combustion.

Briefly returning to the solid phase, there is some evidence to suggest that the thermal decomposition of the oxidizer used herein, ammonium perchlorate (AP), is sensitive to applied voltage (25). The suggestion was made that charge carriers play a significant role in thermal decomposition. Based on tentative findings, it was concluded in Reference 25 that AP decomposition was enhanced by an impressed voltage and explained on the basis of an electron transfer model. The study resulted in the assignment of a probable defect structure to AP: cationic Frenkel type or Schottky disorder depending on the temperature where decomposition took place. However, here current heating seems to account for observed and measured enhancement effects (Chapter V).

Computer Predictions

A technique to predict gas-phase charged matter and combustion properties was desired since, as seen, an electric field might influence both. For the formulations selected, a variety of charged gas-phase species were expected. Also, particulate matter would be present in the gas phase which might carry a net charge. In this section, it is possible to qualitatively account for the metal added to the formulations used. Previously, nothing has been said herein about the role of particulate metal (aluminum) on combustion.

A developed computer program was used to provide predictions. The basic program is described in detail elsewhere (39). The computer program was based on the minimization of the Gibbs free energy of the reacting system and accounted for both gaseous and particulate matter. Herein, the program was modified to consider the effects of combustion inefficiency (through the creation of nonreactive matter, described shortly) upon properties of the gas phase.

Briefly, the basic computer program involved the use of a Taylor series expansion of the Gibbs free energy, written as a function of composition Y and temperature T, about a point (Y_o, T_o). Both gas and particulate species, charged and neutral, were summed in the free energy expression. The series expansion was terminated after second order terms. This total expression was minimized subject to mass balance constraints using Lagrange multipliers (by conventional variational technique involving constraining conditions). To make the system of resulting equations determinate, it was assumed that reaction processes were adiabatic. The solution process was then the simultaneous convergence on both combustion temperature and composition, converted to number density. Other assumptions made were that:

1. the overall gas phase was ideal
2. charged species were singly ionized
3. the gas phase was quasi-neutral
4. condensed phase entropy of mixing was negligible.

Inherently, the state of thermal and chemical equilibrium was assumed. Particulate matter was, likewise, assumed in thermochemical equilibrium with gaseous matter.

Two nonreactive particulate species were created to account for combustion inefficiencies. Both nonreactive species were assumed to possess thermal properties identical with their respective parents (ordinary aluminum and carbon). These nonreactive species essentially served to suppress parent reactions. That is, the parent element was

restricted from undergoing reaction, in varying degree, by the presence of the nonreactive specie, in amount such that elemental mass was conserved. The degree of restriction of reaction (termed combustion efficiency) was denoted by a percent of the input weight of the element. Thus, for instance, the notation $80/Al_r$ means that 80% of the initial aluminum by weight is allowed to react during the combustion process. The balance of aluminum by weight serves as non-reactive aluminum. However, it is emphasized that the amount of parent matter allowed to react and the amount that actually reacts need not necessarily be the same. Thus, for example, for the reaction

$$C_1 Al + C_2 O_x \rightleftharpoons C_3 Al_y O_z + C_4 Al \tag{10}$$

where x, y, z are integers and C_1, C_2, C_3, C_4 are stoichiometric coefficients, $C_4 \neq 0$ could result.

Input to the computer program merely required a percentage breakdown by weight of the propellant ingredient elements. Trace elements with low ionization potentials, such as potassium, sodium and cesium, were also included in this percentage. Trace element values used are presented in Table VII. Discussion of Table VII is placed in Chapter V. The other input variable besides combustion efficiency was combustion pressure. The computer output consisted of an iterated combustion temperature, other overall gas-phase properties such as molecular weight, plus iterated number densities for approximately 200 charged, neutral and particulate products.

The machine data considered most pertinent are presented in Figures 20,21,39,40. Experimental results, discussed in Chapter V,

are superimposed on this machine data. Additionally, Figure 30 presents the computer predicted relationship between aluminum allowed to react and gas-phase products involving aluminum oxide and metallic (unburned) aluminum. This figure is used later (Chapter V) to translate experimental findings to Figures 39 and 40. It is noted that all figures containing computer data apply to the case where no nonreactive carbon exists in the gas phase. Based on experimental findings (Chapter V), it was reasonable to neglect the nonreactive carbon for final computer computations.

Select observations regarding computer predictions are given below. These predictions are contrasted later with experimental results (Chapter V).

1. The electron number density was found to be always approximately an order of magnitude less than the positive ions number densities (Na, K) and the negative ion number density (Cl).

2. Ionic and electron number densities were increased approximately an order of magnitude above their respective densities from the "pure" formulation by accounting for parts-per-million of impurities. However, charge densities were near saturation by accounting for trace impurities (since, for example, a 1% by weight potassium nitrate or cesium perchlorate ionizable salt added to the "pure" formulation resulted in charge densities only slightly above values with trace impurities).

3. The ratio of aluminum oxide (Al_2O_3) to metallic aluminum product was independent of combustion pressure (Figure 30).

Machine computations were also attempted in order to obtain meaningful exhaust product compositions. Some experimental measurements were taken from an exhaust station (Chapter V) and correlation of exhaust conditions with combustion conditions was desirable. Expansion to exhaust conditions was assumed isentropic. Thus, the computer program additionally involved describing the behavior of the entropy function in the neighborhood of a point (Y_0 , T_0).

Additional input to the computer program was experimentally determined pressurizing gas flow in the exhaust (Appendix G). This gas acted as a reaction quench and diluent. Unfortunately, the ratio of mass efflux of pressurizing gas to mass efflux of combustion gas was so large (Figure 41) that the computer program would not generally converge to a solution where exhaust and combustion product compositions could be related. However, it is obvious that exhaust product concentrations with diluent would be smaller than nondiluted exhaust product concentrations. This fact should be noted when computer concentration predictions are contrasted with experimental results (Chapter V).

Figures 31 and 32 illustrate computer predicted ratios of combustion concentration of carbon monoxide to carbon dioxide. Combustion efficiency again is the parameter in these figures. Experimental exhaust concentration results, discussed in Chapter V, are superimposed upon these figures.

Ancillary Factors

For the experimental arrangements used (Chapter IV), there was a conduction loss from the gas phase to the cool inhibiting and

pressurizing gas. This conduction loss theoretically affects the burning rate (54). Also, the side flow gas used to inhibit the propellant sample might convectively influence the burning rate. Fortunately, this latter influence was found to be extremely weak even at a combustion pressure of one local atmosphere (Appendix G). Both of these experimental factors were expected to be independent of impressed voltage.

An electric field could effectively alter various gas-phase conduction, mechanical, radiation, and reactional mechanisms. Some specific mechanisms are placed below. Many of these might be interrelated or related to previous discussion.

Conduction. An electric field could affect combustion temperature, the reaction zone thickness through the alteration of reactional mixing lengths, or the thermal conductivity through subtle changes to the level of turbulence. Changes to any of these factors individually would alter conduction given by the Fourier conduction law.

Mechanical. Electric current heating might cause melting of propellant ingredients. Should these ingredients flow over other ingredients while on the burning surface, burning might either be inhibited or enhanced depending on the natural requirement for surface premixing. For instance, the flow of a non-energetic binder prematurely over oxidizer particles might prevent oxidizer particles from receiving flame energy or might even quench the particles.

Radiation. Radiation energy associated with the burning system arises from both the combustion gas and particulate species. Evidently, irradiance to the burning surface from a gas phase, entrained

with particulate matter, is significant (11). Accordingly, an electric field might:

1. cause redirection of the motion of particulate matter to the extent that radiation feedback to the burning surface is altered

2. alter the formation of particulate matter to the extent that radiation to the burning surface or surrounding gas is modified

3. cause a change in the overall flame zone luminosity or alter flame species emission characteristics.

Reactional. A number of electric field induced reactional effects have been discussed previously. Conceivably, an electric field might also alter:

1. the independent displacement of ionized intermediates and radicals intimate to the rate controlling chain

2. the gross composition of combustion products.

III EXPERIMENTAL APPROACH

This investigation centered on experimental elements. Both exploratory and diagnostic experiments were conducted. Experiments of an exploratory nature were designed to determine experimental arrangements and to obtain relative high voltage effects on burning propellants for the various arrangements. Experiments of a diagnostic nature were designed to determine flame properties, examine such relevant factors as the pressure dependency of voltage induced effects, and to deduce mechanisms causing alterations to the burning rate under high voltage conditions.

Burning Rate Device Experiments

Since a major measurement in this investigation was the measurement of burning rate, it was necessary to consider various methods for obtaining burning rate. The conventional method, using timing wires in contact with the propellant, was considered unsatisfactory with high voltages in the vicinity of the wires. DeStefano (10) reported electrical signal interference as well as actual wire motion with the impression of high voltages. Thus, a non-contact method for measuring burning rate was sought. Additionally, a continuous burning rate measurement technique was desired. Stones (45) desired a continuous device.

The experimental approach used was to conduct tests on burning propellants to compare the measurement of burning rate using each type of device noted in Table I and using, in addition, a previously untried continuous burning rate device, named herein an Optron (Chapter IV, V, Appendix H). Both a primary and an alternate burning rate device needed to be selected.

Ionization Experiments

For the propellants used, there was the desire for experimental corroboration of computer predicted gas-phase charge densities, particularly the electron density. The approach used was to probe the gas phase with a Langmuir probe at one combustion pressure to seek the electron density. Additionally, the gas-phase DC electrical conductivity was measured, also at one pressure, to gain further information about the microscopic nature of the propellant flames used. To project to other combustion pressures the thermochemical equilibrium computer program was used. However, it was necessary to experimentally determine impurity levels for the computer input.

Electric Parameters Experiments

For the study of an electric field imposed upon burning propellant, the approach used was to investigate flame-field characteristics generally at one combustion pressure employing a limited number of electrode geometries, using two or occasionally three initial voltage settings from two DC high voltage units. Preselected and presized propellants were used. The most interesting arrangements were selected for further experiments.

Included in the six electrode configurations selected for study were the geometries used by each investigator noted in Table I. For those particular electrode arrangements where the propellant served not only as one electrode but also as a resistive component, it was necessary to make provisions to measure the bulk solid-phase DC electrical conductivity. Also, an experiment was designed to study the role of current heating of the solid propellant matter.

To further understanding of flame-field characteristics, apparatus was designed to monitor the applied voltage, other voltages of interest, and both normal and avalanche, or arcing, currents. In addition, since it was desirable to explore the distribution of the impressed voltage between the electrodes, a high voltage rake, capable of recording voltages at its tips, was fashioned to attempt to measure regional field strengths without interference with the applied voltage.

Electric Effects Experiments

The concentration of the investigation was upon burning rate changes induced by the imposition of high voltage on the burning system. For the experimental arrangements selected, experiments were needed to seek to identify mechanisms responsible for burning rate changes under voltage conditions.

First, measurements of burning rate over a pressure range, with and without applied voltages, were taken. Secondly, high-speed closeup photographic coverage was desired to study both the burning surface and particulate matter under voltage conditions. Then, an

extensive sequence of experiments was conducted to gather and quantitatively analyze combustion residue as a function of combustion pressure, again, with and without an imposed voltage. Overall combustion efficiency consistent with previous discussion was deduced from this data. Next, it was felt further insight into the mechanics of the reaction system might be obtained by trapping exhaust gas emissions and then performing quantitative analysis on selected gas stables (CO and CO_2) and qualitative comparisons of other stable species. Such experiments were conducted at various pressures with and without applied voltage. Lastly, experiments were designed to attempt an optical measurement of the combustion temperature, again, with and without voltage.

IV APPARATUS

Assembly Area

The main apparatus used for experiments was assembled at two locations. Experiments at local atmospheric pressure were conducted in an electrically isolated exhaust hood located inside a laboratory trailer especially equipped for high voltage studies on burning propellant. Experiments at pressures higher than atmospheric pressure were performed in a test-cell with essentially a laboratory environment which was modified for this high voltage study.

Control of test-cell operations was accomplished from a control room located behind the cell. Preset sequencing of equipment events, with a nominal accuracy of 100 msec between events, was possible from this room. Visual observations between the cell and the control room were made through a transparent blast window constructed between the cell and the control room.

The atmospheric pressure site was basically a duplicate of the test-cell site except that the combustion bomb used in the cell was not necessary and exhaust emissions were vented through the hood. Additionally, preset sequencing control apparatus was more versatile at the atmospheric site. The functions automated by the sequencing equipment are given later in the chapter.

Overall Assembly

Figure 2 shows the overall test-cell assembly. Not shown in this photograph are such auxiliary equipment as cameras or the optical pyrometer. Figure 3 shows a simplified overall test-cell equipment schematic. Not all apparatus illustrated was used for each experiment. As details of other apparatus are described, particularly those used for ionization and electric parameters studies, appropriate schematics are given.

Propellant Arrangements

The procedure used to prepare propellant samples is contained in Appendix F. The code identifying propellants is placed in Table III. In this section, discussion is restricted to describing the propellant sample as an item of apparatus and the mounting of the sample.

Depending upon the electrode geometry used, the propellant served either as part of the media between electrodes or as one electrode and a resistor. Propellant samples were sized according to the planned experiment and were approximately ½ inch square and 1½ inches or 2 inches in length for ionization experiments and 3/8 inch square and 1½ inches in length for other experiments. For all burning experiments, propellant samples were mounted centrally onto a nitrogen mixing chamber (next section). The mounting piece was a copper rivet to which the propellant sample was either bonded or, preferably, tacked. The copper rivet was fit into a metal insert

positioned on the top of the nitrogen chamber. In the instance where the propellant was an electrode, the rivet and metal insert served as part of the electrical connection for high voltage. A high voltage cable connected the metal insert piece to a tap located on the outer wall of the nitrogen chamber.

Nitrogen Chamber

Nitrogen gas was forced along the sides of the propellant sample to inhibit burning except from the top of the sample. A cylindrical plexiglass mixing chamber was used for this purpose. Nitrogen gas entered the bottom of the chamber through a fitting with radial exit ports, swirling the inlet gas. Nitrogen gas exited the top of the chamber through twenty-four 1/16 inch diameter holes patterned to enclose the sides of the propellant sample. The nitrogen side flow also prevented the flame from fanning out above the unburned propellant.

As the combustion pressure was increased for the metallized formulations used, a smoke mantle partially covered the burning sample and prevented a clear view inside the combustion bomb. The patterned chamber top was replaced by a porous diffusion plate in a futile attempt to displace the smoke. Ultimately, the patterned chamber top was used with additional exit holes bored in the top and sides and also with some of the inlet nitrogen diverted around the chamber. An overall flow pattern was apparently created inside the combustion bomb that was sufficient to clear the smoke. However, Propellant B persisted in generating more smoke than could be completely displaced.

Figure 4 illustrates the propellant and nitrogen chamber setup. This sketch is not to scale. Appendix G contains further discussion

of the nitrogen as a side burning inhibitor, pressurizing gas, and diluent.

Combustion Bomb

A pressure vessel was modified in order to perform high voltage experiments for combustion pressures greater than local atmospheric pressure. A cylindrical stainless steel combustion bomb with an inside diameter of 5 inches and an inside length of 13 inches was used for this purpose. Viewing windows were located every 90° and centered near mid-length of the vessel. Two windows approximately 5 inches in length and 1/2 inch wide, made of 3/4 inch thick Herculite tempered plate glass, located 180° apart, were used for optical measurements access. The other two window ports, also located 180° apart, were modified to become high voltage connections. A 1/4 inch stainless steel rod was force-fit into a high-strength, high-electrical resistance material named Lexan, and machined to the size of the customary windows. The Lexan-rod arrangement purposely protruded inside the bomb and also outside the bomb. Four additional high voltage connections were also located in the bomb lid. Figure 5 shows the exterior of the combustion bomb, illustrating these features.

It was necessary to electrically isolate the entire experimental system. To this end, the bomb was mounted upon 7/8 inch thick micarta insulating material. All other apparatus interfacing with the bomb was also mounted on micarta (Figure 3). The nitrogen gas inlet line was isolated by a section of high-pressure, high-electrical resistance hose. The 1/2 inch diameter stainless steel exhaust line was shrouded in rubber and strapped with tygon tubing. Necessary electrical leads

from the bomb were connected in series to buffer resistors rated at 1080 megohms. High voltage cabling was insulated with 10 KV/mil material or inserted into tygon tubing. A 100 KV, one-to-one, oil bath transformer, described elsewhere (52), was used to isolate the propellant ignition circuit.

Table IV shows the extent of the electrical insulation of the combustion bomb. It was necessary to keep the system free of corrosive combustion products and room dust to maintain the values given in Table IV (atmospheric site apparatus was similarly electrically insulated).

The bomb was further modified to maintain an essentially constant pressure after the ignition pressure surge. The small propellant sample size helped in this regard by reducing the amount of combustion debris deposited along the exit line. Additionally, the small sample size afforded a small ignition pressure surge (1 atm., typically, at an initial pressure of 15 atm.) and minimized post-test cleanup. The main modification, however, to ensure constant pressure combustion, was to provide a 1/2 inch diameter exhaust port in the center of the lid of the bomb and then flow the combustion gases and nitrogen through a 1/2 inch diameter straight through valve. This valve was preset for a particular flow condition at a particular combustion pressure (Appendix G). The combustion bomb pressure, including any ignition surge, was recorded on a calibrated direct reading gage threaded into a 1/8 inch diameter port located on the side of the bomb.

Figure 6 illustrates the interior of the combustion bomb and shows the propellant sample and nitrogen chamber. The Lexan-rod high voltage connections are barely visible in the photograph. Also shown

in the photograph is the ignition post where the ignition wire was connected through the propellant. The leads from the ignition post were connected to the isolation transformer through the receptacles in the bomb lid. The ring electrode and the high voltage rake shown in the photograph are discussed later in the chapter.

Electric Apparatus

High Voltage Supplies

Both an unregulated current and a regulated current DC high voltage power supply were used during the study. The unregulated current power supply, variable from 0 - 25 KV and 0 - 5 mA, is seen in Figure 5. The delivered voltage was set negative with respect to ground. To record the currents drawn through the high voltage circuit with the apparatus designed for this purpose (next section), it was necessary to allow this power supply to "float" a few volts above ground potential.

The regulated current power supply, variable from 0 - 100 KV and 0 - 100 mA, is shown in Figure 7. This figure also displays preset sequencing and recording apparatus used at the atmospheric pressure site. Not shown in this photograph, but an auxiliary part of the regulated power supply, is a large oil bath housing the high voltage transformer-rectifier. Polarity of this high voltage unit was changed by rotating an electrical connection board located under the oil. Currents resulting from impressed voltages could be controlled, nominally, from 0% to 100%. Multiple safety features were incorporated into the regulated unit since careless operation could be extremely dangerous.

Voltage and Current Circuits

Voltages at any point in the high voltage circuit were measured by connecting a buffered circuit to that point. This circuit was designed to divert microampere currents from the high voltage line to drive sensitive recording galvanometers. The impedence of the measuring circuit was such that the circuit being monitored should not be disturbed (Chapter V). Buffer circuits were electrically shielded from each other to prevent cross-talk and the buffer resistors (1080 megohms) were housed in a plexiglass container to prevent dust contamination.

Net currents passing through the high voltage circuit under load were measured by connecting monitoring circuits across known resistors positioned in series between the ground electrode and the high voltage supply ground. The diverted microampere currents again drove sensitive recording galvanometers. Zener diodes were placed across the current monitoring circuits to protect the galvanometers from receiving too high a current which would torque the mirror assembly in the galvanometer until its holding coil failed. For a particular current range, if the diverted current rose too high, the Zener diodes allowed the excess current to bypass the measuring circuit. Then, of course, the recorded current was no longer accurate.

Figure 8 illustrates wiring schematics for both the voltage and the current monitoring circuits. This figure does not show the calibration network associated with the current circuit.

Electrode Geometries

In addition to the propellant as an electrode, a screen, a plate and a ring were used as high voltage electrodes during the investigation. The screen electrode was made of 15 mil diameter nichrome wires, spaced 1/16 inch apart. The stainless steel plate electrode was 1/2 inch wide and approximately 2 inches in length. The ring electrode was a 1 inch inner diameter copper ring. The nichrome screen could be fashioned over the copper ring.

Figure 9 shows sketches of the six electrode geometries studied. In the first three sketches the propellant serves both as an electrode and as a resistor. In the next two sketches the propellant represents part of the media between electrodes. The last geometry shows an axial wire buried in the propellant. In this latter configuration the propellant acts partially as an electrode and partially as a media between electrodes.

Figure 10 illustrates a typical completed arrangement of electric apparatus. The arrangement shown was used for electric parameters experiments.

Optical Instruments

Burning Rate Devices

Four separate optical schemes for measuring the burning rate of propellant samples were examined for use. In addition, the conventional burning rate measurement scheme, using timing wires through the propellant, was used for comparative test purposes (Chapter V).

A 16mm Bell and Howell camera, running at 64 frames/second, was focused on the burning propellant from a distance of approximately 36 inches. Both ASA 160 color film and ASA 125 color film were used. The camera lens was stopped to f/9 for all exposures. Timing pulses were superimposed on the edge of the film at a rate of 10 pulses/second. On occasion, a Kodak sun-gun was used for auxiliary lighting purposes. A dimensional reference was imposed on the film by exposing a ruler where the propellant normally sat. Film was analyzed on a Vanguard Model 16 or 16C Motion Analyzer.

The photodiode arrangement examined for use is described in detail elsewhere (34,52). Briefly, six Texas Instrument LSX-600 photodiodes, spaced 1/4 inch apart, were aligned along the propellant axis at a distance of approximately 8 inches from the propellant. As the propellant regressed to a photodiode position, visual flame light would reach the photodiode through a series of collimating baffles in the photodiode holder and the photodiode would pass current which drove a recording galvanometer. The response of the system was greatly enhanced by collimating light from an arc-lamp located on the opposite side of the propellant. This light beamed onto the photodiode holder as the propellant, blocking the beam, regressed past.

It was necessary to install shielded wiring from the photodiodes to eliminate interference among the recording galvanometers while the high voltage supply was on. Occasionally, arcs discharged from the high voltage circuit to the grounded photodiode head assembly and then through a photodiode circuit severely torquing the mirror arrangement in the galvanometer. Such operational difficulties possibly could have been eliminated by "floating" the entire photodiode

assembly. This was not attempted because another method of measuring burning rate, developed herein, was found more suitable.

An unusual optical instrument was used in order to obtain a continuous measurement of burning rate. The instrument, hereafter called the Optron, was operated to continually sweep across the burning surface and then servo-track with the surface as it regressed. The device was also simultaneously used as a simple photomultiplier responding to light. With such features, a continuous burning rate was measured along with an overall burning rate based on ignition until burnout.

The Optron used was a Model 800 equipped with a variable range lens resolving to 0.02% of the fullscale displacement or fullscale field-of-view. For the propellant heights used, then, a typical resolution to about 7 microns was expected. Actually, resolution was limited to approximately an order of magnitude above this value by virtue of the size of an aperture hole which allowed electrons that passed from the photocathode to enter the photomultiplier (Appendix H). The lens was equipped with a variable f-stop setting.

The Optron was preset to orthogonally sweep across the burning surface at 100 Hz (although, occasionally, only one point on the burning surface was tracked). As the propellant burned, servo-tracking of the relative light-over-dark interface provided by the flame-over-propellant interface yielded the burning rate (Appendix H). The servo-mechanism recycle time was approximately 3 microseconds. That is, if the instrument lost its "lock-on" the light-to-dark interface, the instrument would servo-wheel to regain the "lock-on" at an oscillation rate of 50 KHz.

A relative light-to-dark intensity of at least 50 lumens was required for proper Optron operation. A relative intensity of greater than 50×10^3 lumens would temporarily saturate the electronics of the instrument. Neutral density filters were used for the higher combustion pressure experiments to preclude component saturation. The instrument was set a precisely known distance from the propellant sample since the indicated burning rate was proportional to working distance (Appendix H).

The Optron was focused both optically and electrically upon the propellant sample before burning commenced. Optical adjustments were made by centering the sample, in sharp focus, onto an optical viewer graticule to a calibrated fullscale ($\pm$ 5 volts) position. Electrical adjustments were made by viewing the top surface of the propellant on a Tektronic RM 45A oscilloscope to position the orthogonal sweep length and amplitude, and to verify the fullscale voltage setting. The differential voltage output of the Optron was connected to an X-Y Plotter recording device.

Figure 5 shows a photograph of the Optron head aligned with one optical access window of the combustion bomb. Figure 11 displays the Optron electronics and the auxiliary oscilloscope. Also shown in this latter figure is recording apparatus. Appendix H and Chapter V provide details of the operation and performance of the Optron as a burning rate measurement device.

Closeup Camera

A 16mm Hycam camera was used for closeup study of the burning propellant. The ASA 160 color film used was exposed at a framing

rate of 2000 frames/second at a lens setting of f/4. Timing marks were superimposed on the film at a rate of 120 pulses/second. Extension tubes were required for closeup focusing.

Temperature Pyrometer

An IDL 650 brightness pyrometer was used briefly until a Shawmeter two-color pyrometer arrived. Operation of these two instruments was similar.

The sensing head of the pyrometer was positioned at a distance of 17 7/8 inches from the propellant sample. The instrument viewed the propellant through one of the Herculite plate glass windows. The pyrometers were calibrated at the Air Force Calibration Laboratory, Newark AFS, Ohio, at a working distance of 17 7/8 inches between the focusing lens and the 1/4 inch aperture of a Rocketdyne blackbody. The Herculite glass was not used during calibration. In operation, the field-of-view of the instrument was adjusted to a 3/8 inch diameter circle. The center of the circle was positioned approximately 13/16 inch from the bottom of the propellant sample.

The comparative wavelengths for the two-color instrument were approximately 0.665 microns and 0.467 microns. The differential voltage output from the two-color device deflected a 0 - 100 MV meter, calibrated in temperature. Figure 5 illustrates the Shawmeter pyrometer aligned with the other optical access window of the combustion bomb.

Immersion Probes

High Voltage Rake

A high voltage rake was designed to measure spatial point voltages, without interference, at points of interest in the vicinity of the combusting system. Figure 12 displays the rake used inside the combustion bomb. Figure 6 shows the rake positioned along the propellant sample, slightly imbedded in the sample. A similar rake was also used at the atmospheric pressure site.

The rake assembly was fabricated out of plexiglass and the rake tips were 10 mil diameter tungsten wires. The spacing of the tips could be varied but a spacing of 1/4 inch was typical. Portions of the tungsten wires were occasionally consumed while immersed in the hostile gas-phase environment. The rake was easily disassembled for wire replacement. The small currents drawn through the rake were used to drive recording galvanometers in the voltage monitoring circuits.

Ionization Probes

Two other immersion probes were designed for use in this study. One probe was designed to approximate an infinite length-to-diameter cylinder and was used as a Langmuir probe. The other probe was designed to measure the DC electrical conductivity of the gas phase.

The Langmuir probe was constructed of 15 mil diameter tungsten wire which was positioned across a yoke made of micarta. An effective length-to-diameter ratio of approximately 50 was realized. Voltage was supplied to this wire from a variable 0 - 40 volt DC power supply. The remote electrode used was a 4-inches square wire screen made of

15 mil diameter nichrome, spaced 1/16 inch apart. The distance between the wire probe and the remote screen electrode was 1 1/2 inches.

For reasons discussed in the next chapter, it was necessary to traverse the tungsten probe across the propellant flame. A rolling probe platform was arranged for this purpose. The remote screen electrode remained over the entire flame. It was also necessary to depart from the conventional Langmuir probe technique of sweeping the probe voltage and measuring the collected current, all in a short time interval (Chapter V). For experiments here, a probe voltage was preset and both the collected current and applied voltage recorded as a function of time, again using galvanometers.

Figure 13 shows the Langmuir probe immersed in the gas phase of Propellant A. The probe was held stationary for this photograph. The glowing combustion debris buildup upon the wire probe is clearly observable.

The DC electrical conductivity probe was fashioned using two 15 mil diameter tungsten wires, spaced 1/2 inch apart, stretched again across the micarta yoke. Figure 15 shows this arrangement. The main difference between the Langmuir probe and the electrical conductivity probe was the ratio of the area of the applied voltage electrode to the area of the other electrode (Chapter V). In operation, using the conductivity probe, the tungsten wires were positioned at the flame and nitrogen side flow interface, straddling the propellant. Hence, this probe was continually cooled.

Figure 14 illustrates the ionization probes schematic. This figure additionally shows both the Langmuir probe and the electrical

conductivity probe positioned for measurement. Calibration deflections of the recording galvanometers were made by switching the 220K ohm resistor, shown in the figure, into the circuit.

Solid-Phase Electrodes

The bulk DC electrical conductivity of the solid propellant was measured using the technique described by Turner (52). Basically, two 20 mil diameter electrode wires were imbedded in a propellant sample of known size at a known distance between wires and the resistance between the wires measured. An alternate method was to measure the resistance of a propellant sample of known size, appropriately wedged between finely machined surfaces of two copper electrodes, with these electrodes mounted on micarta. Figure 16 shows this arrangement. This figure also shows a heavy silicon thermal insulation spread onto the outer surfaces of the copper electrodes. This device was mainly used as the electrode arrangement for studying current heating of the propellant to simulate electrode geometries where the propellant acted as a discrete electrical component (Chapter V). Propellant resistances were measured with either a General Radio Corporation 1862-C Megohmeter, operated in the ungrounded position at a discharge voltage of 500 volts, or a Hewlett Packard Vacuum Tube Voltmeter, Model 412A or 410B.

Sampling Devices

Exhaust Emissions Apparatus

A fraction of the combustion bomb exhaust was diverted from the exhaust line by inserting an impact tube into the exhaust downstream

from the straight-through valve. The tube was made of teflon to preclude a ground path from the bomb. The tube led to a gas trap. Ultimately, the tube was left completely open to also pass entrained solid debris into the gas trap since both glass wool and wire screen inserted into the tube failed to filter solid debris without blocking the flow in the tube.

The gas trap was a 3 liter stainless steel cylinder initially evacuated to 100 microns Hg absolute pressure. A leak checked valve served as the entrance to the trap. Part of the trapped gas was transferred to a 1 meter cell initially evacuated to 10 microns Hg absolute pressure for infrared analysis at standard conditions (Chapter V). The balance of trapped gas was retained for gas chromatographic analysis (Chapter V). Infrared spectra were obtained with a Perkin-Elmer 421 infrared grating spectrometer. Table V presents the instrument settings used.

Combustion Residue Disk

A 1 inch diameter stainless steel disk was positioned 1 1/4 inches above the unignited propellant sample to recover combustion residue. The disk was mounted in the center of a piece of plexiglass which was placed between two snap rings located inside the combustion bomb (Figure 17). The debris attached to the disk was scraped from the disk by a dental pick into sealable plastic sacks.

Recording Equipment

All voltage and current data were recorded on either Dupont Mark 010 or Xerox Astroprint paper fed through either a CEC 5-124A or a CEC 5-123 recording oscillograph, respectively. Both type 342 and 351

magnetic recording galvanometers were used. A Mossley Model 2D-2 X-Y Plotter was used to record the differential voltage output from the Optron as a function of time. Figures 7 and 11 show some of these recording devices.

Automatic Controls

Equipment events at both the test-cell site and the atmospheric pressure site were automated. The functions automated were:

1. combustion bomb pressure increase/decrease
2. combustion bomb pressure vent
3. oscillograph start
4. X-Y Plotter start
5. camera on/off
6. ignition power on/off
7. high voltage on/off.

V RESULTS AND DISCUSSION

The majority of experiments were conducted using Propellants A and B. From Table III it is noted that Propellant A contains a double base (nitrocellulose and nitroglycerine) binder; hence, Propellant A represents a double base modified composite propellant. The binder is obviously energetic. The ammonium perchlorate oxidizer is of unimodal size. Propellant B is a representative composite propellant. The ammonium perchlorate is a trimodal blend. In both Propellants A and B, 200 atomized (15 micron) aluminum metal was added. Propellants AD and AM were considered variations of Propellant A, and Propellants BD and BO were considered variations of Propellant B. Hereafter, these propellants are termed variation propellants. However, ultimate comparisons were made between Propellants A and B.

Experimental preliminaries are placed in Appendix G. These preliminaries served to establish nitrogen conditions, record local electrostatic potentials for nonburning propellant, and attend to apparatus details.

Burning Rate Device Experiments

The experimental setup to compare burning rate devices was simple. Samples of either Propellant A or B were mounted onto the nitrogen chamber set to inhibit side burning at one inlet line pressure, or mean side flow velocity (Appendix G). The combustion pressure was one local atmosphere. Tests were conducted using each propellant to

obtain a burning rate measurement with either the photodiode arrangement, a camera, or the Optron. A like number of tests were conducted on each formulation using each burning rate device. These results were compared with burning rate data obtained on Propellants A and B from a strand-burner, using timing wires. The samples used in the strand-burner were side inhibited using a tygon paint.

Table VI presents the results of these tests for Propellants A and B. From this table, it appears that either the camera or the Optron, used in the servo-tracking mode, provide repeatable burning rate data. The Optron was preferred to the camera from the viewpoint of data reduction but further verification of the precision of the Optron was necessary.

Experiments were conducted in the combustion bomb using Propellant A where, after ignition, the bomb pressure was either increased as fast as possible or decreased by venting the bomb. The Optron output should have been non-linear with time, and indeed, it was. Thus, the continuous tracking capability of the instrument was checked.

Additionally, experiments were conducted in the combustion bomb at a fixed pressure with the Optron viewing the sample through one Herculite window and the 16mm Bell and Howell camera viewing the sample through the other window. Measured burning rates agreed to the third decimal place for these experiments. Some Propellant A and B samples were also drilled through axially using a 40 mil diameter drill bit. After ignition, either a highly irregular burning rate or burning area resulted, or sometimes, the flame flashed down the 40 mil diameter hole. The time of Optron output shifts and the film time where irregularities started or stopped consistently agreed. Thus, the instantaneous monitoring feature of the Optron was confirmed.

Hence, the Optron appeared uniquely suitable for a continuous burning rate measurement and was selected as the primary burning rate measurement device. The camera was selected as an alternate for backup and confirmation purposes. Visual observations of the burning of individual propellant samples were also always made to assist in authenticating experimental data.

Ionization Experiments

Ionizable Impurities

Small weighed samples of Propellant A or B were burned in oxygen at one local atmosphere in a small calorimeter bomb. The residue remaining after the sample was burned was taken up into water and then aspirated into a Perkin-Elmer Model 303 Atomic Absorption Spectrophotometer to determine cesium, potassium, and sodium impurity levels for the computer input (Chapter II). Table VII displays these results. Propellant B contains over twice the amount by weight of ammonium perchlorate as Propellant A. Since ammonium perchlorate provides a major source of trace impurities, the greater range of impurity levels resulting for Propellant B seems reasonable. As noted earlier, average trace levels of impurities were used for computational purposes.

Gas-Phase Electron Density

Over 100 individual tests using Propellants A and B were conducted at a combustion pressure of one atmosphere to determine experimental values of charged species number densities. Electron number densities were of particular interest. The Langmuir probe used is

described in Chapter IV. Extensive development of measurement technique was required to obtain useful results.

Contamination of the tungsten probe when immersed in the hostile combustion environment presented a major problem. Combustion debris buildup on the probe effectively changed the probe area. Additionally, the debris continued to burn while attached to the probe resulting in severe thermionic emission from the probe. For suitable data, the probe also required preoxidization to eliminate non-linearities of probe current associated with changes in contact potential of the probe while immersed in the gas phase. Probe preoxidation was accomplished by momentarily immersing the probe in an acetylene-oxygen flame. Finally, the probe developed hair-line fissures after prolonged periods of immersion, affecting probe continuity. Even discounting these factors, computations using the Dushman thermionic emission equation indicated that emission currents would become an accountable factor at a probe surface temperature as low as 1750°K (52), a temperature well below the theoretical combustion temperature (Figure 39 or 40). Thus, probe cooling was also necessary.

To eliminate the debris buildup, shorten probe immersion times, and provide probe cooling, a scheme was devised where the probe was rapidly traversed through the propellant flame, cooled in the nitrogen side flow, and then returned back through the flame. Several passes could be made on each propellant sample, thereby increasing the data gathered. Even with this approach, resulting in immersion times of the order of 30 msec, some emission current spikes were still recorded. Thus, the conventional probe technique of sweeping the probe voltage and recording corresponding current appeared questionable. It was

decided to preset a probe voltage and record probe current and probe voltage as functions of time and then discount emission current surges. This technique proved satisfactory and yielded at least representative data. Slight debris buildup still persisted, however, when the probe was immersed in the gas phase of Propellant A. Absolute probe cleanliness was virtually impossible.

Figures 18 and 19 display the probe currents measured versus preset probe voltage for Propellants B and A, respectively. The scatter of data about the arithmetic mean is also shown in these figures. Approximately 200 data points are incorporated in the scatter bands. Interpretation of these figures for the purpose of determining electron number densities involved the following consideration.

With the probe voltage negative with respect to the remote electrode, negative species should be repelled from the probe and positive species attracted to the probe. Ultimately, the probe current should saturate reflecting the magnitude of the number density of positively charged ions. With the probe voltage positive, negatively charged species should migrate to the probe. The two positive voltage current plateaus shown in Figures 18 and 19 imply that two different negative species coexist in the gas phase. One of these species collects at a lower voltage than the other species. Based on mobility considerations, electrons require a smaller driving force mechanism (field strength) to drift to a probe than negative ions. Thus, the first current saturation plateau with the probe voltage positive was assumed to be due entirely to electrons and the second plateau due entirely to other much less mobile negative species. The plasma potential ϕ_p was taken, by convention, to be the electron saturation potential.

The number density of electrons η_e was calculated using the following expression, applicable to an infinite cylindrical probe (Appendix E):

$$\eta_e = \eta_{e)_r} \left[1 + \frac{\frac{3}{4} d_p}{2\lambda_e} \ln\left(\frac{\ell_p}{\frac{d_p}{2} + \lambda_e} \right) \right] \qquad (11)$$

The factor $\eta_{e)_r}$ is given by

$$\eta_{e)_r} = \frac{2.5}{e} \sqrt{\frac{m_e}{kT_e}} \frac{I_e}{A_p} \qquad (12)$$

In Equations (11) and (12), ℓ_p is the effective probe length (taken to be the length of probe scarred by the gas phase), d_p the probe diameter, A_p the probe area, and λ_e , m_e , T_e , and I_e , the mean free path, mass, temperature, and current of the electrons, respectively. The determination of other parameters necessary to perform computations using Equation (11) follows.

From Equation (12), it is seen that the electron temperature must be known. Assuming for the moment a collisionless gas, for electrons satisfying a Maxwellian distribution, the electron current density at the probe surface J_s is related to the electron random thermal current density J_r by

$$J_s = J_r e^{-\frac{e\phi}{kT_e}} \qquad (13)$$

The notation ϕ represents the difference between the probe potential and the plasma potential. Ideally, Equation (13) applies in the region of the current-voltage characteristic plot bounded by positive ion saturation and electron saturation. Logarithmic differentiation of Equation (13) with respect to ϕ yields a simple expression relating the electron temperature to the slope of a logarithm of current density versus potential plot. Electron temperatures determined in this manner, using the mean data from Figures 18 and 19, were well over an order of magnitude higher than the computer predicted combustion temperatures.

It was difficult to reason that the indicated electron temperature could be so significantly different from the combustion temperature, particularly in view of the low voltages used and the high density of the gas phase. However, it was also known that:

1. even slight probe contamination produces a first order influence on electron temperature deduced from Langmuir probe data (50)

2. in continuum regime plasmas (where collisional phenomena cannot be ignored), the current-voltage slope flattens with increasing pressures, effectively distorting a deduced electron temperature (51).

Thus, the ideally deduced value of electron temperature was considered totally unreliable. It became necessary to select an electron temperature. The electron temperature was assumed to be the combustion temperature as predicted by the computer, corrected for combustion efficiency (later section).

An electron mean free path of 4×10^{-5} cm was estimated using the Sutherland approximation to correct for temperature. The formula given in Reference 38 was used. The electron current was obtained by subtracting the measured positive ion saturation current from the measured electron saturation current since the probe collects total current.

Using all of the above in Equation (11), experimental electron number densities deduced for Propellants A and B, respectively, were

$$\eta_e)_A = 1.6 \times 10^{11} \frac{\text{electrons}}{\text{cm}^3}$$

and

$$\eta_e)_B = 2.3 \times 10^{12} \frac{\text{electrons}}{\text{cm}^3}$$

Figures 20 and 21 show computer predicted electron densities versus combustion pressure with combustion efficiency (Chapter II) as a parameter. The above experimental values are also placed on these figures. As will be seen (later section), both Propellants A and B seem to undergo combustion at one local atmosphere near the $60/Al_T$ point. Thus, excellent experimental and computer agreement is seen for Propellant B using this information. For Propellant A, it is necessary to consider the experimental technique further (although experimental

number density accuracy to within an order of magnitude using a Langmuir probe has been considered adequate in some cases).

As previously remarked, slight debris buildup persisted when the probe traversed through the gas phase of Propellant A. Due to the short term duration of the probe in the gas phase and the quenching action of the nitrogen side flow, this debris consisted largely of unburned aluminum metal (later section). Referring to Figure 20 then, a lower electron number density could be anticipated using the probe. Probe contamination probably produces a first order effect on electron number density. In Reference 50, the contamination effect on number density was considered to be a second order term.

Computations by Turner (52), using Figures 18 and 19, essentially corroborated computer predictions for number densities of ions. For those calculations, the ionic temperatures used were the computer predicted combustion temperatures whereas ionic mean free path lengths were taken from computations that agreed with experimental air-propane flame data (4). Turner also selected an electron mean free path approximately an order of magnitude greater than used herein, again using computations that corroborated air-propane flame data. For halogenated hydrocarbon flames, of course, electron attachment effectively reduces the electron mean free path.

A final comment is important regarding the area ratio of the remote electrode to probe. For probe operation according to probe theory, it is necessary that the remote electrode never operate near saturation current. This insures that there is no voltage drop between the gas phase and remote electrode, thereby referring probe voltages actually to the gas phase rather than merely the remote electrode. To

insure further that the probe saturates without saturation at the remote electrode, the remote electrode area must be large compared to the probe area. Based on random thermal current density considerations, this area ratio is related to the square root of the mass ratio of ionic species. Conservatively, for the formulations used, an area ratio of the remote electrode to the probe should be greater than 250. However, a value of 100 was the practical limit since a finer mesh remote electrode screen was burned through and a thinner diameter probe was consumed when immersed in the gas phase.

Gas-Phase Electrical Conductivity

The DC electrical conductivity of the gas phase of Propellant A, AD, and B was measured using the twin probe scheme described previously (Chapter IV). The combustion pressure was one local atmosphere. A voltage of 20 VDC was impressed across the probes located at the edges of the combustion zone and the currents drawn and the applied voltage measured as functions of time. Again, slight combustion debris attached to the tungsten wires when Propellant A (or AD) was used.

The DC electrical conductivity of the gas phase σ_g was computed from Ohm's law ($J = \sigma_g E$), where $E = \frac{\phi_a}{h}$ and $J = \frac{I_m}{A_c}$:

$$\sigma_g = \frac{h I_m}{A_c \phi_a} \tag{14}$$

In Equation (14), h is the distance between electrodes (taken to be the propellant width), I_m the measured current, ϕ_a the impressed

voltage, and A_c the area over which currents flow (taken to be one-half the circumference of the cylindrical probe times the propellant width).

Table VIII presents the values of DC electrical conductivity determined from the defining formula. From Table VIII, it is noted that there was no measurable difference in conductivity between Propellant A and doped Propellant A (AD) which corroborates the statement in Chapter II that trace impurities adequately account for gas-phase ionization levels.

Table VIII also contains DC electrical conductivities computed using Langmuir probe determined electron number densities and computer predicted electron number densities. The following expression, developed in Appendix E, was used for these latter calculations

$$\sigma_g = \frac{e^2 \eta_e \lambda_e}{\sqrt{2.55 k m_e T_e}} \tag{15}$$

The electron temperature used in Equation (15) was taken again to be the computer predicted combustion temperature corrected for combustion efficiency. An electron mean free path of 4×10^{-5} cm was used. Comparing experimental values of the electrical conductivity with the value obtained using computer data for Propellant A illustrates again the effect of slight combustion debris on measured current (passed or collected).

It is noted from the range of electrical conductivity values given in Table VIII that the gas phase represents a weakly ionized gas.

The same conclusion follows immediately from a summation of computer predicted mole fractions of ionic species.

Summary (Ionization Experiments)

The results of this experimental segment led to a number of important statements concerning the propellant flames used. These statements relate mainly to the influence that high voltages might be expected to exert on the combustion process.

1. Based upon an acceptable correlation of electron number densities between computer predicted values and experimentally deduces values, it appears that the mechanism of thermal ionization (or equilibrium ionization) adequately accounts for the source of flame electrons. It also appears reasonable to assume that the electrons are in the state of equilibrium (or near equilibrium) with the rest of the gas phase. Under field strengths applied herein (later section), these conditions should not be appreciably disturbed.

2. It appears that the gas phase contains an appreciable amount of negative ions besides electrons. This should be the case for the formulations used. As previously noted, the computer predicts that this ion is a chlorine ion. The density of negative ions seems to balance the density of positive ions which would tend to counterbalance any net electric field influence involving the heavy ions. However, dissociative electron attachment to create negative ions reduces the free electron number density, possibly hampering the effectiveness of a given electric field.

3. Based on the agreement of the experimental measurement of the gas-phase electrical conductivity with calculated values (considering only electrons), an externally applied electric field would be expected to affect only electrons. The motion of other charged species is completely negligible. Again, evidently the electrons can also be treated in thermal equilibrium with the rest of the gas phase. However, the gas phase is clearly collectively molecular thereby probably restricting the effectiveness of impressed voltage.

Electric Parameters Experiments

Electrical Arrangements Selection

Appendix G contains a summary discussion of nonburning equipotential plots for the six electrode geometries of Figure 9. The presence of conducting gases was, of course, not considered there. Here, experiments were conducted generally at a combustion pressure of one local atmosphere using Propellants A, AD, AM, and B and, variously, each of the six electrode geometries. Either the regulated current or the unregulated current high voltage supply was used. The supplied voltage settings were either 5KV, 15KV or 50KV. The polarity of electrodes was also a variable. For the regulated current supply unit, current controls were set at either 0% or 100%. At 100% current control, the currents drawn through the high voltage under load system would be allowed to rise without built-in restrictions of the power unit. Time histories of currents, applied voltage, and the high voltage rake voltages (next section) were recorded. The burning rate was measured with the Optron.

As noted in Chapter III, the main objective of these experiments was to screen the various electrical arrangements. The findings from the experiments are narrated below. However, discussion of the high voltage rake results is placed in the next section. In the following, current will be variously referred to as avalanche, breakdown, random, or steady current. Avalanche current here means high magnitude transient arcing current. Breakdown current means continual current, accompanied by visual, fairly steady, arcing. Random current is taken to mean low magnitude transient current. Steady current means constant magnitude current that is independent of time.

Electrode Geometry I. It is noted that this configuration does not present a completed electrical circuit. Hence, no currents were drawn through the system and applied voltages were, accordingly, held constant. The only plausible mechanism that might have been involved here was the possibility of charge repulsion or attraction between the charged propellant and charged gas-phase matter. The influence of this mechanism, if present, was not measurable. Applied voltages had no measurable effect upon the burning rate. A few experiments using this geometry were also conducted at combustion pressures of nearly 10 atmospheres with the same negative result. This geometry was abandoned.

Electrode Geometry II. The electrical circuit for this geometry involves the propellant as a resistor and electrode, the gas phase as a conducting media, and the resistive gap between the gas phase and the copper ring. Time varying currents were drawn through the system; hence, the applied voltage also varied with time. The time variation

and magnitude of recorded currents depended upon the propellant, high voltage supply, and applied voltage.

For Propellants A and AD, using the unregulated current high voltage supply with a negative voltage of 5 or 15KV applied to the propellant, random currents were drawn. Current magnitudes ranged to 5 mA over durations of, typically, 80 msec. Occasional avalanche currents also resulted with magnitudes of up to 60 mA over perhaps 40 msec time intervals. The current path was determined to be through the propellant bulk but obviously was not always uniformly spread across the propellant cross-section. If the random currents ever steadied to average values of from 3-5 mA for prolonged periods of time (1 to 2 seconds), the nonburning propellant would usually darken and then pre-ignite along a preferential current path. Currents like this were, fortunately, extremely rare using the unregulated current unit for this propellant. A correlation of Optron output with current indicated that during random current intervals measurable burning rate reductions resulted. Figure 22 illustrates a typical time correlated plot of recorded current, applied voltage, and Optron output for Propellant A. The combustion pressure was approximately 2.5 atmospheres. Using the regulated current high voltage unit with any of the three voltage levels applied always resulted in steady currents drawn through the system with the higher current magnitudes corresponding to the higher applied voltages. At 50KV the propellant would always pre-ignite along a preferred current path, thereby altering the burning area. A large current surge was recorded at almost the instant the voltage was applied for this case. Changing polarity with the regulated current unit at the higher voltage settings only affected the area in the solid propellant

where pre-ignition occurred. For instance, with +15KV applied to the copper ring before the propellant regressed past the ring, steady electron currents drawn from the flame to the ring passed through the nonburning propellant, igniting the propellant if time allowed.

Propellant AM, being a heterogeneous metal mesh and propellant combination, reacted erratically when high voltages were impressed. Repetitive arcing occurred between metal mesh fibers. High frequency noisy buzzing was audible. Recorded currents were alternating in nature with frequencies of 140-180 Hz with a fairly steady root-mean-square value of, typically, 2.5 mA. The power unit was being shorted. Numerous pre-ignition sites along the sample surfaces were observed after the voltage was impressed.

For Propellant B, using the unregulated current unit set at 15KV, repetitive breakdown currents resulted sometime after the high voltage was impressed. At the low voltage setting, breakdown rarely occurred. Again, at 50KV pre-ignition resulted, changing the burning area. At 15KV, recorded currents were alternating in nature with frequencies of 110-200 Hz with a fairly steady root-mean-square value of, typically, 4 mA. Avalanche currents peaked at 100 mA. The unregulated power unit was virtually shorted. Buzzing was audible. Visual breakdown current paths were observed to pass partly around the propellant and seemed to re-enter the propellant slightly below the burning surface (often accompanied by localized rounding of the burning surface). Figure 23 shows a representative time plot of recorded current, applied voltage, and Optron output for Propellant B. The data included in this figure were for a combustion pressure of approximately 10 atmospheres. The similarity between current and voltage traces shown in

this figure and those published by Stones (45) is noted (here, of course, sensitive galvanometers were used). Burning rate increases were noted under 15kV conditions for this propellant. These increases appeared to be due to breakdown currents heating the solid phase near the burning surface.

Electrode Geometry III. The electrical circuit for this configuration eliminates the resistive gap of the previous geometry. For Propellants A, AD, and B, using either high voltage supply with an applied voltage of 15KV, continual currents were always drawn through the system. For Propellant A, and AD, steady current was passed. For Propellant B, visual breakdown currents again resulted. The unregulated current high voltage unit was basically shorted. Again, solid-phase current heating seemed to be involved. Only burning rate increases were measured. These increases were most notable for Propellant B.

Electrode Geometry IV. In this configuration the propellant represents part of the media between the ring electrodes. With 15KV impressed across the rings, wild irregular arcing occurred from one ring through the gas phase to the other ring. At the lower impressed voltage (5KV), the repetitiveness of arcing subsided. Avalanche currents recorded with 15KV applied peaked at about 250 mA. The applied voltages had no measurable influence upon the burning rate. This result seems consistent with the result reported by Silla ( ). However, no flame deflections nor local flame extinctions were visually observed here. This geometry served no further use.

Electrode Geometry V. This configuration provides the best opportunity of all geometries used for ionic winds, if existant, to influence the burning process (19,20,26). Again, with impressed voltages, wild arcs passed from one plate electrode through the gas phase to the other plate. Applied voltages had no measurable influence upon the burning rate. No flame deflections nor distortions were observed. Ionic winds were evidently completely ineffective here. This geometry served no further use.

Electrode Geometry VI. This electrode arrangement was fashioned in order to attempt to route drawn currents harmlessly through the system and to avoid the resistive nature of the propellant. To the gas phase, the wire electrode passing through the propellant represents a highly stressed (point) electrode. Operationally, however, no way was successfully devised to prevent the wire from dissipating heat conducted from the gas phase to the nonburning propellant. Thus, the burning surface was often crown shaped. At combustion pressures higher than atmospheric pressure, this crown was quite pronounced. Repetitive arcing occurred from the wire electrode to the ring. Avalanche current magnitudes of up to 300 mA, lasting perhaps 40 msec, were recorded. Measured burning rates were not repeatable even under no-voltage conditions. The crowning effect noted was considered the cause of these burning irregularities. Thus, this electrode geometry was eliminated.

Based on the results of these screening experiments, only electrode geometries II and III seem promising. Electrode geometry III results in continual currents always being drawn through the system with solid-phase current heating indicated as the cause of burning rate increases

under high voltage conditions. Electrode geometry II appears the most interesting. Both burning rate increases and decreases seem to result under properly applied voltages using different propellants. Therefore, electrode geometry II was selected for further investigation. Apparently the nitrogen resistive gap between the ionized gas phase and electrode ring effectively retards all but vicious breakdown currents.

Electric Field Strength

The high voltage rake, described in Chapter IV, was positioned to measure regional field strengths resulting from applied voltages for the various electrical arrangements. On occasion, the rake clearly interferred with the system being measured. On the other occasions, no visible interference was noted. Nonetheless, the field strengths reported here must be viewed with reservation.

For electrode geometries IV and V, the rake could not be used at all since arcs from one electrode invariably passed along the rake tips enroute to the other electrode. For the other geometries when rakes were positioned along the nonburning propellant, currents evidently localized and, as indicated, interfered on occasion causing ignition sites about the tungsten tips of the rakes. However, for electrode geometry II, on those occasions where the rakes did not seem to cause current interference, the reduction of rake data indicated that:

1. Propellant A essentially represents an equipotential body while Propellant B represents a buffer resistor dropping the entire applied voltage in the solid phase (prior to breakdown)

2. for Propellant A, a maximum gas-phase region field strength of about 0.3KV/cm exists.

The solid-phase results are consistent with nonburning findings placed in Appendix G. The gas-phase results for Propellant A indicate that the apparent gas-phase field strength is much lower than the applied field strength (discussed below) with a large voltage drop necessarily occurring then either in the resistive gap or well downstream from the burning surface. A rake placed approximately 4 inches from the burning surface verified that large voltage drops occur in the region where combustion species are undergoing quenching action (ionic winds may be effective there but this is of no concern to burning rate).

The applied field strength for electrode geometry II and Propellant A was computed from applied voltage versus time records and average burning rate data, allowing a time related computation of electrode spacing. The applied field strength deduced in this manner, discounting the region where the propellant was within 1/4 inch of the electrode, ranged from 4KV/cm to 14KV/cm. This field strength was assumed to be one-dimensional, in a direction parallel to the direction of regression. This seemed to be reasonable based on experimental preliminaries (Appendix G).

The range of applied field strength given above pertains to all combustion pressures checked. In fact, over the combustion pressure range where the rake was used (1 - 10 atm), neither the applied nor resulting field strengths were found sensitive to combustion pressure. Admittedly, however, rake experimental results must be taken cautiously.

Solid-Phase Measurements

The solid-phase bulk DC electrical conductivity of Propellants A, AD, B, and BD was measured using the solid-phase apparatus mentioned in Chapter IV (imbedded wires). Additionally, the propellant sample temperature was elevated by placing the samples in a curing oven. Bulk resistances were then taken as a function of oven temperature for each of the numerous samples of each propellant. Approximately 1/2 hour was allowed for the samples to reach the indicated oven temperature. Samples were never manually disturbed to ensure that contact resistances were constant.

Figure 24 displays typical results of these tests. The electrical conductivity was computed from the defining formula given previously [Equation (14)], where resistance replaced voltage and current in accord with Ohms law. From Figure 24 it is seen that:

1. the presence of ionizable salts produce no effect upon the solid-phase DC electrical conductivity

2. the extremely resistive propellant at standard temperature becomes significantly less resistive at even modest temperatures.

The second statement suggests that significant solid-phase current concentrations should exist for Propellant B (or BD) in the solid-phase subsurface heating zone (the zone beneath the solid-gas interface heated by the gas phase) when high voltages are impressed across this burning propellant. This most logically explains the observation

given earlier that breakdown currents bypassing this propellant seemed to re-enter the propellant slightly below the burning surface.

An additional experiment was conducted to provide some understanding of the detailed role which currents play while passing through the propellant bulk. The experimental apparatus shown in Figure 16 was used for this purpose. Propellant samples were sandwiched between the copper electrodes shown so as to provide the contact resistance necessary to yield the same DC electrical conductivity at 21°C as was obtained using imbedded wires. Thus, a reference was established. Known currents were then passed through the copper bar-propellant system for specified time intervals and the resistance between the electrodes then measured with the megohmmeter. Later, the same samples were placed in the curing oven and the propellant resistance recorded against the oven temperature.

Correlating these results for Propellant A yields Figure 25. Regretably, this same experiment for Propellant B was not possible since, as previously noted, currents largely bypassed this propellant. Samples of Propellant B also tended to ignite when visual currents broke around the sample. Figure 25 also shows time intervals corresponding to burning times available for continual current passage at various combustion pressures. From Figure 25 the heating effect of continual and, presumably, uniform currents upon propellant bulk is seen. However, the applicability of this simulated experiment to the burning situation with impressed voltages for Propellant A must be questioned since continual currents were extremely rare (for electrode geometry II). Figure 25 is presented to illustrate that small currents

can indeed heat propellant. If this current is concentrated, the heating effect is localized and intensified (later section).

Summary (Electric Parameters Experiments)

The findings of this experimental segment indicate that electrical arrangements are very important in the realization of high voltage effects on burning propellant. The electrode geometry, type of high voltage supply, nature of resulting currents, and the resistance features of the system all seem contendable factors. Additionally, the following can be stated.

1. For electrode arrangements where the propellant represents part of the media between electrodes, only wild arcing results from the presence of ionized gas. No unusual flame phenomena occurs, a condition understood from knowledge of the makeup of the propellant flames used.

2. When the propellant is utilized as an electrode, it is circumstantially conclusive that electric currents involving the solid phase represent the accountable factor. Without proper arrangements preheating or pre-ignition of the non-burning propellant seems to overwhelm all else. Currents drawn by the ionized gas phase can pass through the unburned solid or breakdown partially around the unburned solid. Propellants exhibiting conditions for concentrations of current should enhance the effectiveness of solid-phase current preheating.

3. For electrical arrangements where the propellant still serves as an electrode but where solid-phase currents seem ineffectual, burning rate decreases result. Yet the electric field strength seems small near the propellant electrode.

Regarding the last statement, it is possible that both the plasma characteristics of the gas phase and thermionic emission from the propellant electrode act to retard the apparent gas-phase field strength. It is known that a plasma can self-generate secondary electric fields counterbalancing external electric fields (7,38,43) and that thermionic emission from an electrode can negate the conventional electrode voltage drop (5,24).

Electric Effects Experiments

Experiments were conducted to investigate the precise magnitude and nature of burning rate changes observed under voltage conditions. As noted earlier, electrode geometry II was selected. Additionally, the unregulated current high voltage supply was used. Applied voltage settings were either 5KV or 15KV negative to the propellant. Both Propellants A and B were used. Variation propellants, like Propellant AM or BO, were also used on occasion.

The status of understanding at this stage was that:

1. an electric field imposed on the gas phase of the propellants used affects electrons and electron encounters might be important to the combustion process (Chapters II, V)

2. an electric field imposed upon the gas phase probably affects basic properties of the gas phase; however, many properties could be involved (Chapter II)

3. electric currents involving the solid phase simply explain burning rate increases, real or "apparent" (Chapters II, V).

Combustion Pressure Influence

Approximately 125 systematic tests were performed where the burning rate of the propellant sample was measured as a function of combustion pressure (bomb pressure plus ignition pressure surge), using the Optron. The parameter was the high voltage. Currents and voltages were recorded as a function of time. Voltage application was most often arranged so that both no-voltage and voltage burning situations occurred for the same sample. The continuous burning rate measurement from the Optron allowed both voltage and no-voltage burning rates (recall Figures 22 and 23). Possible burning rate variations from sample to sample were eliminated by using this technique.

Current and voltage traces recorded for Propellants A and B were found to be essentially independent of combustion pressure. Again, for Propellant A, largely random currents were drawn at either voltage setting. For Propellant B, breakdown currents largely resulted with 15KV applied but rarely occurred with 5KV applied.

Figures 26 and 27 display the results of burning rate experiments for Propellants A and B, respectively. Approximately 150 data points are given. From these figures, the precise effect of an applied voltage on burning rate is seen. The actual percentage of change induced by applying high voltage is noted to be relatively small in either case.

However, no attempt was made to seek the maximum change. Comparing Figures 26 and 27, it appears that:

1. burning rate increases for Propellant B are independent of combustion pressure but dependent on applied voltage

2. burning rate decreases for Propellant A are independent of applied voltage but dependent on combustion pressure; as the combustion pressure increases, the burning rate changes induced under voltage conditions decrease.

It is worth noting that the first comment above is consistent with electrical energy solely influencing the burning rate since the ability of the system to conduct current, as measured by the DC electrical conductivity of the gas phase, is only weakly dependent on pressure (38,). The second comment seems consistent with the suggested importance of electron encounters upon the burning process. It is further noted from Figure 26 that at high combustion pressures, where diffusional mechanisms probably completely dominate the burning process, the effect of impressed voltage is not measurable.

Camera Data

The Hycam camera (Chapter IV) was set to film Propellant A undergoing combustion at about 6 atmospheres. Resolution to 100 microns was desired and obtained. No-voltage tests were filmed and then correlated with test runs where 15KV was applied at a preset time from ignition (also yielding no-voltage data for the time interval before voltage was applied).

Film reduction revealed nothing of comparative interest. There was no observed difference in the appearance of the burning surface with an imposed voltage. The apparent size of aluminum agglomerates and the time from agglomeration formation until the agglomerate left the burning surface were determined to be unchanged by the voltage. Also, 1000 agglomerates were tracked in the gas phase. Careful data reduction resulted in assumed unidimensional speed distributions for these particles. One speed distribution was supposed to apply to particles entrained in the gas phase with no-voltage. The other distribution involved the agglomerates in motion under high voltage. It was ultimately concluded that the agglomerates all belonged to the same population and the supposed conditional difference of voltage was nonexistant. Thus, the remark made by Watermeier (26,53), that aluminum particulate matter would be very likely strongly repelled from or attracted to the burning surface were the surface an electrode, seems to be conjecture (in Chapter II, this potential effect was stated somewhat more specifically).

Observation of the Bell and Howell camera film, where ASA 125 color film was used without auxiliary lighting, left the impression of a qualitative reduction in the overall gas-phase luminosity for Propellant A with imposed voltage. This reduction, if real, was not noticed with the naked eye. Burning rate changes, however, were corroborated for both Propellants A and B by film analysis of both ASA 125 and 160 color film.

Combustion Residue Analysis

Solid residuals from combustion were gathered for Propellants A and B as a function of combustion pressure. The parameter again was

applied voltage (either no-voltage or 15KV). Residue disks, described in Chapter IV, were used to capture the debris. Collection was from ignition until burnout. Typically, two samples were consumed to obtain a sufficient quantity of matter for accurate analysis at a given condition. Approximately 40 samples of residue were gathered.

Quantitative analysis of the residue was performed in the following sequence.

1. Carbon, hydrogen, and nitrogen quantities were determined by burning a weighed amount of residue sample in a Perkin-Elmer Model 240 Elemental Analyzer.

2. Metallic (unburned) aluminum quantities were determined by reacting a weighed amount of residue sample with 25% sodium hydroxide to evolve hydrogen gas. That amount of hydrogen was compared with the amount liberated from the reaction of a known quantity of aluminum foil with 25% sodium hydroxide. Corrections were made for the hydrogen found in the first step above and also for variations of standard conditions.

Residue samples were also subjected to X-ray diffraction checks to qualitatively verify that the balance of matter was aluminum oxide (Al_2O_3). Nothing else was observed; thus, the balance of residue was assumed to be aluminum oxide. Accuracy of the first quantitative step above was considered to be $\pm$ 1% of determined values and was assessed at $\pm$ 2% of determined values for the second step. If X-ray diffraction checks were totally correct, the overall experimental error can be reasonably put at this latter value.

Figures 28 and 29 illustrate the results of aluminum analysis for Propellants A and B, respectively. A linear least-squares fit is shown for no-voltage data. From these figures, the following is noted.

1. For Propellant A with no voltage, the ratio of aluminum oxide to metallic aluminum increases with combustion pressure. Based on the combustion efficiency considerations of Chapter II, then, as the combustion pressure increases, the apparent combustion efficiency increases (Figure 30).

2. For Propellant A with an imposed voltage of 15KV, combustion seems to be significantly less efficient than without voltage at modest combustion pressures. This voltage effect diminishes as the combustion pressure increases.

3. For Propellant B with or without voltage, the ratio of aluminum oxide to metallic aluminum is independent of combustion pressure (over the range of pressures tested). Impressed voltage produces no effect on the apparent combustion efficiency of Propellant B.

It is noted that voltage-results are probably conservative since residue gathered for voltage conditions included the residuals for the portion of the burning interval before voltage was applied. Again, the high voltage supply unit was sequenced on, at a preset time from ignition.

The relationship between the ratio of aluminum oxide to metallic aluminum and combustion efficiency has been previously given (Figure 30). As also noted, this figure applies to all combustion pressures for both

Propellants A and B. That is, the computer predicted ratio of aluminum oxide to metallic aluminum product is independent of combustion pressure (Chapter II). From Figures 28 and 29, it is seen that this pressure independence is experimentally confirmed for Propellant B, in apparent agreement with the findings of Reference 29. For Propellant A, this prediction can be only approximately verified. Translating experimental findings at no-voltage from Figures 28 and 29 to Figure 30, it is seen that combustion of samples of Propellant B occurs near the $60/Al_r$ point and, for Propellant A, over a band centered near $60/Al_r$. Under voltage conditions for Propellant A, the band of combustion efficiency is wider. Combustion inhibition seems clear under applied voltage for Propellant A.

The results from the elemental analyzer involving carbon residue revealed nothing of comparative interest. Nearly 99% by weight of the residue apparently involves aluminum. Carbon constitutes, at most, one-half of 1% by weight of the residue. Any high voltage effect on carbon, if present, may have been masked in this small percentage. However, the debris "coat" reported by Stones (45) with applied voltage was not observed. The small amount of carbon found did suggest that nonreative carbon (Chapter II) could be neglected.

Chemical analysis was also performed on combustion debris collected from the Langmuir probe after repetitive traversals through the gas phase of Propellant A. The percent by weight of metallic aluminum in this debris was found to range from 87 to 92%. Again, the carbon content in the debris was negligible.

Exhaust Emissions Data

Combustion exhaust gas specimens from approximately 25 samples of Propellants A, AM, B and BO were captured. The apparatus used has been

described previously (Chapter IV). Again, either 15KV or no-voltage conditions were contrasted. The sample collection time was kept constant for voltage conditions and was changed only to compensate for the time intervals available at the various combustion pressures. Sampling techniques used had been previously developed (40).

The trapped specimens were analyzed both quantitatively and qualitatively under local standard conditions. Quantitative analysis was performed using a gas chromatograph to obtain CO and CO_2 concentrations. Standards for CO and CO_2 were run before each gas specimen was analyzed. Quantitative infrared analysis for CO and CO_2 concentrations was also conducted. An infrared spectrum, covering a wavelength band of 2.5 microns to approximately 18 microns, was obtained at least once for each specimen. Practices recommended in Reference 18 were used.

Infrared deduced CO and CO_2 concentrations were obtained from working curves prepared for these species where percent transmittance was plotted against partial pressure, or concentration, for a total pressure of one local atmosphere. The analytical wavenumbers chosen for CO and CO_2 were 2170 cm^{-1} and 3720 cm^{-1}, respectively. Water band interference near the CO_2 analytical wavenumber was compensated for, to the extent possible, by using "wet" CO_2 to prepare the CO_2 working curve.

Experimental results from both the gas chromatograph and infrared analyses are given in Figures 31 and 32 for Propellant A (and AM), and Propellant B (and BO), respectively. Both voltage and no-voltage results are included in these figures. Also illustrated in these figures are the computer predicted combustion ratios of CO to CO_2 product concentration for Propellants A and B, respectively, at the various levels of combustion efficiency (Chapter II). However, as indicated in Chapter II, experimental conditions and computer conditions are not the same.

Experimental results include the effect of inhibiting and pressurizing gas dilution on exhaust products (Appendix G) as well as expansion effects involving the straight-through exhaust valve. There was also a vast difference between the combustion temperature where combustion products formed and the temperature at which exhaust analysis took place. Hence, results here are only comparative with respect to voltage conditions.

Nonetheless, experimental exhaust findings placed in Figures 31 and 32 essentially corroborate the computer predicted trend that the ratio of CO to CO_2 concentrations at combustion conditions is independent of combustion pressure. However, an imposed voltage does not seem to have any discernible effect on this ratio.

It is worth noting that gas chromatograph results and infrared results presented in Figures 31 and 32 appear discordant. Actually, gas chromatograph results include a systematic experimental error. It was found that samples of exhaust specimens injected into the chromatograph columns were being blocked by combustion debris. This was rectified for concluding experiments by employing a larger molecular seive size in the columns. However, repeating the other experiments using the larger molecular seive size was not considered worthwhile in view of the negative result under voltage conditions (obtained from infrared data).

A qualitative comparison of the infrared spectra obtained from each gas specimen revealed some interesting features. Of course, only certain species (those exhibiting a change in dipole moment due to the absorption of incident radiation) could be detected and of those detected (CO, CO_2, CH_4, C_2H_2, C_2H_4, HCN, H_2O, HCl, NO_2, N_2O, NOCl, HNO_3),

only a few (the first six indicated) were found to be stable. The other species continued to undergo gas or wall reactions. Nonetheless, the overall infrared spectra revealed that:

1. each propellant yields a distinguishable infrared spectrum for exhaust conditions for the same combustion conditions (Figures 33,34,35 and 36)

2. the variation propellants (Propellants AM and BO) indicate stronger exhaust concentrations of hydrocarbon species (C_xH_y) than the basic propellants (Propellants A and B) (compare Figures 33 and 34, and Figures 35 and 36)

3. under impressed voltage, Propellant A indicates stronger exhaust concentrations of C_2H_2 and CH_4 than Propellant A without voltage (Figures 37 and 38)

4. voltage conditions do not alter Propellant B exhaust concentrations.

Taking the second and third qualitative findings above collectively, the third finding might be expected since combustion is apparently inhibited by impressed voltage for this propellant. Propellants AM and BO were observed to burn irregularly when contrasted with Propellants A and B at the same combustion pressure. Propellant AM burned irregularly due to erratic metal mesh combustion. Propellant BO liberated black soot and burned slowly compared to Propellant B. Clearly, the overall combustion efficiency associated with these variation propellants must be questioned. Thus, as stated earlier (Chapter II), gas-phase compositional changes might result from applied voltage. Here, exhaust

composition changes seem to result from retarded combustion. It might also be speculated that increased hydrocarbon exhaust products under voltage conditions imply that reactional mixing between the energetic hydrocarbon double base binder products and oxidizer products is affected. However, this would be a gross extrapolation. Detailed combustion zone spectroscopic studies would be required to verify this conjecture.

Combustion Temperature

Experiments to measure the combustion temperature were attempted. The optical apparatus and arrangements used were described previously (Chapter IV). For a propellant classed similar to those used, the gas phase seems to reasonably represent a grey target (11). Under the assumption that this is also the case here, two-color pyrometry results are at least fundamentally valid. However, the inadequacy of the experimental conditions became apparent soon after checkout experiments began. The following was found.

1. The combustion zone depth (as measured by the thickness of propellant samples) affected the indicated temperature. At low combustion pressures, a sample thickness of literally inches appeared necessary to obtain realistic indicated combustion temperatures.

2. The indicated combustion temperature fluctuated with time.

3. The Herculite glass window altered the indicated combustion temperature.

4. Any smoke or combustion debris that passed between the target and pyrometer sensing head also influenced the indicated combustion temperature.

Thus, only relative voltage and no-voltage comparative measurements were realized.

It was possible to determine the apparent effect of the glass intervening media at one combustion pressure. Experiments were conducted at a combustion pressure of one local atmposphere using a fixed thickness propellant sample with and without the Herculite glass placed between the sample and pyrometer. Additionally, the distance from the sample to the glass edge was varied. Under these conditions, the Herculite plate glass increased the indicated combustion temperature (taken at one time) by an amount, constant with distance, of approximately 100°K.

For remaining experiments, contrasting 15KV and no-voltage, a fixed thickness propellant sample was used. Indicated temperatures were taken at one time, the time as viewed through the pyrometer optical eyepiece when the propellant regressed to the bottom edge of the field-of-view circle (Chapter IV). The apparent effect of the Herculite glass was subtracted from each data point taken.

Indicated combustion temperatures, from approximately 65 samples of Propellant A or B burning at various pressures, with and without voltage, revealed nothing of comparative interest. For Propellant A under voltage conditions, some indicated temperatures were lower (at most, 150°K) than indicated without voltage. However, judging the overall experimental precision, it was concluded that impressed voltage produced no change to indicated combustion temperatures.

Evidently, the usual irregularity of combustion temperature associated with composite propellant flames can be expected to exceed 150°K (1,8).

Figures 39 and 40 present computer predicted combustion temperatures for Propellants A and B, respectively. Combustion efficiency again is the parameter. Imposed on these figures are experimental results translated from combustion residue analysis, using Figure 30. Thus, indirect temperature measurements confirm that impressed voltage has no extensive effect on combustion temperature.

Summary (Electric Effects Experiments)

The results of this final experimental segment lend additional insight into the mechanisms causing burning rate changes under applied voltages. The following statements can be made in this regard.

1. There is no evidence to suggest that there is any gas-phase mechanism contributing to measured burning rate increases. Solid-phase current interactions seem to be singularly involved.

2. Measured burning rate decreases clearly involve gas-phase phenomena. The high voltage effect on burning rate is combustion pressure sensitive, indicating reactional interference under voltage conditions. The combustion of metal ingredient was found to be reduced in extent by an applied voltage, indicating more inefficient combustion under voltage conditions. Also, exhaust products contain a greater amount of hydrocarbon species when combustion has taken place under high voltage conditions, which seems to

further indicate more inefficient combustion under applied voltage.

Based on the first statement above, it is noted that Equation (6) might now be used to correlate the effects of breakdown current heating on the solid phase. The findings of Figure 27 allow the computation of the elevated temperature T_p^* due to breakdown current, knowing the temperature sensitivity of burning rate. A value of π_r = 0.081%/°F has been reported for Propellant B ( ). However, the experimental determination of π_r involves temperature pre-conditioned propellant. Here, for Propellant B, the propellant was not uniformly preconditioned in bulk by current. As noted in previous sections, for this propellant current is apparently concentrated. Nonetheless, computations using Equation (6), with the π_r value noted above and data from Figure 27 (at 5 atmospheres), indicates an effectively localized solid-phase temperature increase of 130 - 300°C. This range of temperature increase may be realistic since, as noted earlier, experiments to assess current heating for this propellant failed partially because breakdown currents often caused ignition. Clearly, during those experiments, ignition temperatures were reached.

Some comments regarding the possible correlation of findings herein with other related work are worthwhile. Stones (45) used a propellant formulation approximately as resistive as Propellant B. Additionally, under applied voltage, the power unit used by Stones virtually shorted and breakdown currents peaked to the limit of the unit. Stones may have mistaken breakdown current effects for evidence of ionic wind effects. Certainly more voltage and no-voltage data as

a function of combustion pressure would have been desirable with emphasis on observing the nature of drawn currents.

Except in a gross sense, it is difficult to compare the work of Silla) with that herein. The disappearance of field induced burning rate reductions with increasing pressure seems compatible and understood on the basis of diffusional mechanisms controlling the burning rate at high pressure. Yet, relatively, a high pressure here was a low pressure there, except when air was used as the pressurizing gas. An air environment, of course, allows after-burning which might have been extensively affected by the transversely applied AC electric field.

Aberrant and Omitted Data

Calibration data and data resulting from development and checkout tests are generally not included herein. Data from test runs where known malfunctions occurred are also omitted. In this latter category are burning rate data from high voltage tests where currents knifed through the nonburning propellant to the extent that pre-ignition occurred along a preferred current path. These burning situations were termed "flash-downs".

Results from two other test runs are not included. Propellant A was involved in both cases and an applied voltage of 15KV was used in conjunction with electrode geometry II. During burning under voltage, the burning propellant sample extinguished (once, perhaps for a full second), then reignited to burn to completion. The electrical data gathered during these two test runs were not considered unusual. The Optron sensor lost "lock-on" the burning surface since the light-over-

dark target disappeared during the interval of extinguishment. These two tests were considered aberrant.

VI CONCLUSIONS

The goal of this research, as previously stated, was to provide information in order to assess the practical control of propellant burning rates by means of an externally applied electric field. The findings herein do provide data important to the disclosure of mechanisms responsible for voltage induced burning rate changes. The summary statements of Chapter V taken with the considerations of Chapter II complement the conclusions reached here. For the formulations and arrangements used, the following was concluded.

1. Either burning rate increases or decreases result from externally applied high voltage.

2. Ionic winds are not involved in burning rate changes. The composition of the gas phase precludes effective involvement of this mechanism associated with space charge.

3. Burning rate increases are due exclusively to currents affecting the solid phase. "Apparent" increases result from preferential path currents preigniting the nonburning propellant, changing the burning area. Continual current preheats the nonburning propellant and continual breakdown current in apparent concentration causes essentially real burning rate increases.

4. Burning rate decreases are realized in the absence of appreciable countereffect from electric current. These decreases are associated with flame electrons, very probably through electrically induced reactional interference involving electron encounters. Under voltage conditions, combustion efficiency is clearly impaired.

The above conclusions are not sufficient to lead to generalizations regarding the total effectiveness of applying high voltage across a burning propellant in, say, a small solid motor. Aside from problems that would be associated with incorporating electrical hardware into a solid motor (or gas generator), there are a number of fundamental differences regarding the combustion of small samples of propellant placed in a combustion bomb and grains of propellant loaded into a full-scale system. For instance, the propellant burning rate, combustion temperature, and overall combustion efficiency can all be vastly different for the two situations. Additionally, in the confines of a combustion chamber where the propellant volume approximates the chamber volume, a burning rate change induced by applied voltage might result in the onset of a cascading burning rate. That is, a sustained burning rate decrease, say, might result in a decreased chamber pressure causing a further decrease in the burning rate, and so on. Thus, many practical details associated with high voltage impressed upon a full-scale system require additional consideration. These factors were not studied here.

However, the experience gained during the investigation does authorize considered opinion in regard to the attempted use of this technique on a full-scale system at conventional operating pressures. That is, that largely uncontrolled rapid propellant consumption would result, for electrode geometries where the propellant served as an electrode, since the high voltage power unit would short, delivering the highest possible current. Wild arcing would result for electrode geometries where the propellant acted as part of the media between electrodes. The use of this candidate method to exercise command control of burning propellant remains to be demonstrated.

In retrospect, it is worth emphasizing that several useful experimental techniques and instruments were developed for use during the study. Noteworthy in this regard are:

1. the development of the Optron to provide reliable, accurate, and continuous measurements of propellant burning rates

2. the development of a Langmuir probe technique to provide comparative measurements of ionic species resulting from combustion of metallized propellants

3. the development of a simple, accurate method of assessing combustion efficiency by chemical analysis of recovered combustion residue.

The last two developments required the use of a modified thermochemical equilibrium computer program. The application of any of the above to other combustion research is certainly worth serious consideration.

BIBLIOGRAPHY

1. Adams, J. M. "The Measurement of Gas and Particle Temperatures in Rocket Motor Chambers and Exhaust Plumes," Aerojet General Corp., TP-11 (May 1967).

2. Calcote, H. F. "Electric Properties of Flames; Burner Flames in Transverse Electric Fields," Third Symposium (Int) on Combustion, Baltimore: Williams and Wilkins, 1949.

3. Calcote, H. F. "Electric Properties of Flames; Burner Flames in Longitudional Electric Fields," Industrial and Engineering Chemistry, V43., p 2726 (Dec. 1951).

4. Calcote, H. F. "Ion and Electron Profiles in Flames," Ninth Symposium (Int) on Combustion, New York: Academic Press, 1963.

5. Cobine, J. D. Gaseous Conductors. New York: Dover, 1958.

6. Cook, M. A., and Gwyther, T. "Influence of Electrical Fields on Shock of Detonation Transition," AFOSR-56, AD No. 629239 (1965).

7. Delcroix, J. L. Introduction to the Theory of Ionized Gases. New York: Interscience Publishers, Inc., 1960.

8. Derr, R. L., and Osborn, J. R. "An Experimental Investigation of the Gaseous Phase Reaction Zone in a Composite Solid Propellant," JPL Report No. TM-67-6 (Sept. 1967).

9. Dimmock, T. H., et. al., "The Electrical Properties of Ionized Flames - Part II, Electrostatic and Magnetohydrodynamic Deflection," Thiokol Chemical Corp., AFOSR-990, (Aug. 1961).

10. DeStafano, L. A., "The Effect of an Applied Electric Field on Propellant Combustion," Frankford Arsenal Report M67-23-1, (June 1967).

11. Felton, R. F., "A Technique to Measure the Irradiance of a Burning Solid Propellant Surface," (tentative title), Doctoral dissertation, Air Force Institute of Technology. To be published.

12. Gaydon, A. G., and Wolfhard, H. G., Flames: Their Structure, Radiation and Temperature. London: Chapman and Hall, Ltd., 1960.

13. Guenault, E. M., and Wheeler, R., "Propagation of Flame in Electric Fields; Distortion of the Flame Surface," Journal of the Chemical Society (London), p 195 - 199, (Jan. 1931).

14. Hermance, C. E., "A Physical Model of Composite Solid Propellant Combustion which includes the Oxidizer Particle Size and Surface Heat Generation," AIAA Paper 66-112. Third AIAA Aerospace Sciences Meeting. New York, New York., 1966.

15. Hermance, C. E., "A Detailed Model of the Combustion of Composite Solid Propellants," undated notes.

16. Jensen, D. E., and Kurzius, S. C., "Determination of Positive Ion Concentrations in High Velocity Laminar Flames," Aero Chem Research Laboratories, Inc., TP-186 (Oct. 1966).

17. Kelly, J. R. "Electromagnetic Effects on the Propagation and Structure of Gaseous Detonations," Sc. D. Thesis, M.I.T., July, 1965.

18. Kendall, D. N., Applied Infrared Spectroscopy. New York: Reinhold Publishing Corp., 1966.

19. Lawton, J., Mayo, P. J., and Weinberg, F. J., "Electrical Control of Gas Flows in Combustion Processes," Proceedings of the Royal Society, A303, p 275 - 298 (1968).

20. Lawton, J., and Weinberg, F. J., "Maximum Ion Currents from Flames and the Maximum Practical Effects of Applied Electric Fields," Proceedings of the Royal Society, A277, p 468 - 497 (1964).

21. Lee, J. F., Sears, F. W., and Turcotte, D. L., Statistical Thermodynamics. Reading, Mass.: Addison-Wesley Publishing Co., 1963.

22. Lewis, B., and von Elbe, G., Combustion, Flames and Explosions of Gases. New York: Academic Press, 1961.

23.

24. Loeb, L. B., Basic Processes of Gaseous Electronics. Berkeley: University of California Press, 1961.

25. Maycock, J. N., and Pai Verneker, V. R., "Role of Point Defects in the Thermal Decomposition of Ammonium Perchlorate," Proceedings of the Royal Society, A307, p 303 - 315, (1968).

26. Mayo, P. J., Watermeier, L. A., and Weinberg, F. J., "Electrical Control of Solid Propellant Burning," Proceedings of the Royal Society, A284, p 488 - 498, (1965).

27. McDaniel, E. W., Collision Phenomena In Ionized Gases. New York: Wiley, 1964.

28. Micheli, P. L., "A Stop-Start Study of Solid Propellant," Final Report NASA CR-66487, n.d.

29. Miller, R. R., "Some Factors Affecting the Combustion of Aluminum in Solid Propellants," Proceedings of the Second ICRPG Combustion Conference, CPIA Publication 105, V. 1, p 331 (May 1966).

30. Mills, R. W., "Flame Inhibition with Electron Attachment as the First Step," Combustion and Flame, V. 12, No. 6, p 513 - 520 (Dec. 1968).

31. Mitchell, J. E., and Wright F. J., "Effects in Diffusion Flames by Radial Electric Fields," Combustion and Flame, (to be published).

32. Payne, K. G., and Weinberg, F. J., "A Preliminary Investigation of Field Induced Ion Movement in Flame Gases and Its Application," Proceedings of the Royal Society, A250, p 316 - 336 (1959).

33. Pejack, E. R., and Velkoff, H. R., "Effects of a Transverse Electric Field on the Characteristics and Heat Transfer of a Diffusion Flame," Doctoral dissertation, Ohio State University, Nov. 1967.

34. Peterson, R. E., and Payne, C. E., "Effects of Electrostatic Fields on Solid Propellant Burn Rate," Report AFRPL-TR-69-40 (1969).

35. Plett, E., "Joulean Heating and Lorentz Force Effects on Gaseous Detonation Flow Fields," Sc. D. Thesis, M.I.T., Sept., 1966.

36. Romig, M. F., "The Influence of Electric and Magnetic Fields on Heat Transfer to Electrically Conducting Fluids," Advances in Heat Transfer. New York: Academic Press, 1964.

37. Rossikkin, V. S., and Timkovsky, V. P., Bulletin Academy Science U.S.S.R., Ser. Phys., p 211 (1941).

38. Samaras, D. G., Theory of Ion Flow Dynamics. Englewood Cliffs, N. J.: Prentice-Hall, Inc., 1962.

39. Selph, C., "A Calculation Method for Determining Equilibrium Compositions of Multiphase Systems," notes. Unpublished.

40. Sharf, P. B., Goshgarian, B. B., and Nelson, H. M., "The Measurement of the Exhaust Composition of Selected Helicopter Armament," Report AFRPL-TR-67-203, USAARU-67-10, (June 1967).

41

42

43. Spitzer, L., Physics of Fully Ionized Gases. New York: Interscience Publishers, Inc., 1956.

44. Steinz, J. A., and Summerfield, M. S., "Mechanism of Burning of Composite Solid Propellants with Special Reference to Low Pressure Combustion Phenomena," Princeton University, Contract No 1858(32), July 1968.

45. Stones, J. L., "The Effects of Electrostatic Fields on the Combustion of Solid Propellant (part title)," Final Report Ministry of Aviation Contract No. PD/31/D14/R1 (Jan. 1967).

46. Strehlow, R. A., Fundamentals of Combustion. Scranton, Pa.: International Textbook Co., 1968.

47. Summerfield, M. S., et. al., "Burning Mechanism of Ammonium Perchlorate Propellants," Solid Propellant Rocket Research, Progress in Astronautics and Rocketry. Vl., New York: Academic Press, 1960.

48. Summerfield, M. S., and Caveny, L. H., "A Feasibility Study of Command Control of Solid Propellant Burning Rate," Report AFRPL-TR-69-249, (Feb 1970).

49.

50. Thornton, J. A., McLeman, E. A., and Penfold, A. S., "Investigations Concerning Energy Storage Using a Low Pressure Gas Discharge," Report AFRPL-TR-68-86 (March 1968).

51. Travers, B. E. L., and Williams, H., "The Use of Electrical Probes in Flame Plasmas," Tenth Symposium (Int) on Combustion., p 657 - 667, Combustion Institute, Pittsburgh, 1965.

52. Turner, S. W., "The Effects of Electrostatic Fields on Flame Spread Rates of Solid Propellant," Doctoral dissertation, University of Arizona, 1970.

53. Watermeier, L. A., "Optical and Electrical Properties of Solid Rocket Propellant Flames," Report BRL 1275, (March 1965).

54. Williams, F. A., Combustion Theory. Reading, Mass.: Addison - Wesley Publishing Co., Inc., 1965.

APPENDIX A

TABLES

TABLE I. Comparison of Past Experiments on Electric Field Effects on Burning Rate

ITEM	REFERENCES				
	10	34		45	53
Propellant Class: (M-metallized)					
Double Base (DB)	-	-	X	X(M)	X(M)
Composite	X	X(M)	X	-	-
Composite/DB blend	-	X(M)	-	-	-
Combustion Pressure:					
Range (atm.)	1	1	1-100	15-40	1
Pressurizing gas	-	-	N_2/Air	N_2	-
Burning Rate Device:					
Timing Wires	X	-	-	-	
Photodiode	-	X	X	-	
Photomultiplier	-	-	-	X	(U)
Camera	-	-	X	X	
High Voltage: (KV DC)	25	15	13	15	25
(KV AC)	-	-	14	-	-
Measured: Voltage	X	X	X	X	X
Current	-	-	-	X	-
Electric Field Direction (compared to burning direction): Parallel	X	X	X	X	X
Transverse	-	-	X	-	-
Electrodes:					
Propellant between electrodes	X	-	X	-	X
Propellant as electrode	-	X	X	X	X
Magnitude of Field Effect on Burning Rate: Increase	-	-	-	75%	-
Decrease	21%	10%	40%	-	10%
Combustion Pressure Influence (under electric field): Increase/decrease effect w/ pressure	-	-	X	-	-
Maximum change at a pressure	-	-	-	X	-
No change with pressure	-	-	-	-	-

(U) Unknown

TABLE II. Representative Gas-Phase Properties

PROPERTY	VALUE
Current flux (J)	10^{-2} amperes/cm^2 (1)
DC electrical conductivity (σ_g)	10^{-4} (ohm cm)$^{-1}$
Thermoelectric coefficient (α_g)	10^{-7} amperes/cm$^{\circ}$K (2)
Thermoelectric coefficient (β_g)	4 X 10^{-4} amperes/cm (3)
Combustion temperature (T_f)	3100°K
Propellant temperature (T_p)	300°K
Thermal conductivity (Λ_g)	10^{-4} cal/cm sec$^{\circ}$K (4)
Heat capacity (C_g)	0.3 cal/gm$^{\circ}$K (4)
Heat of reaction (Q)	150 cal/gm (4)
Mass flow/burning area ($\dot{m}$)	0.2 - 4 gm/cm^2 sec
Equation (8) (Ω)	10^{-4} gm/cm^2 sec
Equation (9) (ϵ)	0.999

(1) Maximum continual current measured distributed over the burning area.
(2) Computed for Fig. 18, and $J = \alpha_g \frac{dT}{dx}$, where $\frac{dT}{dx} \simeq 50^{\circ}$K/cm.
(3) Equation (C-4).
(4) Reference 44.

TABLE III. Propellant Code

PROPELLANT	NOMINAL COMPOSITION
A	Ammonium Perchlorate (AP), double base (nitrocelluose and nitroglycerine) binder, aluminum (15% by weight)
AD	Same as A except add 1% KNO_3 at expense of AP
AM	Same as A except cast into aluminum mesh
B	AP, Polybutadiene binder, aluminum (16% by weight)
BD	Same as B except add 1% $CsClO_4$ at expense of AP
BO	Same as B except delete aluminum and fill with binder

TABLE IV. Combustion Bomb Electrical Insulation

LOCATION	RESISTANCE (ohms)
Micarta platform to earth ground	10^{11}
Inlet gas line to earth ground	10^{11}
Exhaust line to earth ground	5×10^{10}
Ignition circuit to earth ground	10^{11}
Lexan - rod to bomb	8×10^{10}
High voltage connections to bomb	2×10^{9}
Plexiglass chamber to bomb	8×10^{10}

TABLE V. Perkin-Elmer 421 Infrared Spectrometer Settings

PARAMETER	SETTING
Interchange	Dual Grating
Slit Program	1000
Gain	5
Attenuation Speed	1100
Scan Time	16 min
Suppression	4
Scale	X 1
Source Current	0.4 amperes

TABLE VI. Burning Rate Device Comparative Results

BURNING RATE DEVICE	AVERAGE BURNING RATE ± PERCENT SPREAD (cm/sec)	
	PROPELLANT A	PROPELLANT B
Camera	$0.108 \pm 4\%$	——
Optron (servo-track mode)	$0.110 \begin{smallmatrix}+4\\-3\end{smallmatrix}$ %	$0.141 \pm 2\%$
Optron (photomultiplier)	$0.100 \begin{smallmatrix}+8\\-10\end{smallmatrix}$ %	$0.133 \pm 6\%$
Photodiode	$0.122 \begin{smallmatrix}+10\\-6\end{smallmatrix}$ %	$0.149 \begin{smallmatrix}+8\\-4\end{smallmatrix}$ %
Timing wire	$0.157 \begin{smallmatrix}+30\\-15\end{smallmatrix}$ %	$0.158 \begin{smallmatrix}+4\\-12\end{smallmatrix}$ %

TABLE VII. Ionizable Impurities

PROPELLANT	Impurity Level (micro gm/gm)		
	Cs	K	Na
A (5 samples)	(1)	38 - 86	125 - 179
B (5 samples)	(1)	102 - 278	62 - 172
A (average)	0	60	150
B (average)	0	190	73

(1) Not detectable

TABLE VIII. Gas-Phase DC Electrical Conductivity

PROPELLANT	DC ELECTRICAL CONDUCTIVITY $(ohm\ cm)^{-1}$		
	Defining Formula	Developed Formula	
		Langmuir Probe	Computer
A	$2\ ^{+1}_{-0.5} \times 10^{-5}$	5×10^{-5}	7×10^{-4}
AD	$2\ ^{+2}_{-1} \times 10^{-5}$	—	—
B	$3\ ^{+1}_{-2} \times 10^{-4}$	7×10^{-4}	6×10^{-4}

APPENDIX B

ILLUSTRATIONS

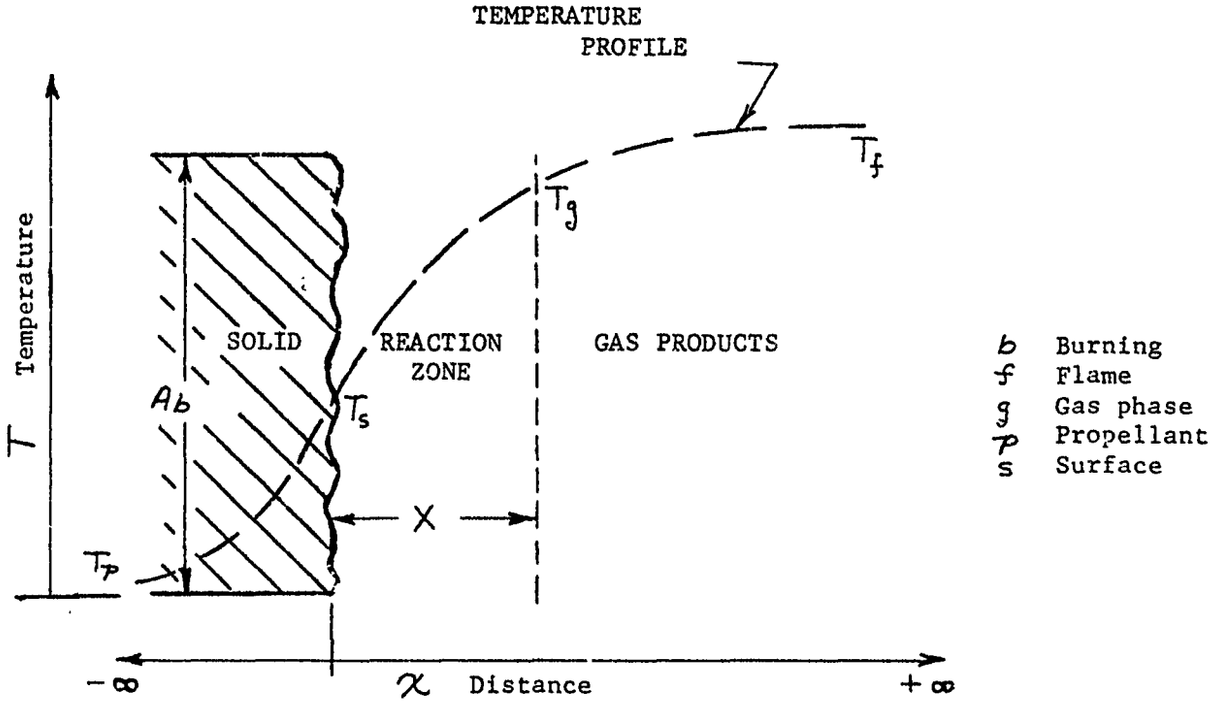

Figure 1. Thermal Model of Burning Propellant

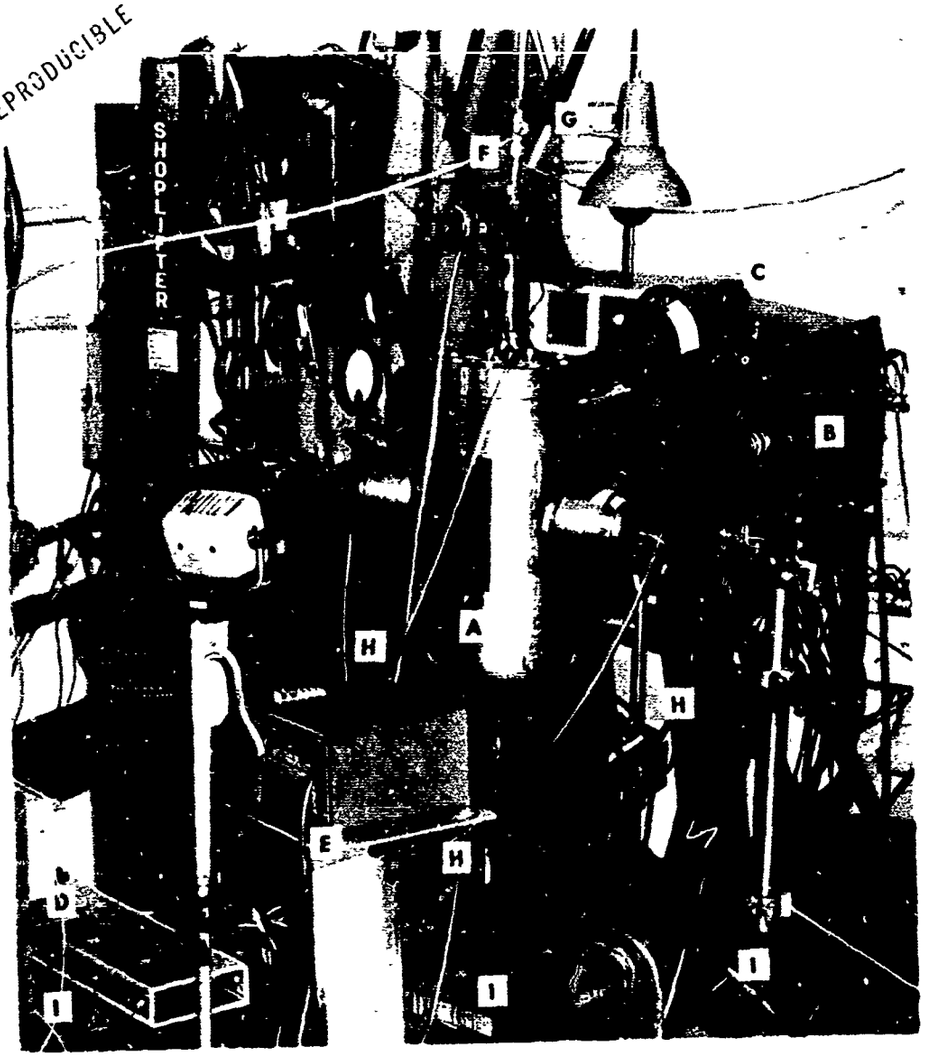

A - Combustion Bomb
B - Optron Sensor
C - Optron Controls, Recording Apparatus
D - Voltage and Current Monitor
E - Timer
F - Emissions Trap Bypass
G - Isolation Transformer Leads
H - High Voltage Leads
I - Electrical Insulation

Figure 2. Test-Cell Assembly

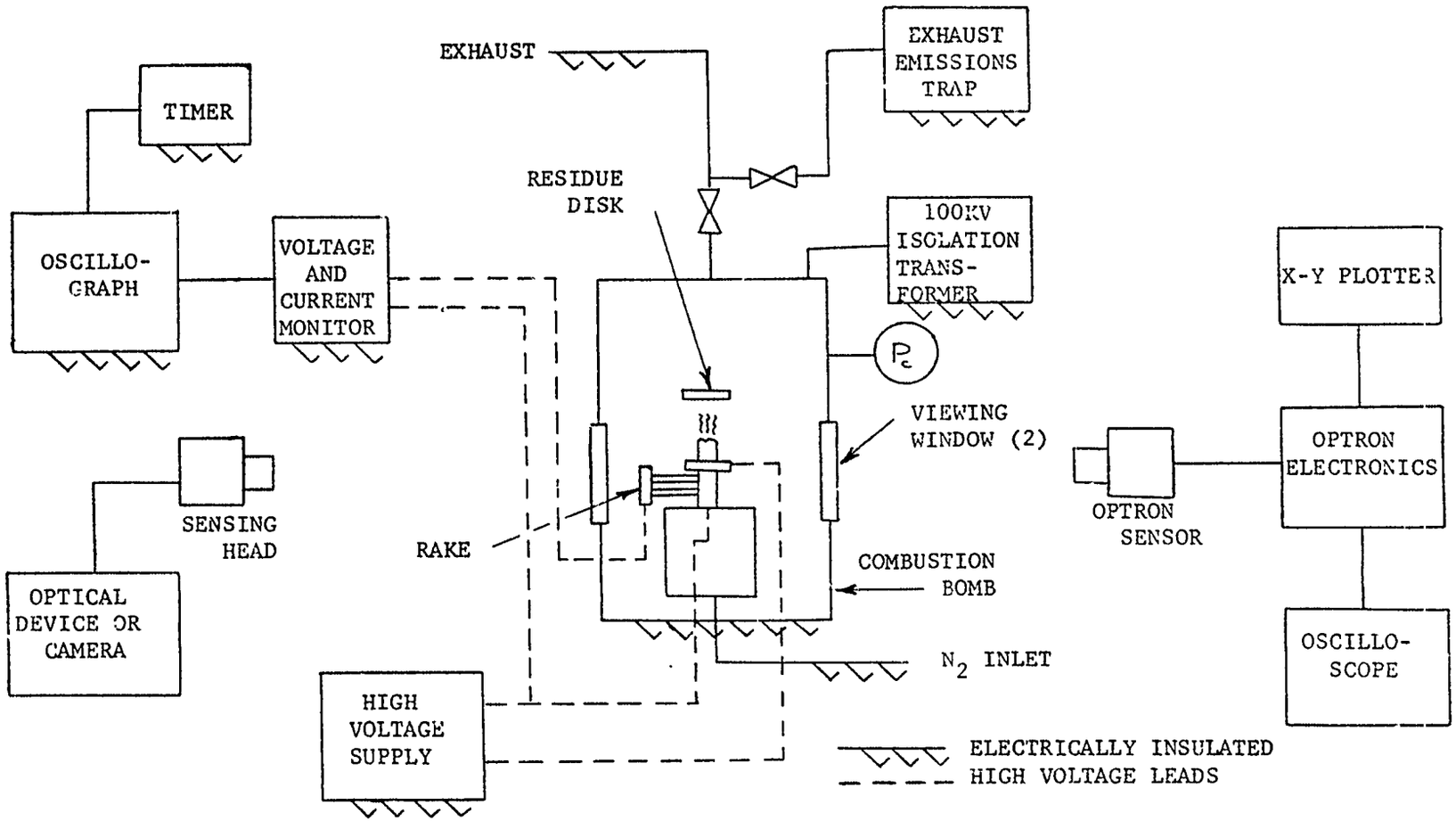

Figure 3. Test-Cell Schematic

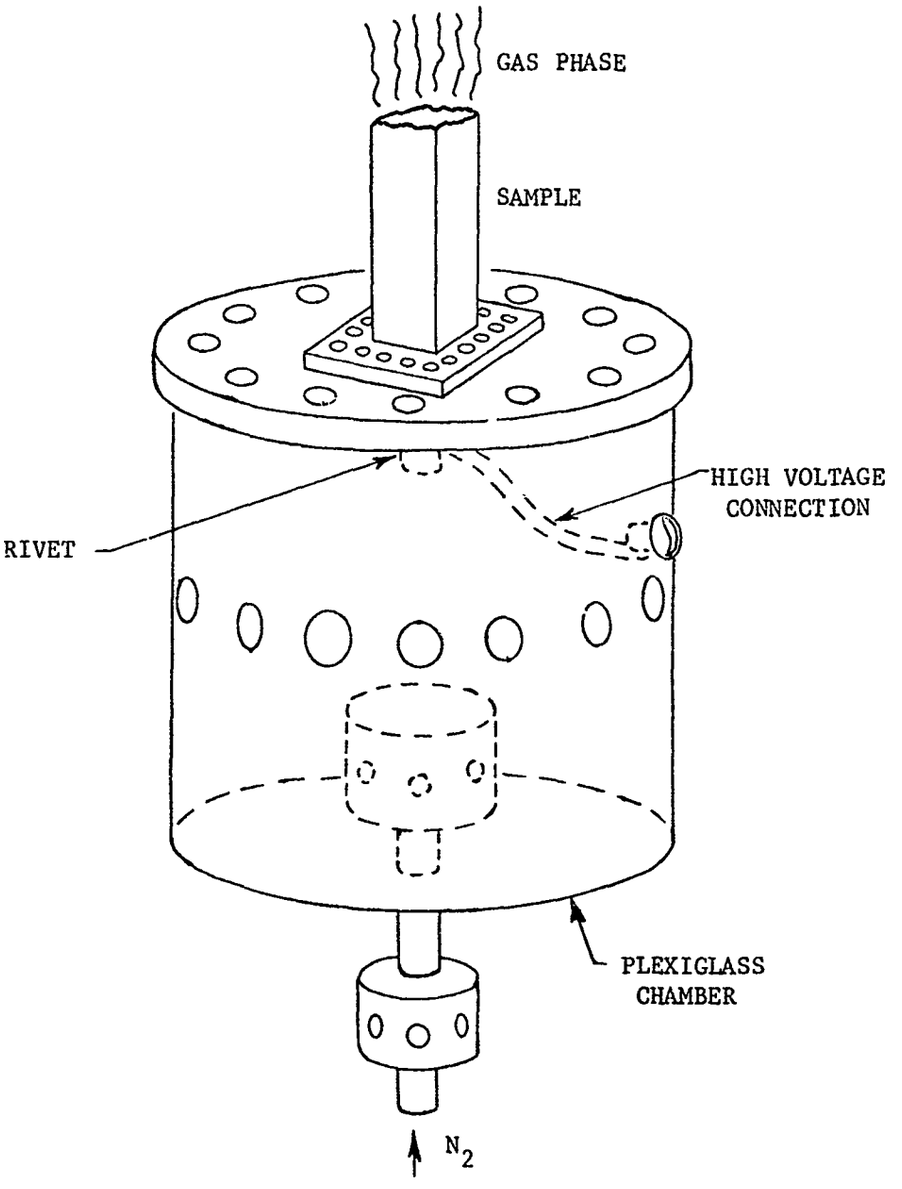

Figure 4. Propellant and Nitrogen Chamber Setup

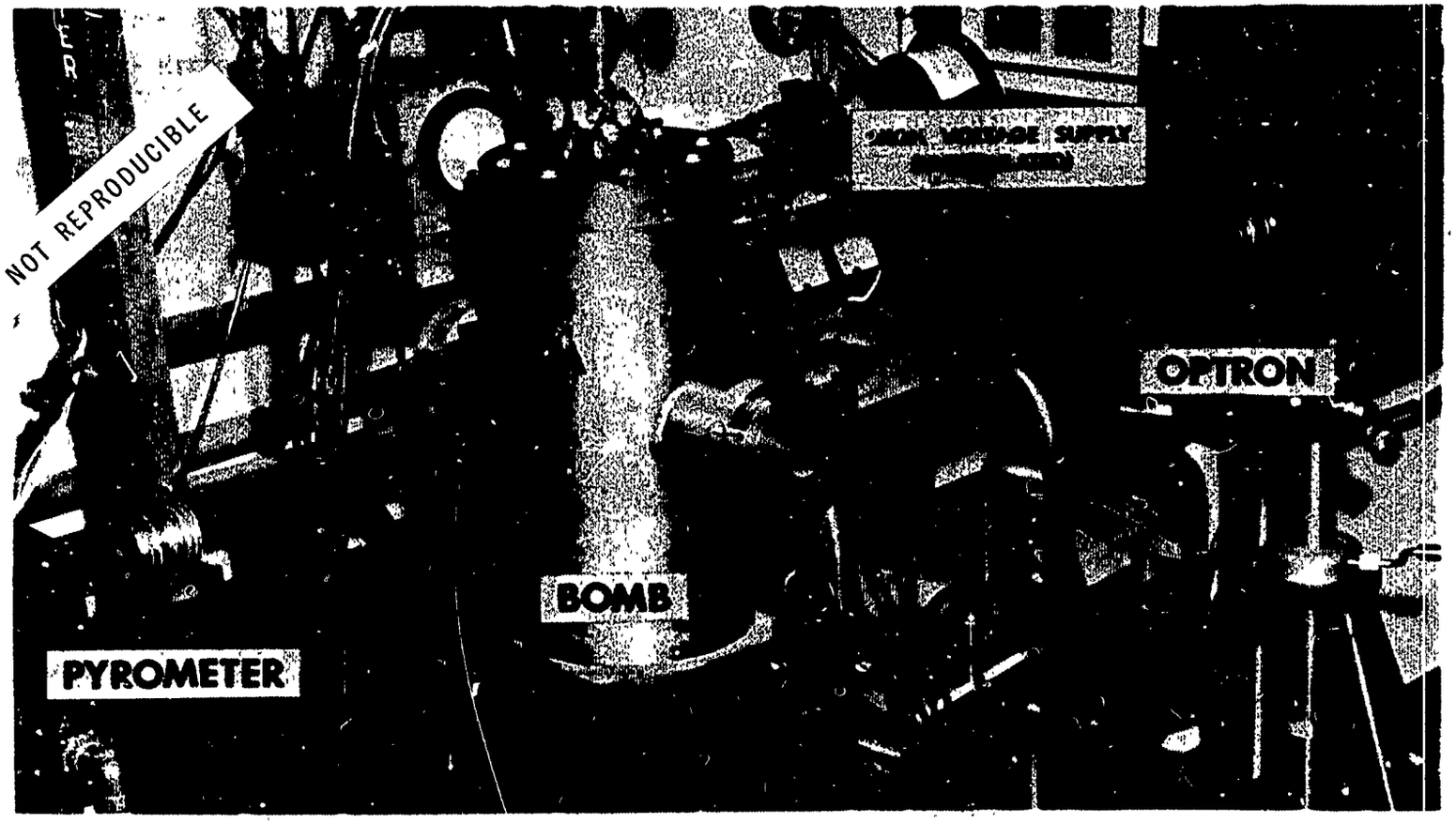

A - Herculite Window (2) B - Electrode Connections (2) C - High Voltage Connections, Ignition Leads

Figure 5. Combustion Bomb

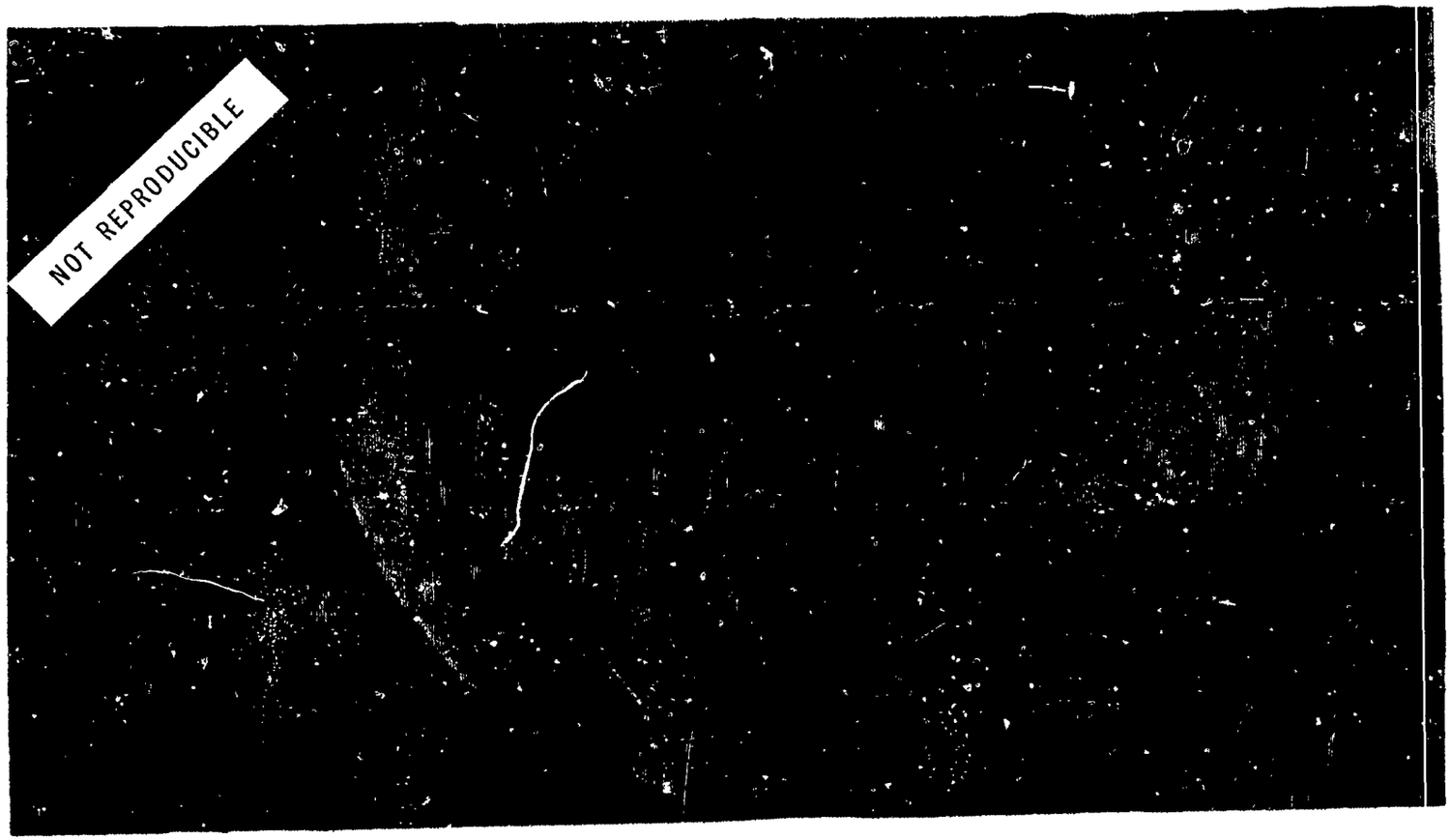

A - Propellant Sample
B - Nitrogen Chamber
C - Ignition Post
D - Ring Electrode
E - High Voltage Rake

Figure 6. Combustion Bomb Interior

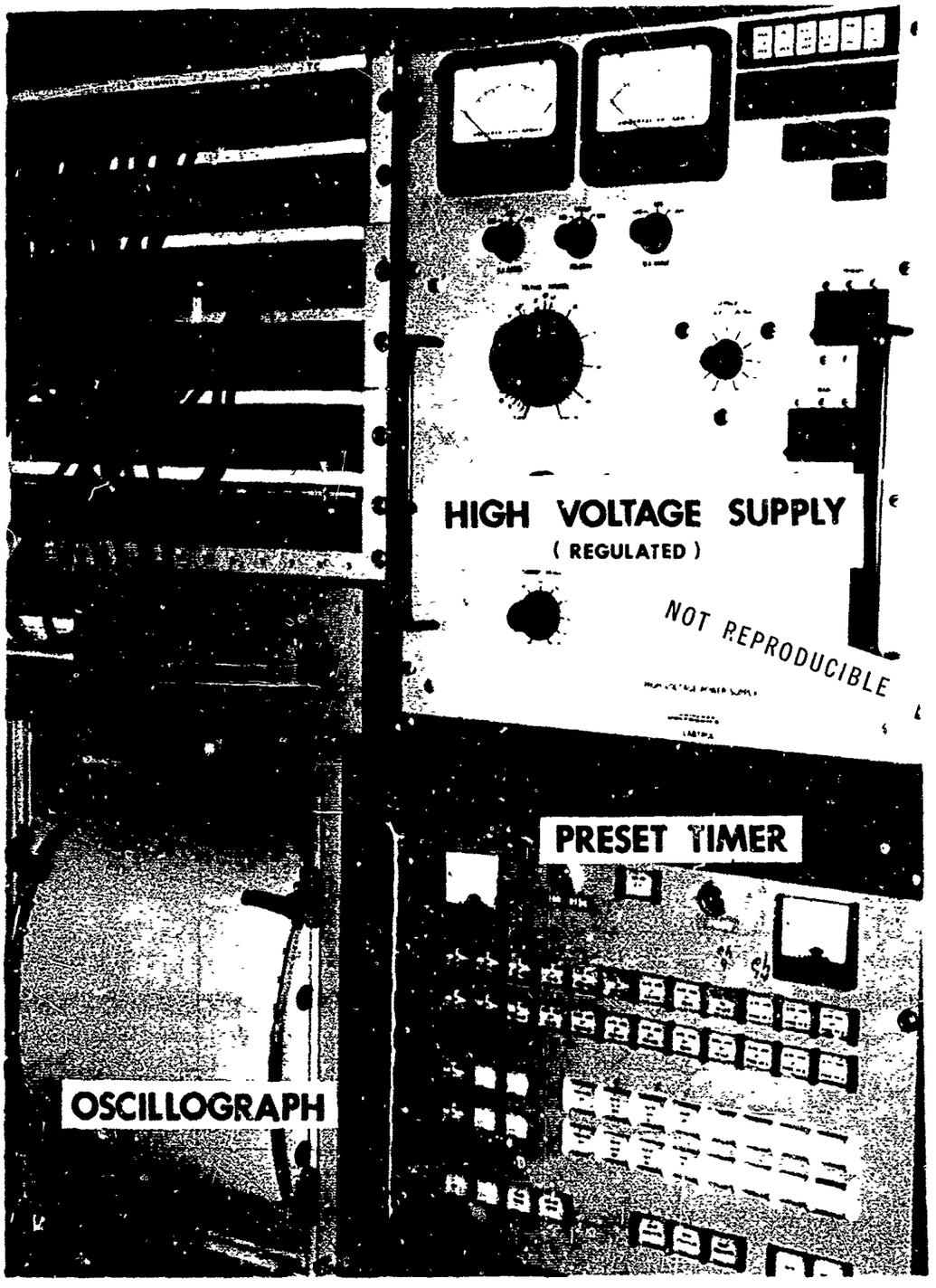

Figure 7. Atmospheric Site Apparatus

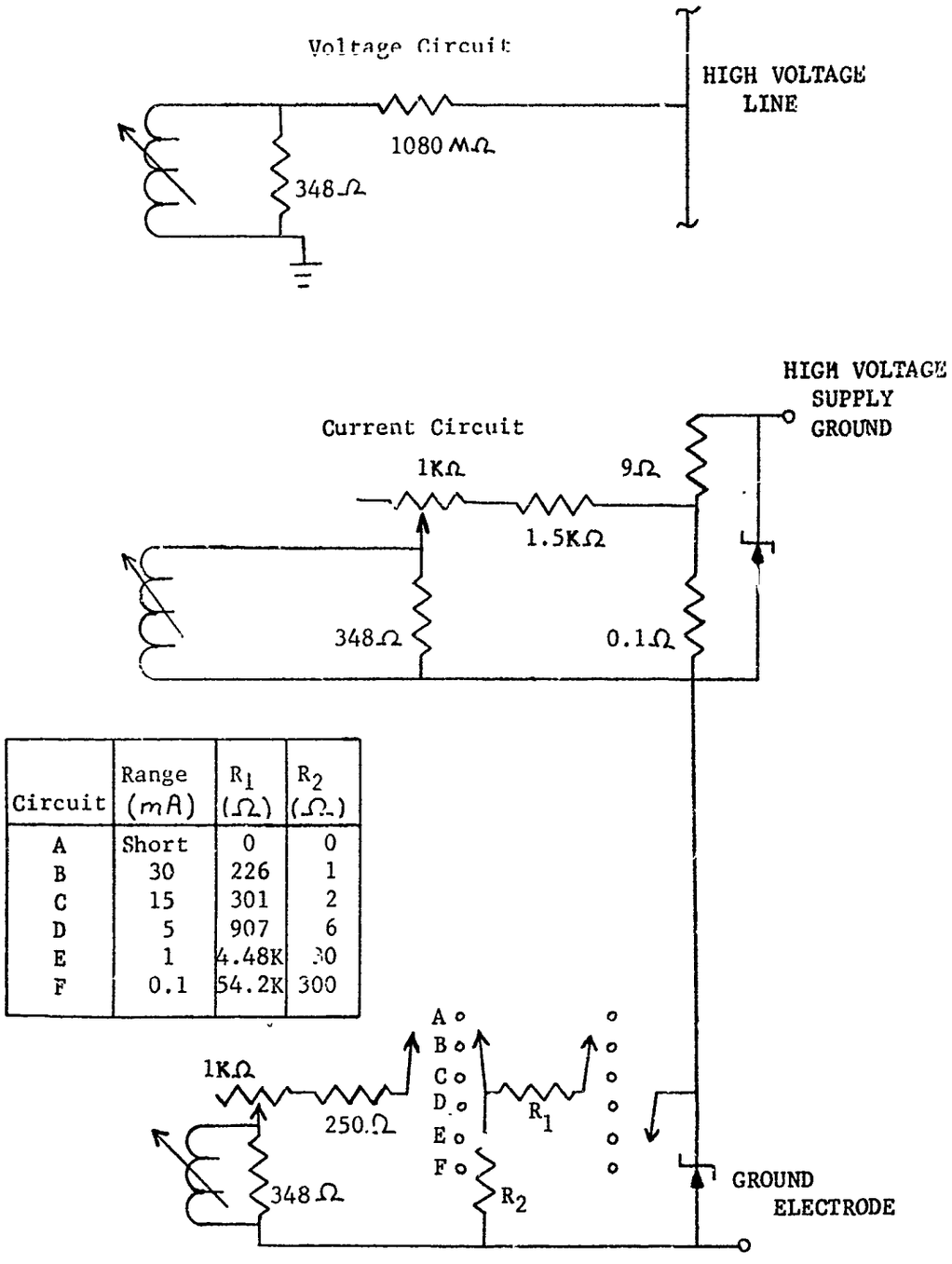

Circuit	Range (mA)	R_1 (Ω)	R_2 (Ω)
A	Short	0	0
B	30	226	1
C	15	301	2
D	5	907	6
E	1	4.48K	30
F	0.1	54.2K	300

Figure 8. Voltage and Current Monitoring Circuits

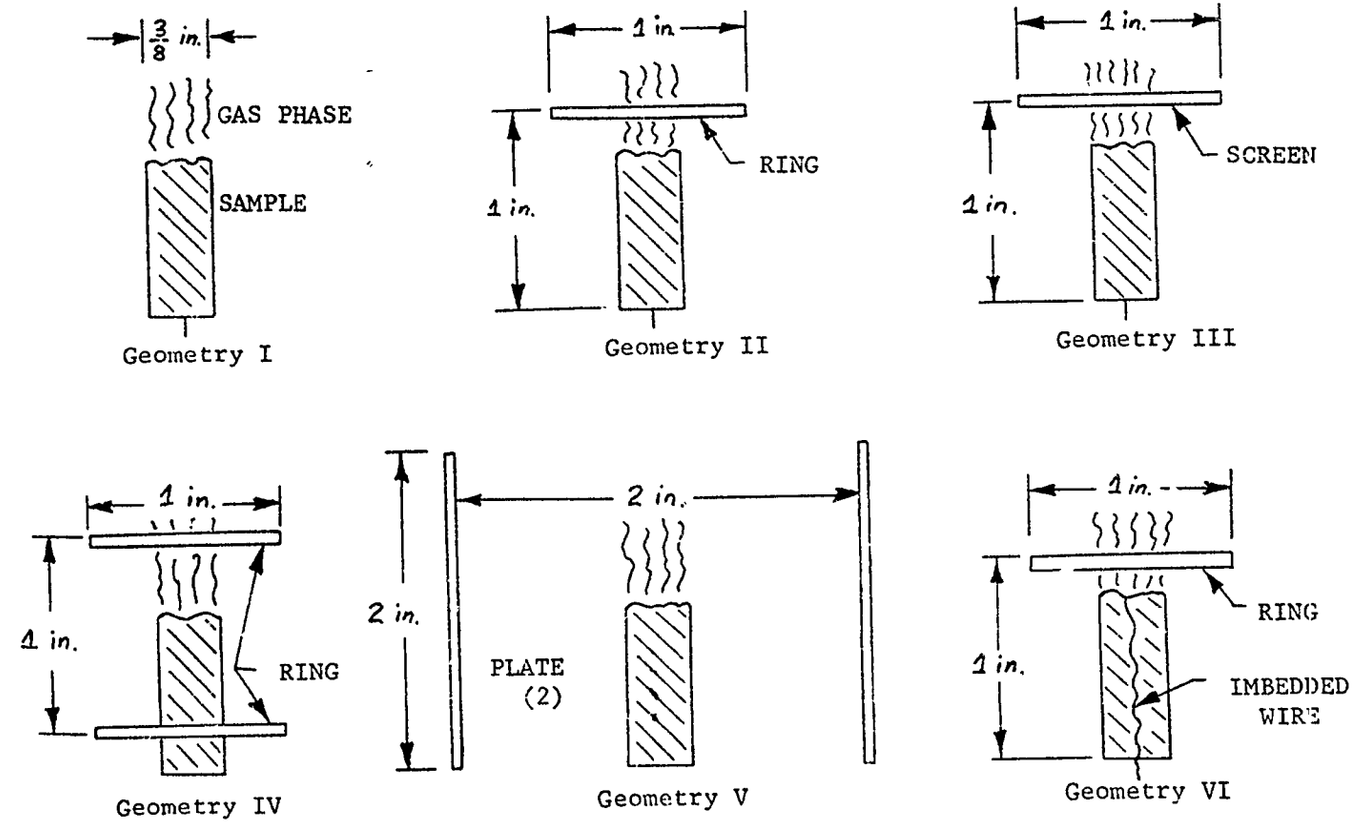

Figure 9. Electrode Geometries

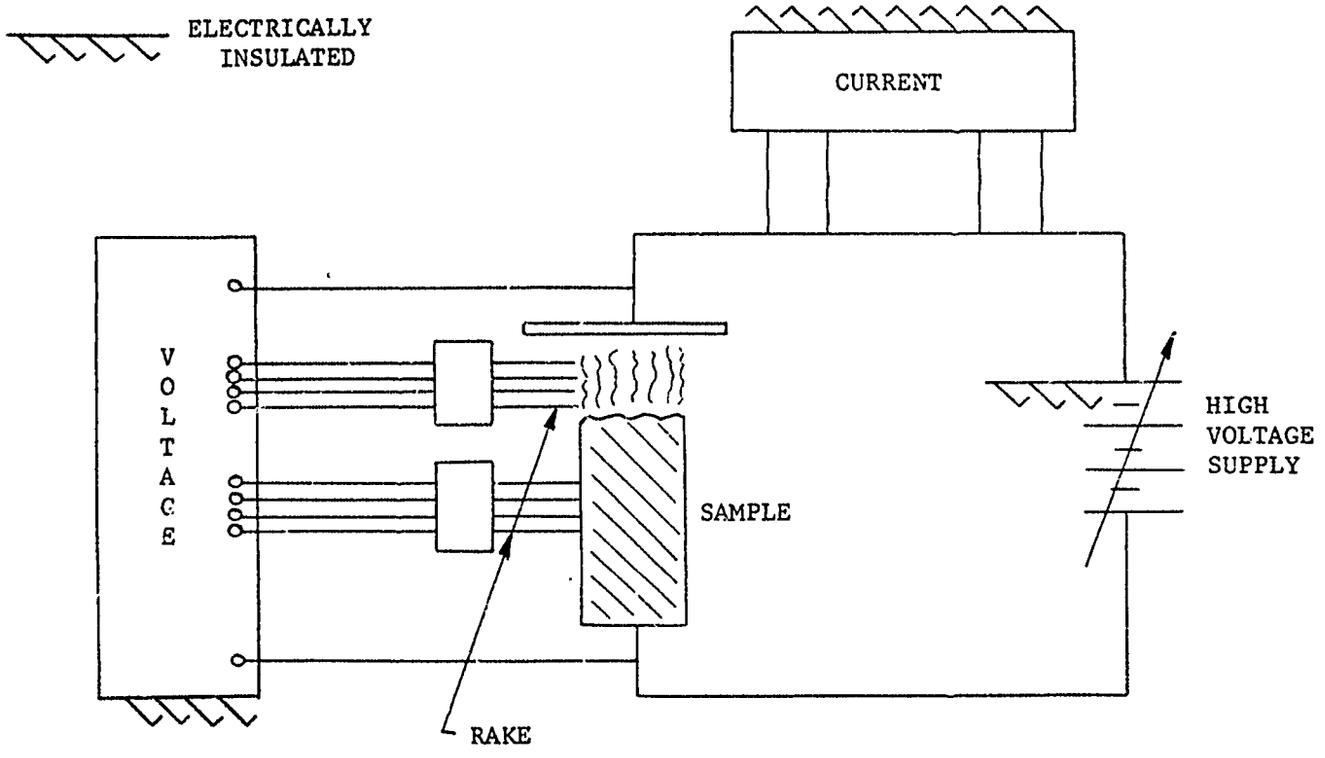

Figure 10. Typical Electric Parameters Experimental Setup

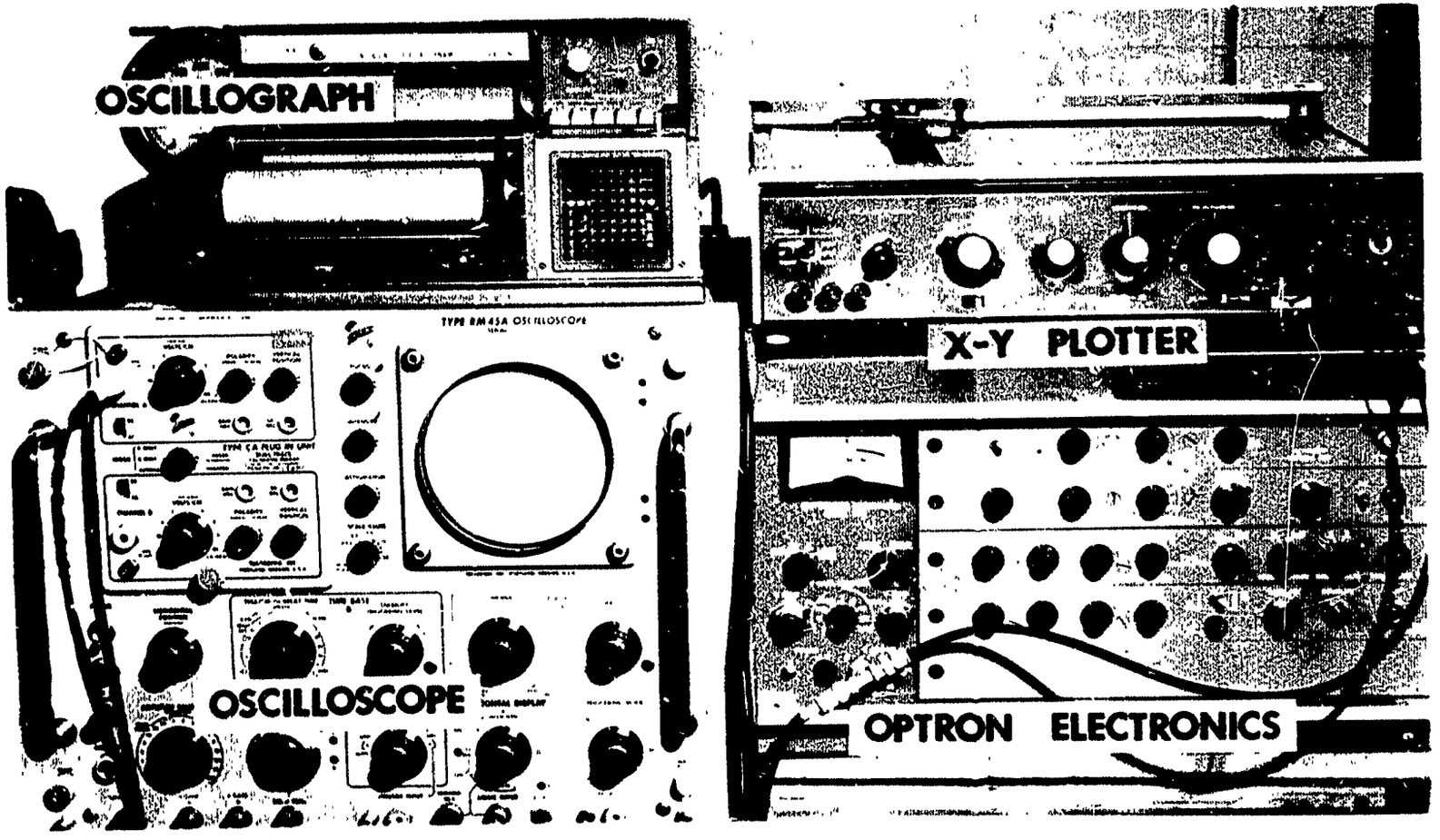

Figure 11. Optron Apparatus

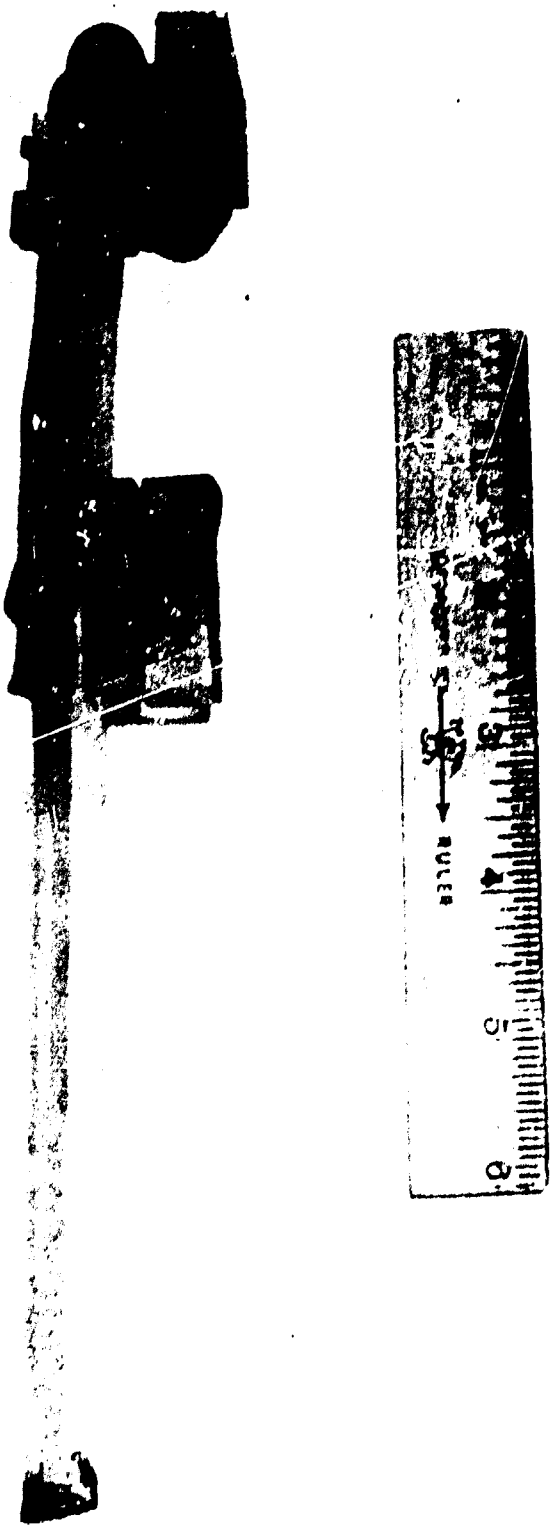

Figure 12. High Voltage Rake

NATIONAL TRANSPORTATION SAFETY BOARD
Washington, D. C. 20591

SA-None File No. A-0003

AIRCRAFT ACCIDENT REPORT

ALITALIA AIRLINES
MCDONNELL-DOUGLAS DC-8-62, I-DIWZ
(ITALIAN REGISTRY)
JOHN F. KENNEDY INTERNATIONAL AIRPORT
JAMAICA, NEW YORK
SEPTEMBER 15, 1970

Adopted: APRIL 28, 1971

E R R A T A

The following changes should be made to the subject report:

Page 10, column 1, lines 10 - 12 delete "at a point approximately 0.1 mile before reaching the outer marker (approximately 2.9 miles from the end of the runway)." and insert: "at a point approximately 2.8 miles from the end of the runway."

Page 11, column 2, (b) Probable Cause, Line 6 insert: "high" following ". . . uncorrectable".

REPORT NUMBER: NTSB AAR-71-9

72331

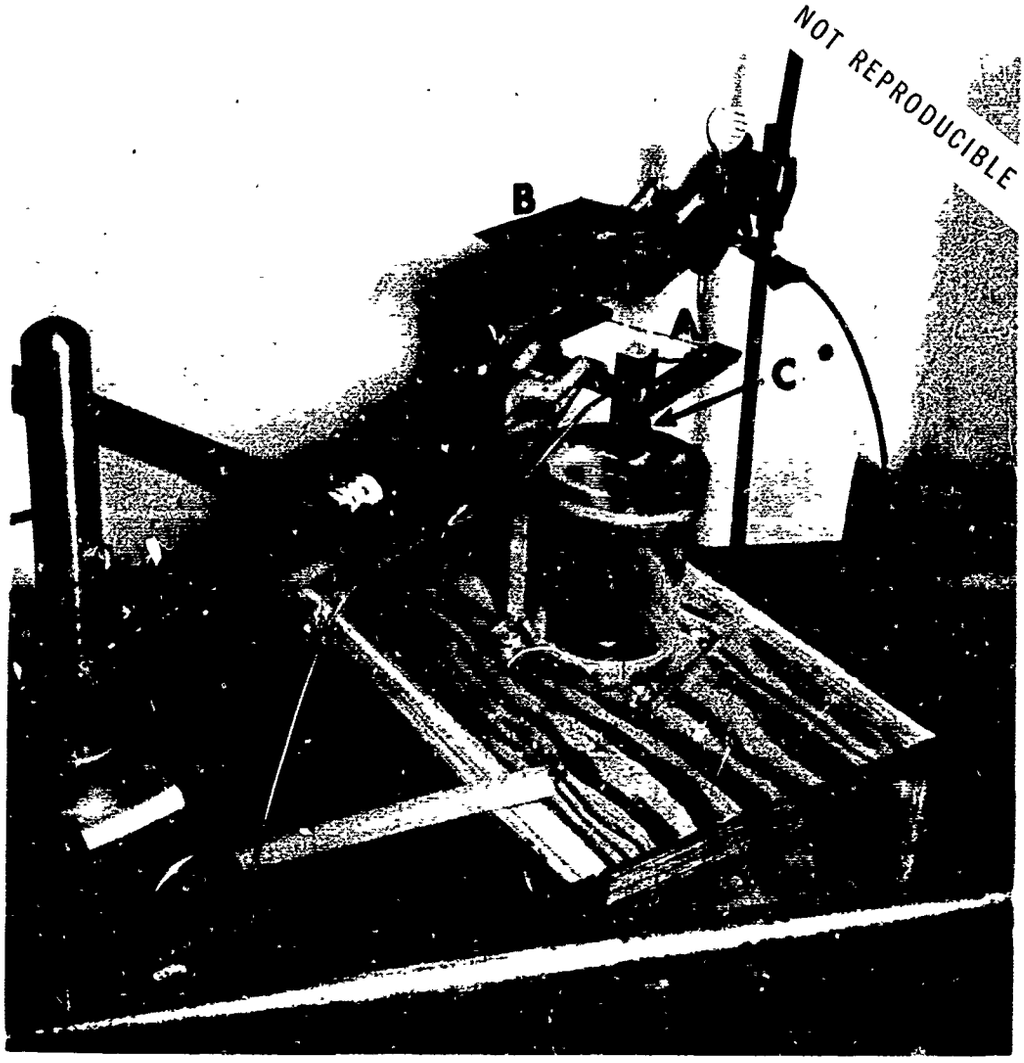

A - Tungsten Probe
B - Remote Electrode
C - Propellant A Sample
D - Nitrogen Chamber

Figure 13. Langmuir Probe Setup

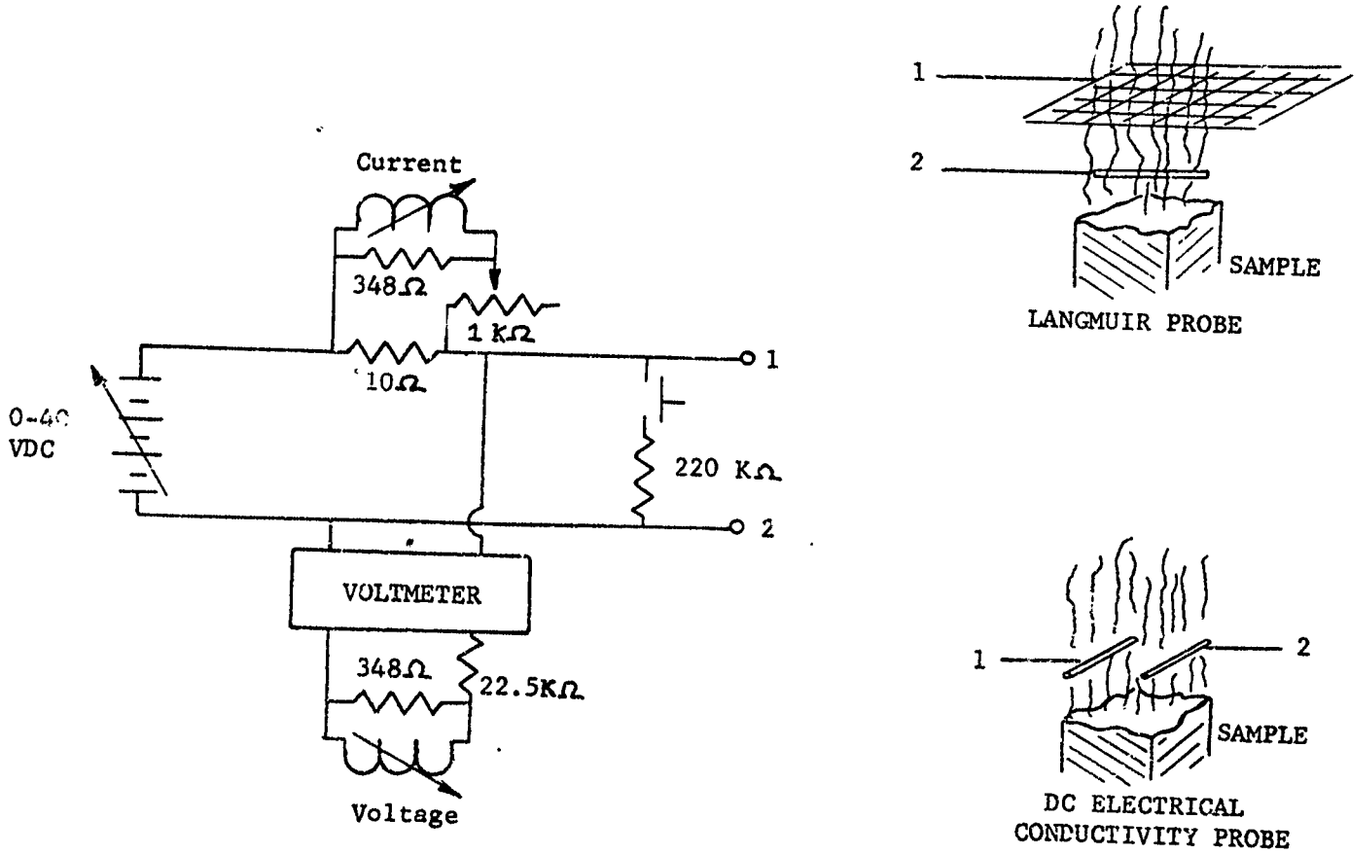

Figure 14. Ionization Probes Schematic

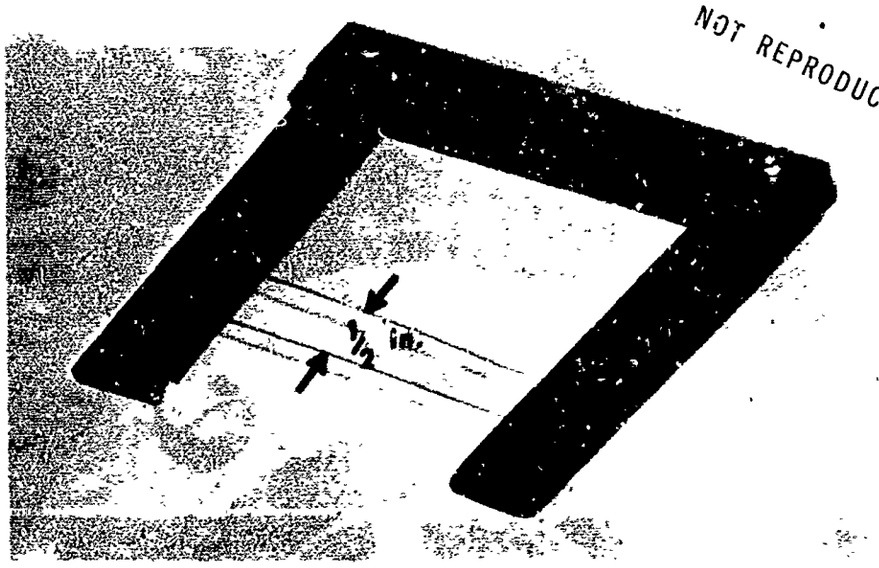

Figure 15. DC Electrical Conductivity Probe

Figure 16. Solid-Phase Electrodes

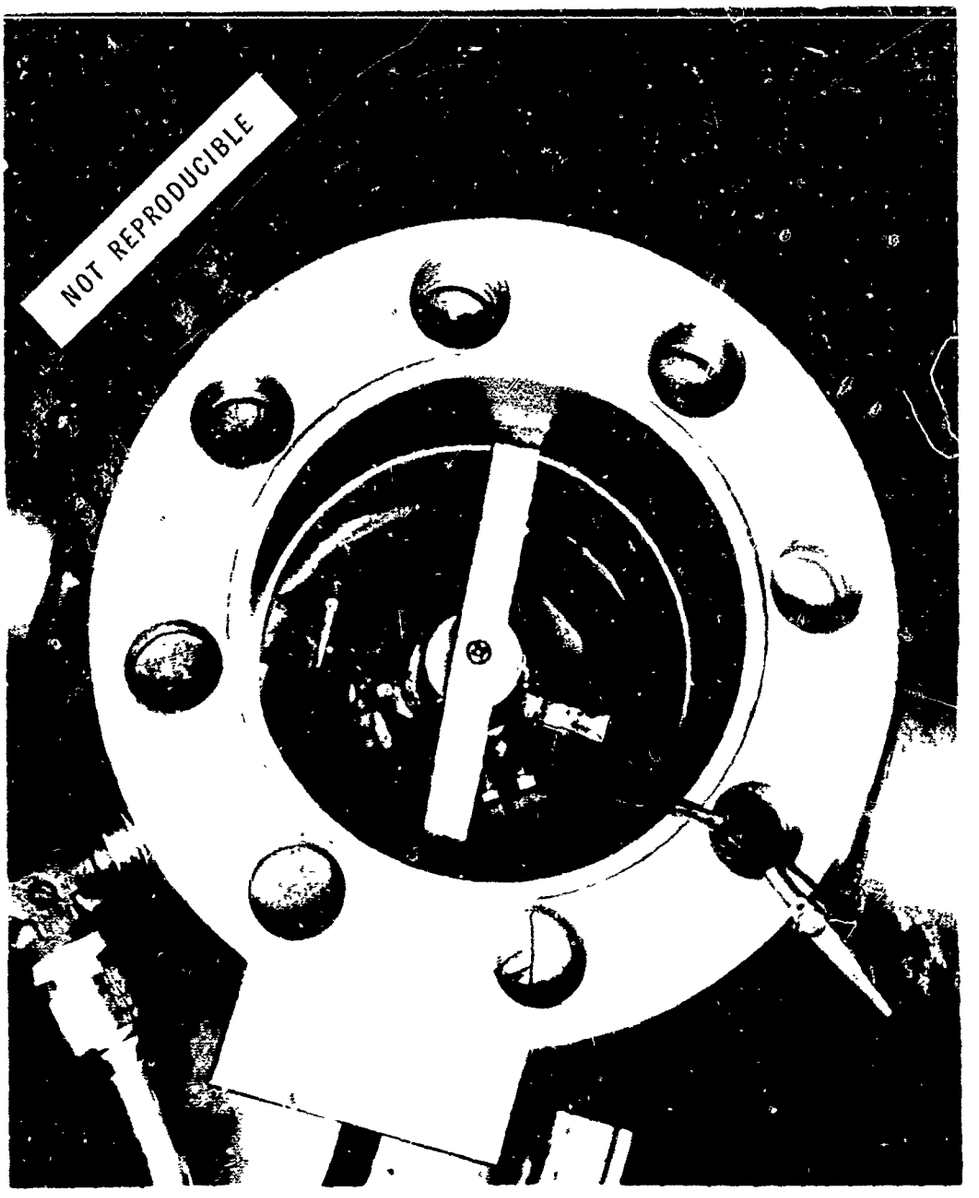

Figure 17. Combustion Residue Disk

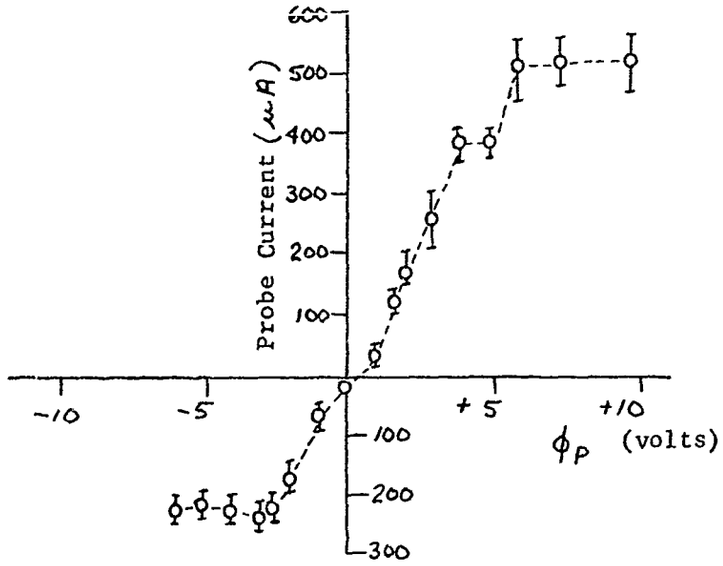

Figure 18. Experimental Plot of Probe Current versus Voltage (Propellant B)

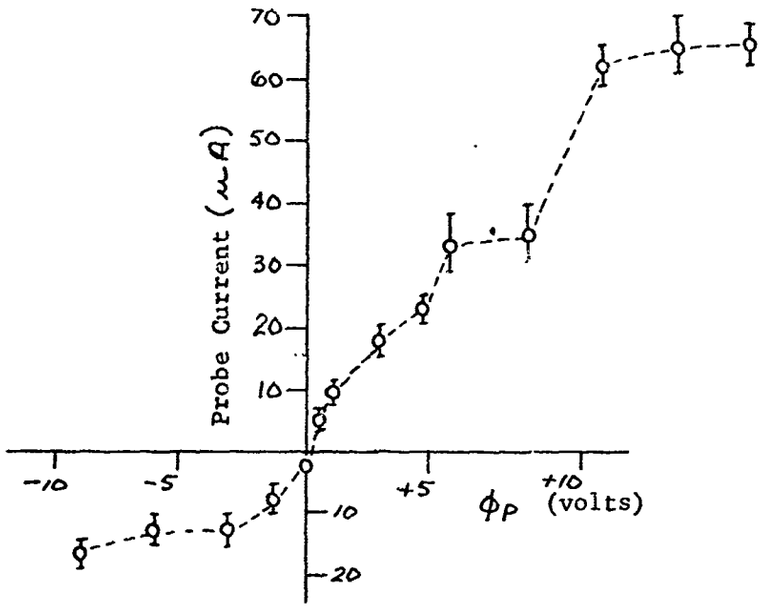

Figure 19. Experimental Plot of Probe Current versus Voltage (Propellant A)

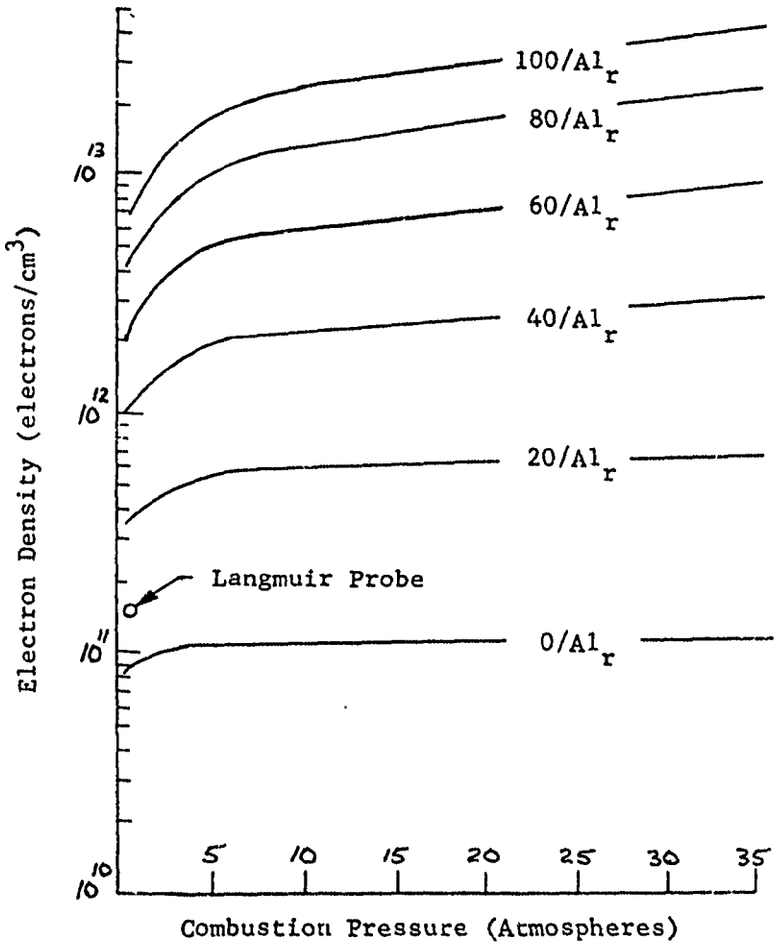

Figure 20. Electron Density versus Combustion Pressure (Propellant A)

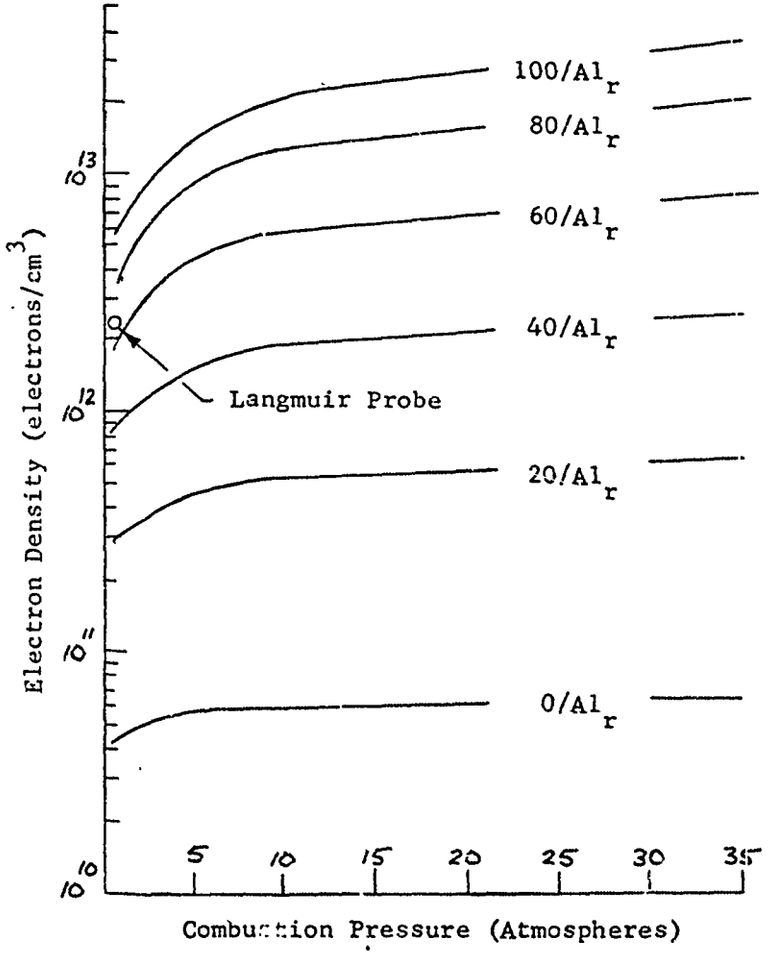

Figure 21. Electron Density versus Combustion Pressure (Propellant B)

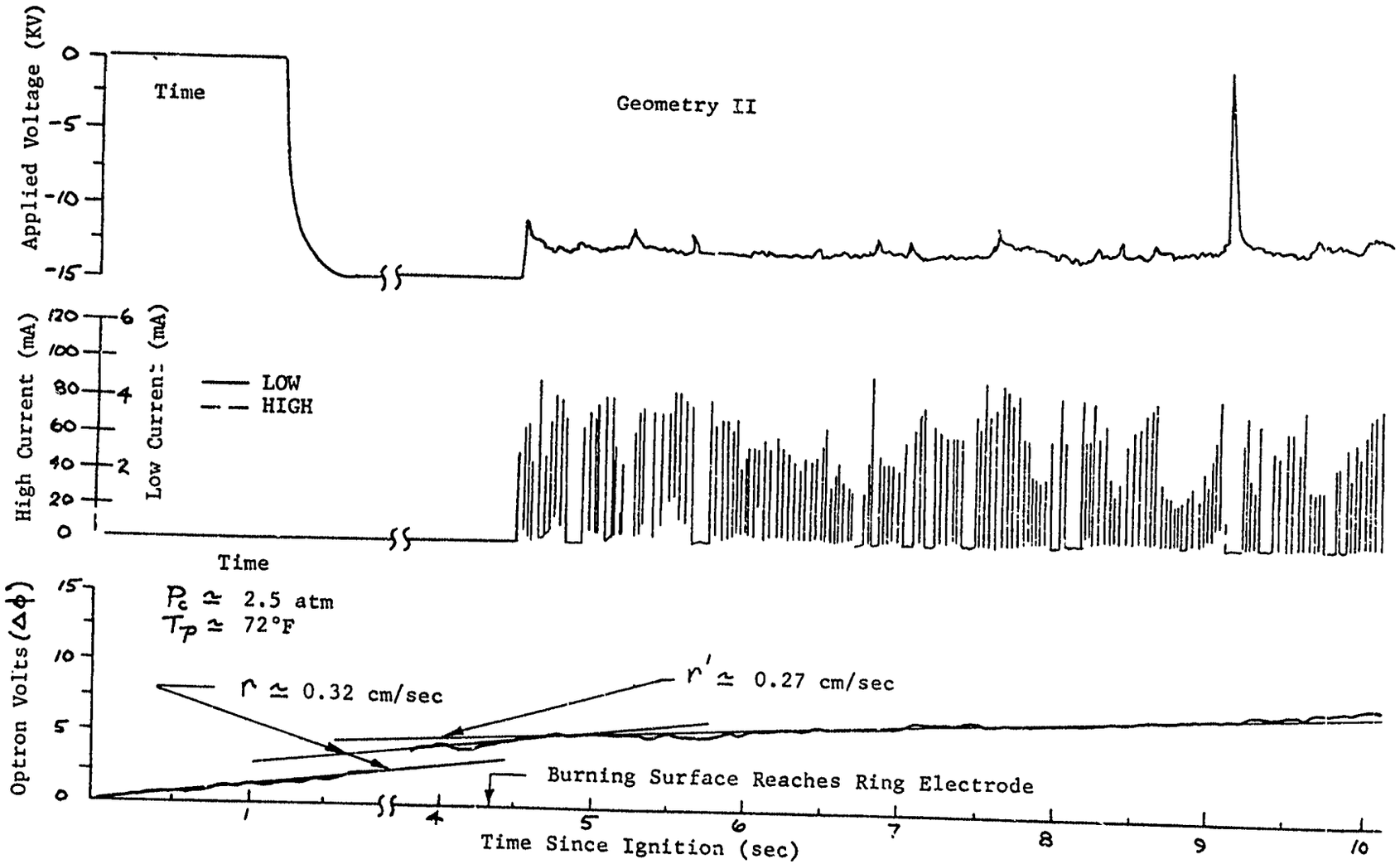

Figure 22. Applied Voltage, Current, Optron Voltage versus Time (Propellant A)

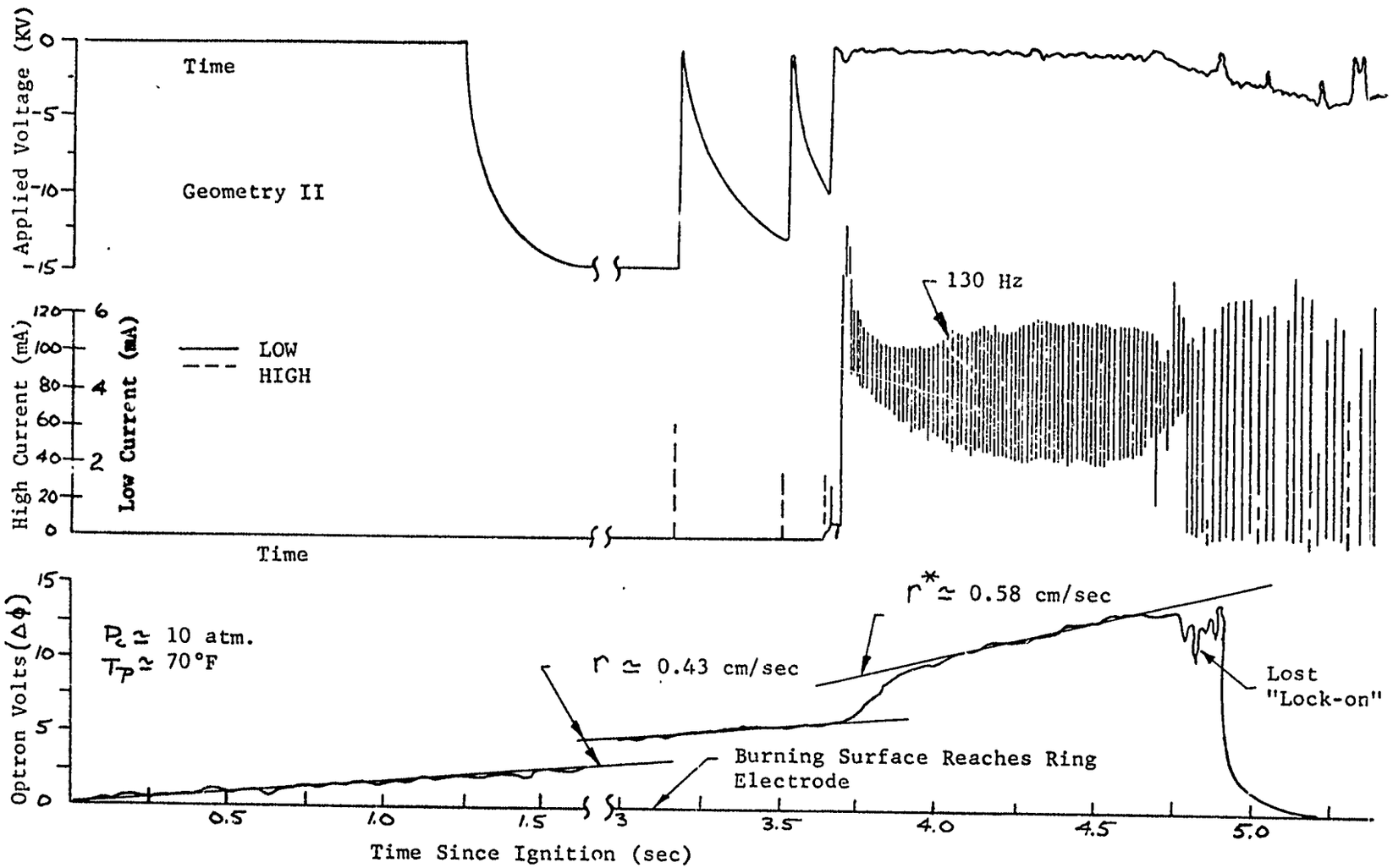

Figure 23. Applied Voltage, Current, Optron Voltage versus Time (Propellant B)

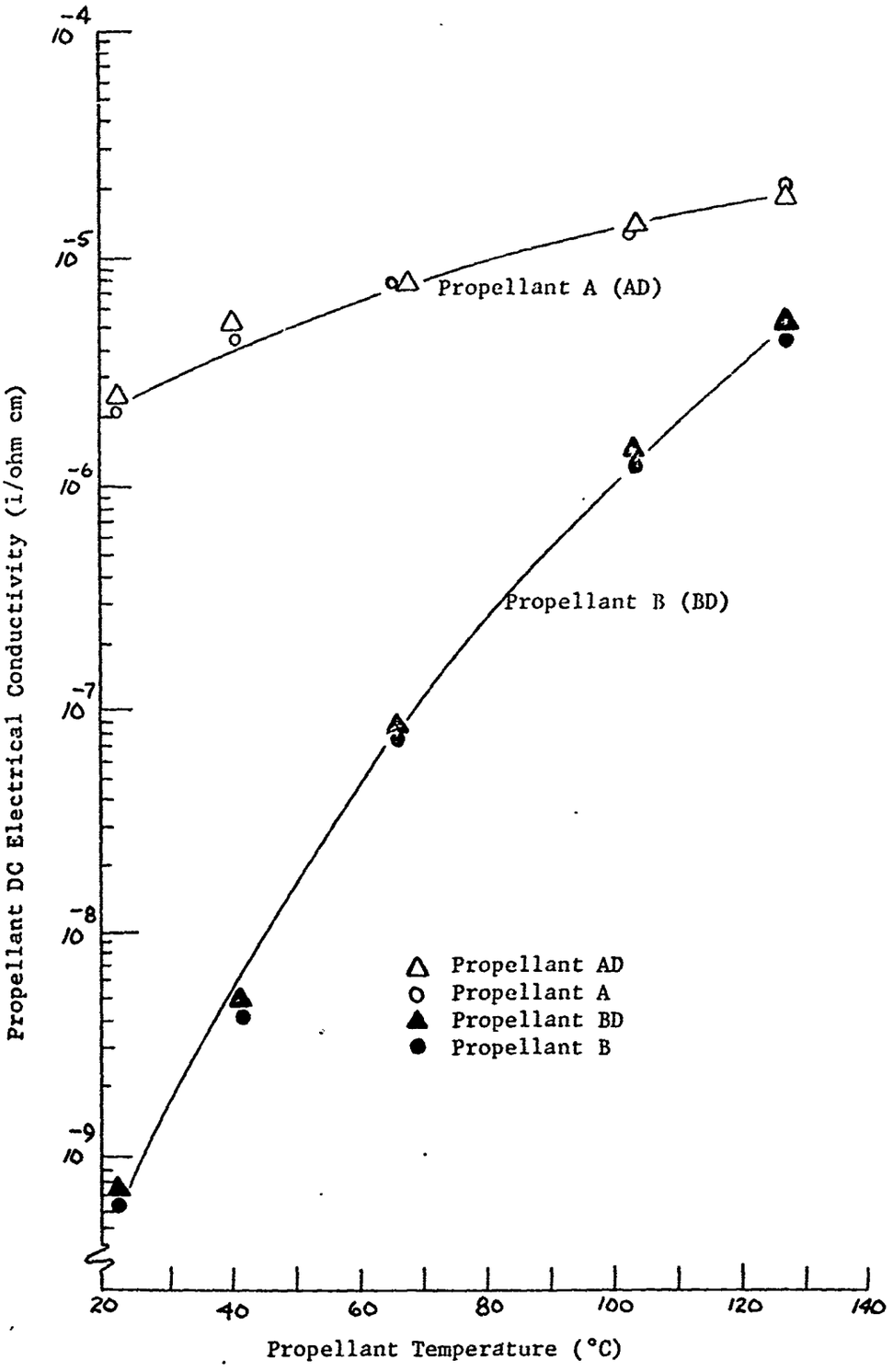

Figure 24. Experimental Bulk Solid-Phase DC Electrical Conductivity versus Propellant Temperature

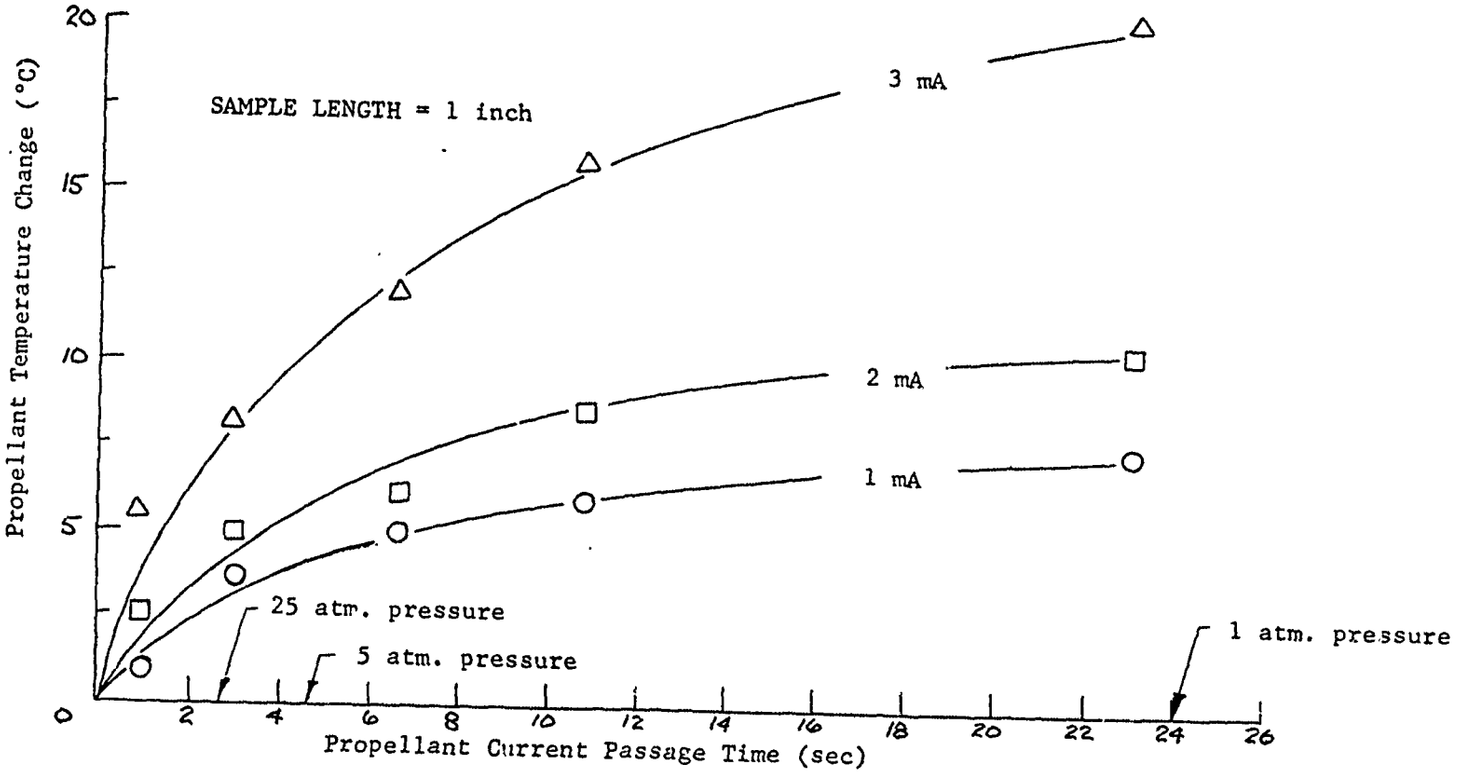

Figure 25. Experimental Simulation of Current Bulk Heating (Propellant A)

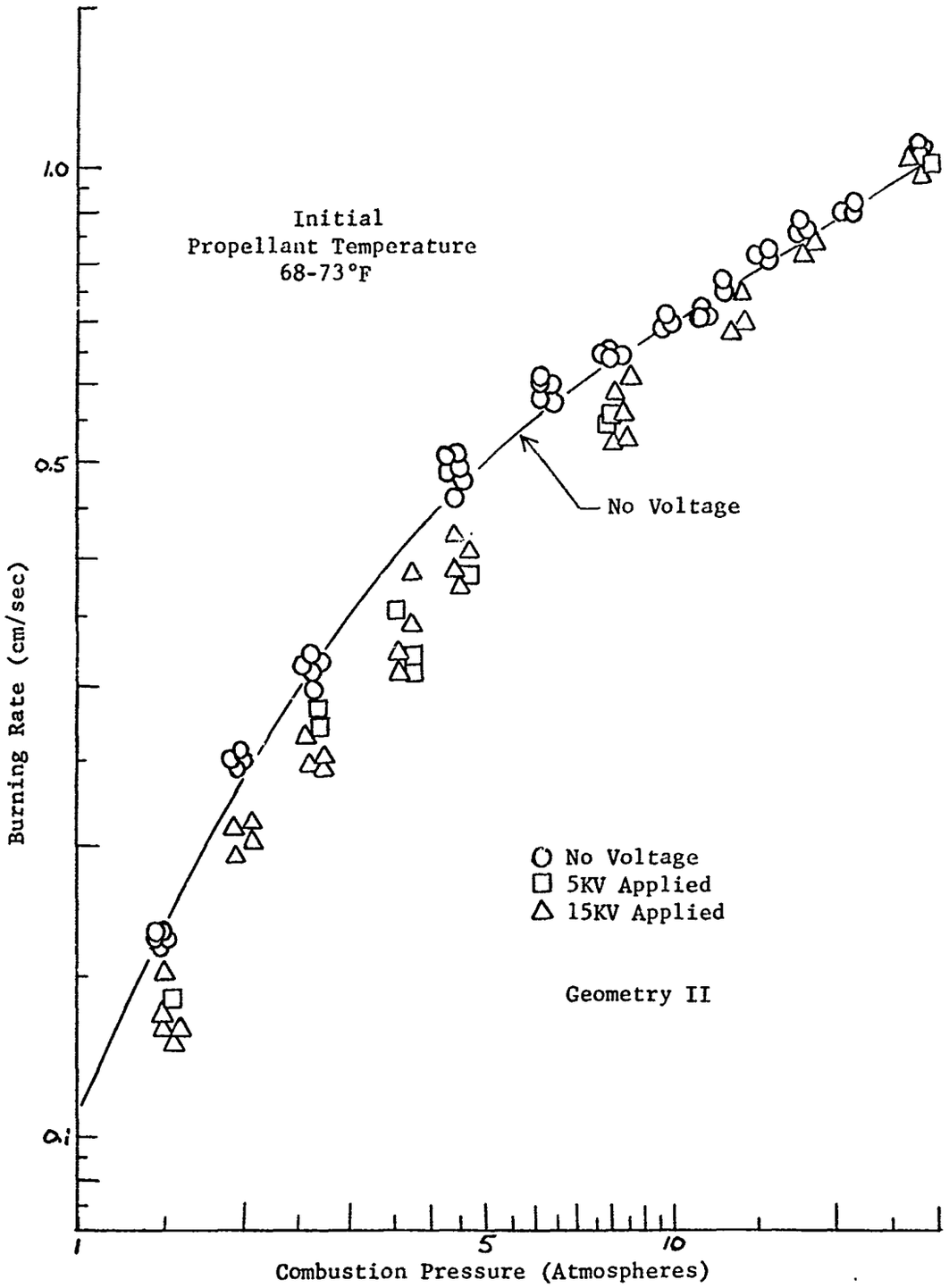

Figure 26. Experimental Burning Rate versus Combustion Pressure (Propellant A)

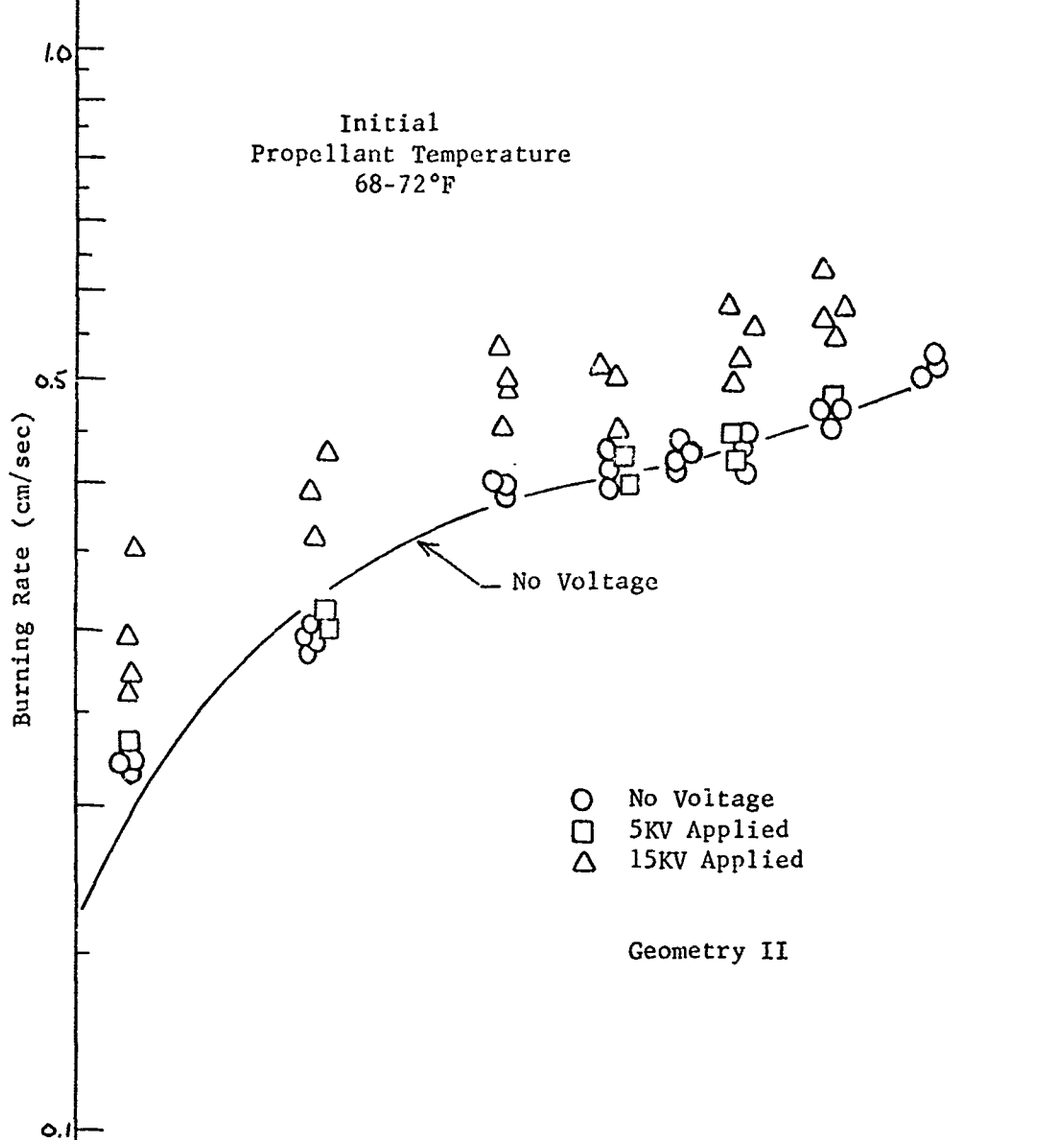

Figure 27. Experimental Burning Rate versus Combustion Pressure (Propellant B)

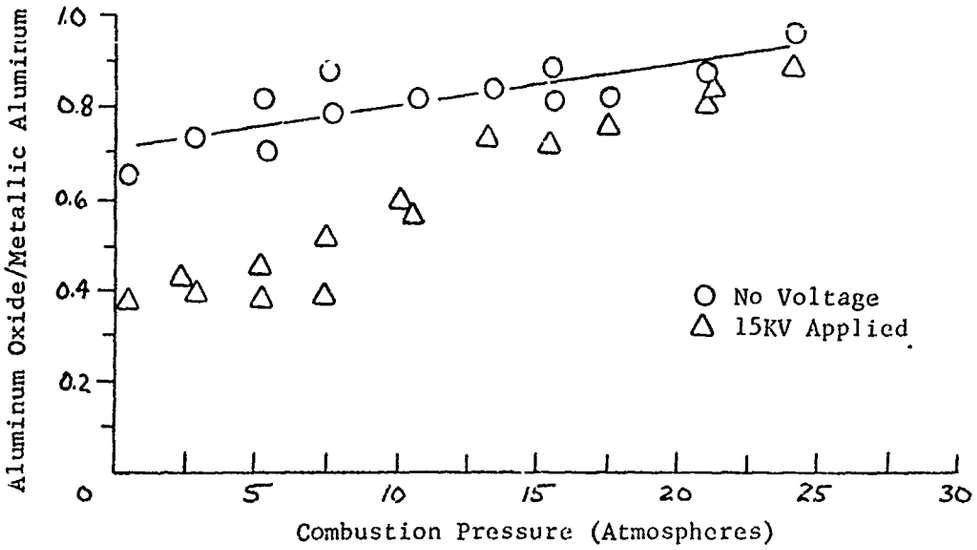

Figure 28. Experimental Ratio of Aluminum Oxide to Metallic Aluminum versus Combustion Pressure (Propellant A)

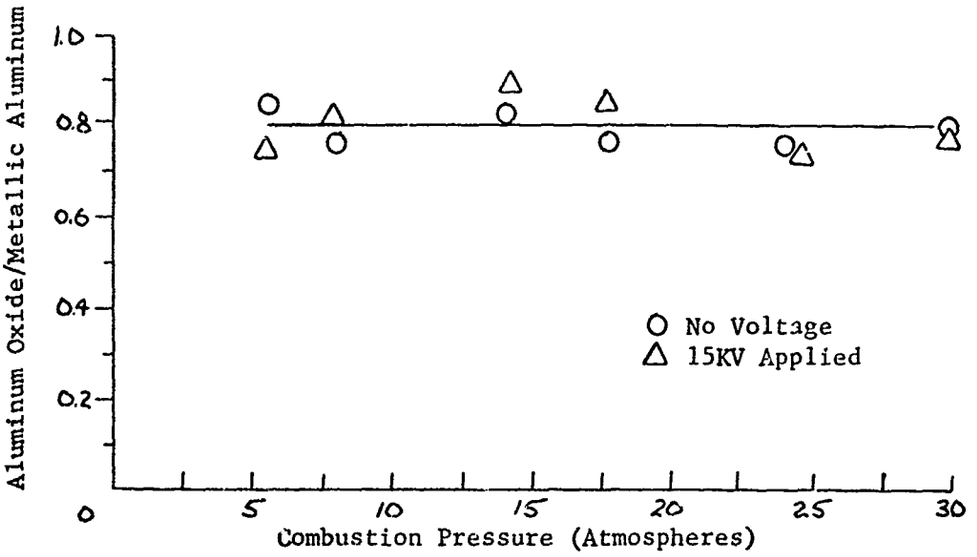

Figure 29. Experimental Ratio of Aluminum Oxide to Metallic Aluminum versus Combustion Pressure (Propellant B)

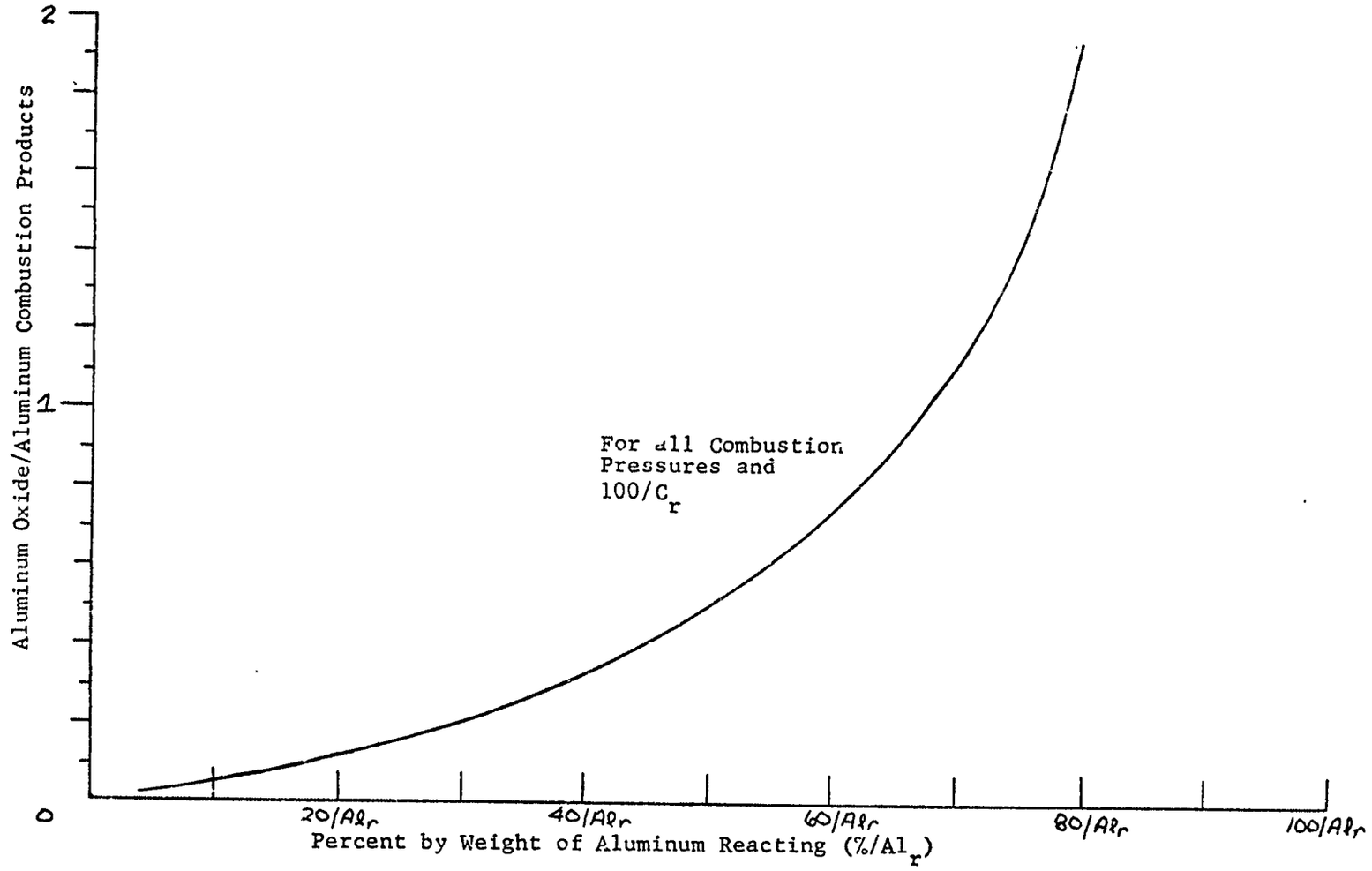

Figure 30. Computer-Determined Combustion Efficiency Relationship for Propellant A or B

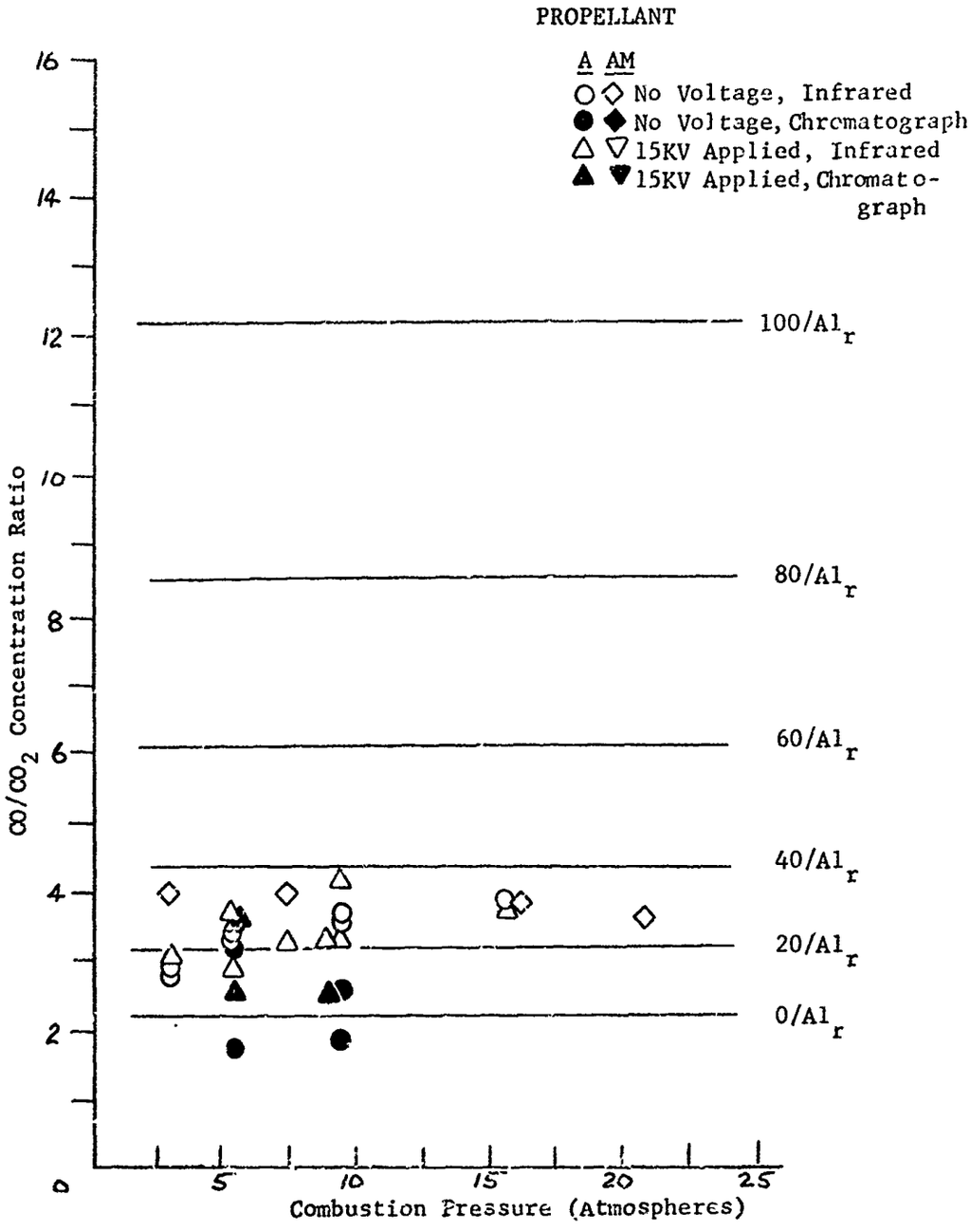

Figure 31. Experimental and Computer CO/CO_2 Concentration Ratio versus Combustion Pressure [Propellant A(AM)]

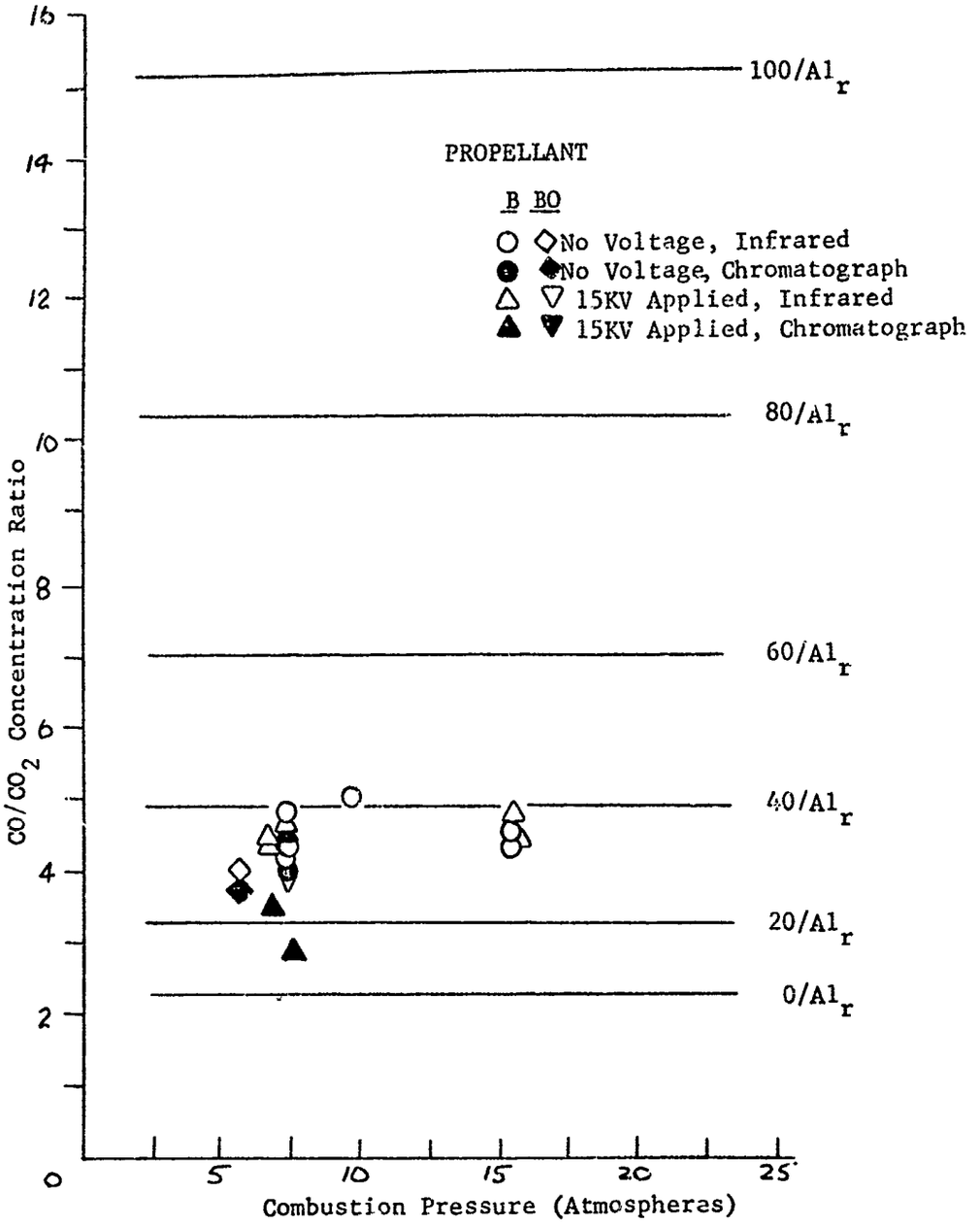

Figure 32. Experimental and Computer CO/CO_2 Concentration Ratio versus Combustion Pressure [Propellant B(BO)]

Figure 33. Infrared Exhaust Spectrum (Propellant A)

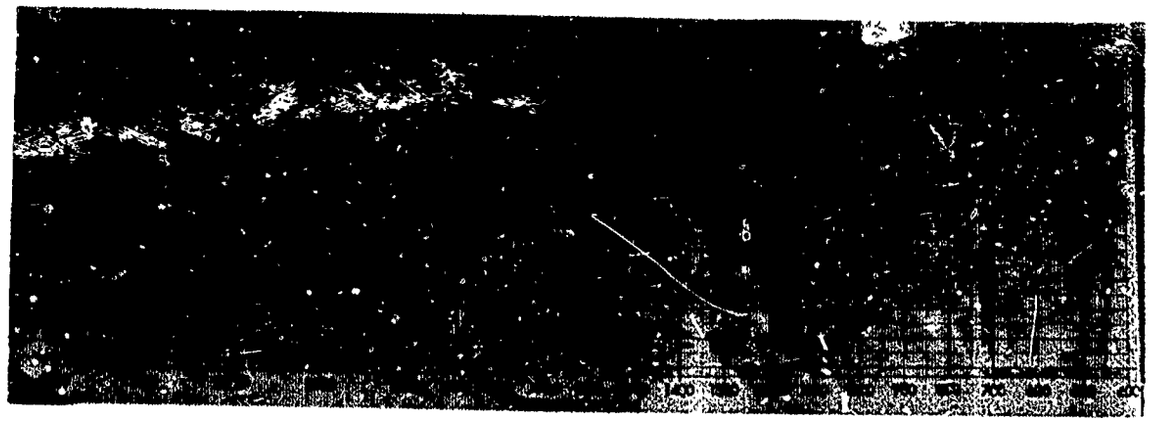

Figure 34. Infrared Exhaust Spectrum (Propellant AM)

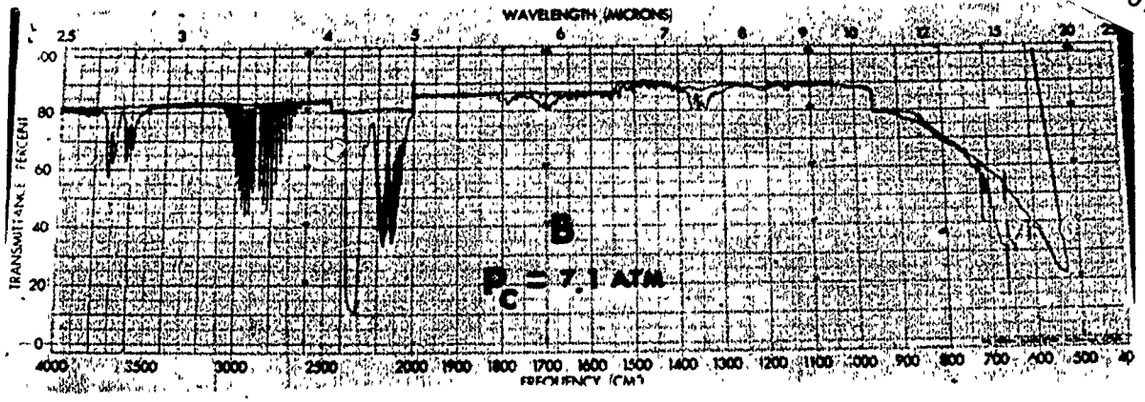

Figure 35. Infrared Exhaust Spectrum (Propellant B)

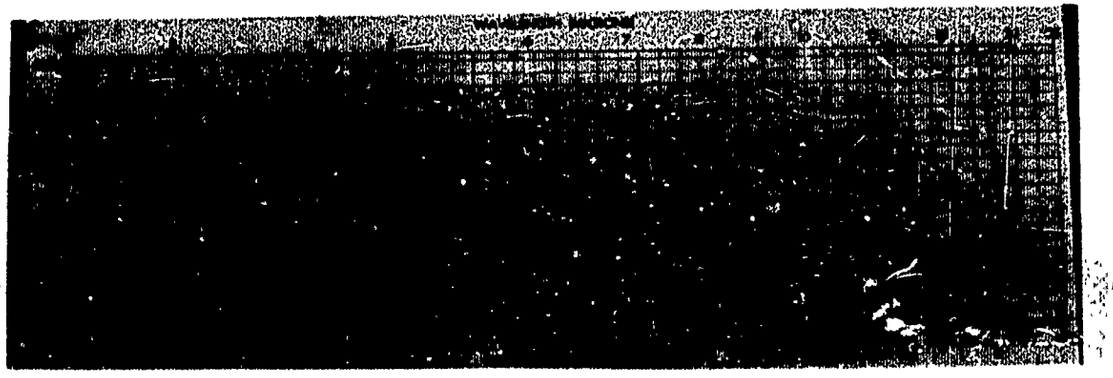

Figure 36. Infrared Exhaust Spectrum (Propellant BO)

Figure 37. Infrared Exhaust Spectrum, No Voltage (Propellant A)

Figure 38. Infrared Exhaust Spectrum with Applied Voltage (Propellant A)

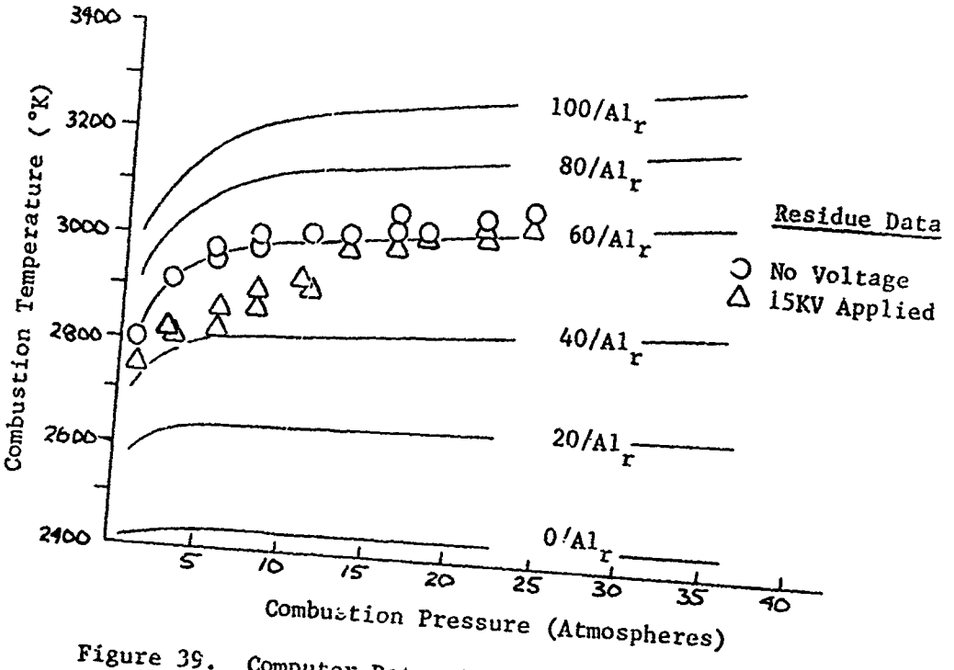

Figure 39. Computer-Determined Combustion Temperature versus Combustion Pressure (Propellant A)

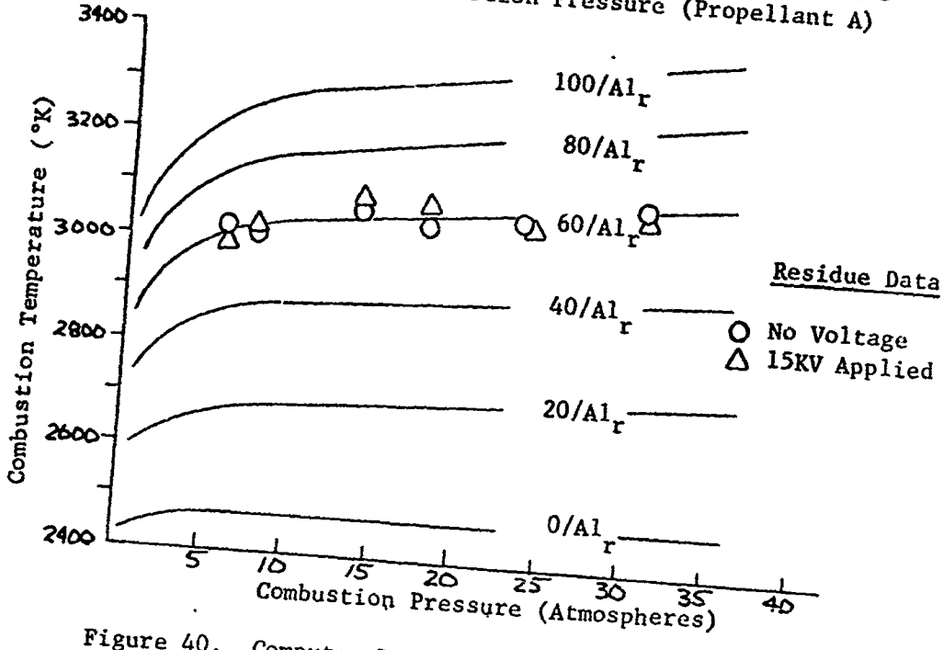

Figure 40. Computer-Determined Combustion Temperature versus Combustion Pressure (Propellant B)

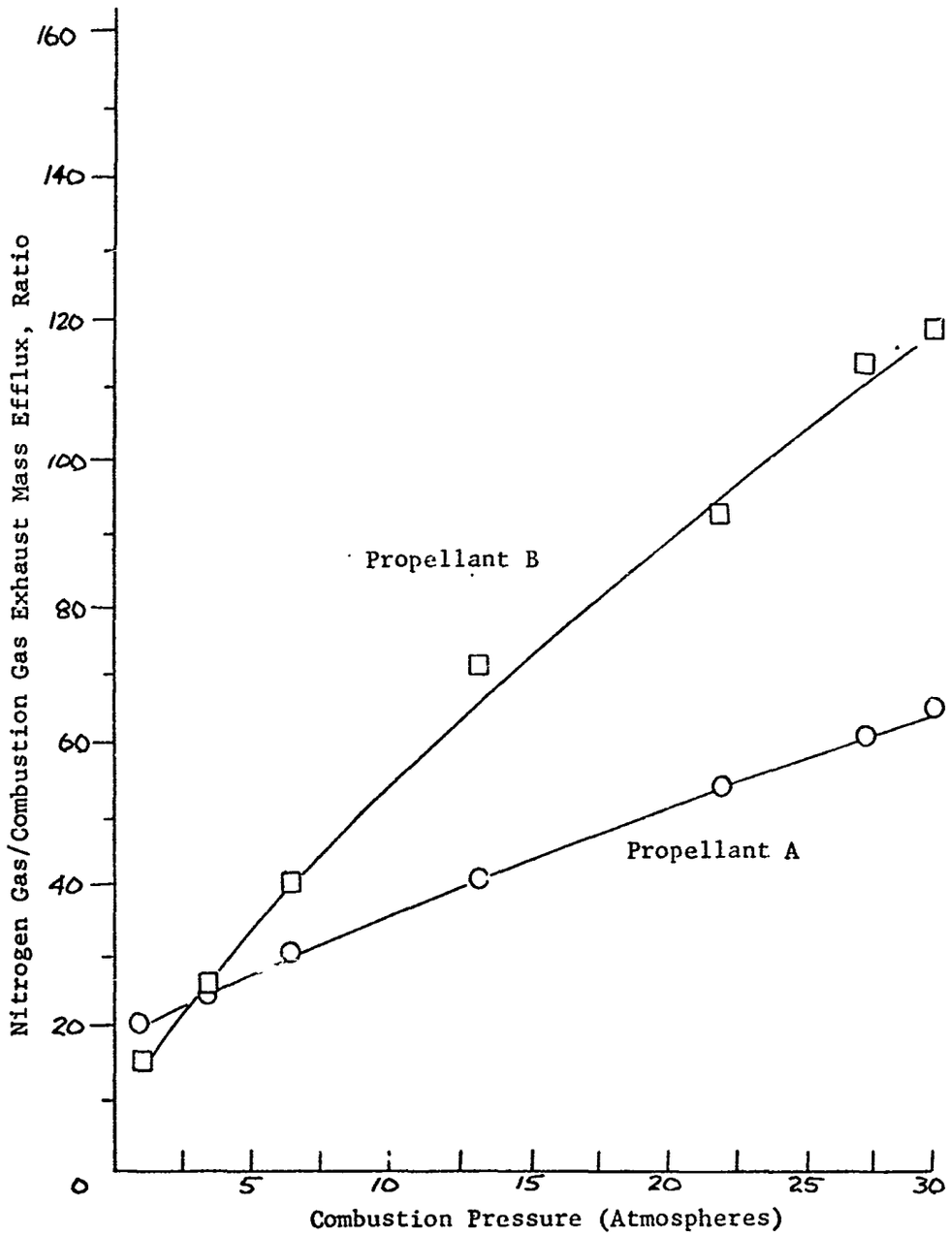

Figure 41. Experimental Nitrogen Gas to Combustion Gas Exhaust Mass Efflux Ratio versus Combustion Pressure

APPENDIX C

GAS-PHASE THERMOELECTRIC COUPLING

The one-dimensional differential form of the conservation of energy expression can be written as

$$\dot{m} c_g \frac{dT}{dx} = -\frac{d(\bar{q})}{dx} + \dot{\mathcal{E}} \tag{C-1}$$

where $\bar{q}$ represents the heat flux vector and $\dot{\mathcal{E}}$ the source energy/unit length. The assumptions leading to Equation (C-1) are consistent with the assumptions leading to Equation (2) (Chapter II).

Consider an electrode arrangement where the burning propellant surface acts either as a cathode or an anode with respect to another electrode located downstream in the gas phase. Allowing only thermal and electrical gas-phase interactions, the gas-phase heat flux toward the burning surface is given by

$$q = -\Lambda_g \frac{dT}{dx} \pm \beta_g E \tag{C-2}$$

where E is the electric field strength, β_g a thermoelectric coefficient, and where the $\pm$ signs correspond to the propellant surface as a cathode and an anode, respectively. In Equation (C-2), the field strength direction was taken to be in the direction of flow of positively charged matter.

The magnitude of the gas-phase current flux J can be written, compatible with Equation (C-2) as[1]

$$J = \sigma_g E \mp \alpha_g \frac{dT}{dx} \tag{C-3}$$

where σ_g is the DC electrical conductivity and α_g another thermoelectric coefficient. The $\mp$ signs correspond, again, to the propellant surface as a cathode and an anode, respectively. The direction of current density is toward the propellant surface when the surface acts as a cathode and in the opposite direction when the surface represents an anode. These directional aspects were accounted for in Equation (C-3).

The relationship between the gas-phase thermoelectric coefficients (α_g and β_g) is given by (38,43)

$$\beta_g = \left(\alpha_g + \frac{5}{2}\frac{k\sigma_g}{e}\right) T_g \tag{C-4}$$

where k is Boltzmann's constant and e the electronic charge. Equation (C-4) is based on the premise that the gas phase consists of molecular species upon which a cloud of free electrons, in thermal equilibrium with these species, have been superimposed.

The source energy/unit length $\dot{\mathcal{E}}$ can be represented by

$$\dot{\mathcal{E}} = \dot{m} Q + J E \tag{C-5}$$

---

[1] It is noted that Equation (C-2) put in terms of entropy current and Equation (C-3) constitute a pair of conjugate equations relating conjugated flows (21).

Equation (C-5) includes both combustion energy and electrical energy associated with the gas phase.

Solving Equation (C-3) for the field strength, inserting the result into Equations (C-2) and (C-5), then combining Equations (C-2), (C-4) and (C-5) with Equation (C-1) results in the following expression

$$\dot{m}c_g\frac{dT}{d\chi} = \epsilon\Lambda_g\frac{d^2T}{d\chi^2} \pm \frac{\alpha_g}{\sigma_g}J\frac{dT}{d\chi} \pm \frac{\beta_g}{\sigma_g}\frac{dJ}{d\chi} + \frac{J^2}{\sigma_g} + \dot{m}Q \qquad \text{(C-6)}$$

where

$$\epsilon = 1 - \frac{\alpha_g\beta_g}{\Lambda_g\sigma_g} \qquad \text{(C-7)}$$

Regarding Equation (C-6), overall charge neutrality dictates that the gas-phase current density gradient is zero; or,

$$\frac{dJ}{d\chi} \equiv \dot{G} - \dot{R} \simeq 0 \qquad \text{(C-8)}$$

where $\dot{G}$ represents charge generation and $\dot{R}$ represents charge recombination. The validity of using Equation (C-8) may also be reasoned on the following basis.

Suppose that the impressed voltage is such that current saturation exists in the gas phase and that charge removal completely overwhelms charge recombination. Then, the current density gradient between electrodes becomes a constant B (20,33). If Equation (C-6) were used to proceed to a solution for the mass flow rate/unit burning

area $\dot{m}$ [like Equation (C-11)], ignoring current heating and thermoelectric coupling terms, and keeping the current density gradient term along, a value of B of the order of 10^2 (amps/cm^2)/cm would be required to make the value of Ω [1] equal to the lowest mass flow rate/unit burning area encountered during the study (Table II). Here, spreading the current density given in Table II over an electrode spacing of one inch, results in a B value of the order of only 10^{-3} (amps/cm^2)/cm.

Hence, using Equation (C-8), Equation (C-6) becomes, upon rearrangement

$$\dot{m}\left(c_g \frac{dT}{dx} - Q\right) = \epsilon \Lambda_g \frac{d^2T}{dx^2} \pm \frac{\alpha_g}{\sigma_g} J \frac{dT}{dx} + \frac{J^2}{\sigma_g} \qquad \text{(C-9)}$$

The integration of Equation (C-9) over the reaction zone thickness yields

$$\dot{m}\left[c_g(T_f - T_p) - Q\right] = \epsilon \Lambda_g \frac{(T_f - T_s)}{x} \pm \frac{\alpha_g}{\sigma_g} J (T_f - T_p) + \frac{J^2}{\sigma_g} \qquad \text{(C-10)}$$

where the ambient temperature was taken as the propellant temperature. Again, the Mallard - le - Chatelier assumption was invoked (Chapter II).

Insertion of Equation (4) (Chapter II) into Equation (C-10), yields a quadratic expression for the mass flow rate/unit burning

[1] Ω would not be given by Equation (C-12) but by: $\Omega = \frac{\beta_g B}{\sigma_g} \Big/ c_g(T_f - T_p) - Q$.

area. This quadratic expression has one solution which is given by the following

$$\dot{m} = \frac{\Omega}{2} + \frac{1}{2}\sqrt{\Omega^2 + \frac{4\epsilon A_g (T_f - T_s)\Gamma (P_s)^{\gamma}}{\left[C_g(T_f - T_p) - Q\right]\left(\frac{RT_s}{m_g}\right)^{\gamma}}} \qquad \text{(C-11)}$$

where

$$\Omega = \frac{J^2}{\sigma_g} \pm \frac{\alpha_g}{\sigma_g}(T_f - T_p) \qquad \text{(C-12)}$$
$$C_g(T_f - T_p) - Q$$

The other solution [i.e., a negative sign before the radical in Equation (C-11)] is regarded as physically improbable since if an electric field does not alter the properties of the system and if $\Omega = 0$ and $\epsilon = 1$, then Equation (C-11) must reduce to Equation (2) (Chapter II). Equation (C-11) leads to Equation (7) using mass conservation.

APPENDIX D

FLAME-FIELD DYNAMICS

The magnitude of the net force/unit volume f acting upon the gas phase due to an electric field of strength E can be represented, for a singly ionized system, as

$$f = (\eta_+ - \eta_-) e E \tag{D-1}$$

The notation η_+ and η_- denotes the number density of positively and negatively charged matter, respectively.

For the propellant flames used, it was found that positive and negative ions exist in nearly like number with the balance of charged matter made up of electrons (Chapter II, V). Since, under an electric field, electron motion completely dominates ionic motion (Chapter V), it is clear that Equation (D-1) reduces to the equivalent of

$$f \simeq \eta_e e E \tag{D-2}$$

Equation (D-2) is written under the assumption that the electric field results in the depletion of all free electrons from the gas volume. Thus, Equation (D-2) represents the maximum body force/unit volume for the special case where ionic motion is completely negligible.

Under the influence of an electric field, a net current/unit area J flows. For an isothermal singly ionized system, the magnitude of current density is given by

$$J = e\sum_{i=1}^{n} \eta_i v_{di} \tag{D-3}$$

The sum in Equation (D-3) is over all charged species. The notation η_i and v_{di} represent the number density and drift velocity for the i th species, respectively. If the drift velocity of each species is assumed small compared with the random thermal velocity of each species, the drift velocity can be linearly related to field strength through the mobility K. Or,

$$v_{di} = K_i E \tag{D-4}$$

Inserting Equation (D-4) into Equation (D-3) and expanding Equation (D-3) for the flames used yields

$$J = e(\eta_+ K_+ - \eta_- K_- - \eta_e K_e)E \tag{D-5}$$

where electrons and other negative ions η_- have been distinguished. Since $\eta_+ \simeq \eta_- > \eta_e$ and $K_+, K_- << K_e$, if $K_+ \simeq K_-$ the magnitude of the net current density becomes

$$J \simeq e\eta_e K_e E \tag{D-6}$$

Thus, from Equations (D-2) and (D-6) it is seen that only electrons contribute to flame-field dynamics as measured by the net body force/unit volume and the current density. Inserting Equation (D-6) into Equation (D-2) yields

$$f = \frac{J}{K_e} \tag{D-7}$$

Using the value of current density given in Table II and a conservative electron mobility of $10^3 \frac{cm^2}{volt\ sec}$ (5), results in a magnitude of f of only $10^2 \frac{dynes}{cm^3}$ ($3.6 \times 10^{-3} \frac{lb}{in^3}$).

APPENDIX E

IONIZATION PROBE THEORETICAL DEVELOPMENTS

Development of Equation (11)

If it is assumed that kinetic and diffusion resistances are simply additive, an immediate result of simple film theory is that (16)[1]

$$\eta_i = \frac{4J_i}{eV_i} + \frac{d_p J_i}{e D_i Sh)_i} \qquad \text{(E-1)}$$

The symbols η_i , J_i , V_i , D_i , $Sh)_i$ denote the number density, current density, average speed, diffusion coefficient, and Sherwood number of the i th ionic species, respectively. The dimension d_p represents the diameter of a cylinder immersed in an ionized gas, with a length ℓ_p large compared to the diameter. It is noted that the first portion of Equation (E-1) is written directly from simple kinetic theory. Also, from simple kinetic theory the diffusion coefficient for the i th species is given by

$$D_i = \frac{1}{3} V_i \lambda_i \qquad \text{(E-2)}$$

where λ_i is the mean free path of the i th species.

[1]This reference was recommended by H. F. Calcote.

The Sherwood number is taken as (16)

$$Sh)_i = \frac{2}{\ln\left[\frac{2(\ell_p + 2\lambda_i)}{d_p + 2\lambda_i}\right]} \qquad \text{(E-3)}$$

For $\ell_p \gg \lambda_i$, Equation (E-3) becomes

$$Sh)_i = \frac{2}{\ln\left(\frac{\ell_p}{\frac{d_p}{2} + \lambda_i}\right)} \qquad \text{(E-4)}$$

With Equations (E-2) and (E-4), Equation (E-1) becomes

$$\eta_i = \frac{4J_i}{eV_i}\left[1 + \frac{\frac{3}{4}d_p}{2\lambda_i}\ln\left(\frac{\ell_p}{\frac{d_p}{2} + \lambda_i}\right)\right] \qquad \text{(E-5)}$$

Again, from simple kinetic theory,

$$V_i = \sqrt{\frac{2.55\,kT_i}{m_i}} \qquad \text{(E-6)}$$

where m and T denote mass and temperature, respectively. Using Equation (E-6) in Equation (E-5), with the current I_i taken over the probe area A_p, Equation (11) results where the i th species are electrons.

It is noted that Equation (11) does not account for mass flow effects. This contribution was treated elsewhere (16), with the result:

$$\eta_i = \eta_{i)_r} \left\{ 1 + \frac{\frac{3}{4} d_p}{\lambda_i} \left[\frac{1}{\frac{2}{\ln\left(\frac{l_p}{\frac{d_p}{2} + \lambda_i}\right)} + 0.55 (Re)^{\frac{1}{2}} (Sc)^{\frac{1}{3}}} \right] \right\} \quad \text{(E-7)}$$

where

$$\eta_{i)_r} = \frac{2.5}{e} \sqrt{\frac{m_i}{k T_i}} \; \frac{I_i}{A_p} \quad \text{(E-8)}$$

and where Re and Sc denote the Reynolds and Schmidt numbers, respectively. Mass flow effects were considered negligible here. Computations to support this omission were based on a Schmidt number of unity and a Reynolds number of the order of 0.1. The Reynolds number was estimated by the expression

$$Re = \frac{\rho_p d_p r}{\mu_g} \quad \text{(E-9)}$$

where r is the burning rate and μ_g the gas-phase viscosity. A viscosity value of 0.07 $\frac{gm}{cm\ sec}$ was considered representative for the formulations used.

Development of Equation (15)

Using Equation (D-4), Equation (D-6) can be written as

$$\overline{J} = e \eta_e v_{de} \tag{E-10}$$

where v_{de} is the drift velocity of electrons. Following Reference 21, if the electron drift velocity is defined as the mean distance traveled between collisions by electrons accelerated uniformly under an electric field of strength E divided by the mean collision time for electrons τ_e, then the drift velocity magnitude is given by

$$v_{de} = \frac{e}{m_e} \tau_e E \tag{E-11}$$

Using the expression

$$\tau_e = \frac{\lambda_e}{v_e} \tag{E-12}$$

, Equation (E-6) for v_e, and Equation (E-11), it follows that

$$J = \frac{e^2 \eta_e \lambda_e}{\sqrt{2.55 k m_e T_e}} E \tag{E-13}$$

From Ohm's law, Equation (15) results.

APPENDIX F

PROPELLANT PREPARATIONS

The propellants used during the study were either manufactured locally or purchased. Both local and purchased propellant was cast into slabs and sacked for storage in a bunker.

Samples were prepared for experiments by dissecting the slabs into selected sizes. Samples with cast surfaces were discarded; thus, only cut surfaces were used. Igniter wire, made of 20 mil diameter nichrome, was inserted through the upper end of the sample perhaps 1/32 inch below the surface. An igniter paste, consisting of boron, silver powder, potassium perchlorate and resin, in methyl ethyl keotone solvent, was then spread over the top surface. Lastly, samples were sacked and stored in a desiccant cabinet, kept at 21°C until required for use.

Periodically, batches of samples were X-rayed to detect macrovoids. Those samples indicating macrovoids were discarded. Random samples, of accurately determined size, were also weighed to compute propellant densities. Typical values of 1.63 gm/cm^3 and 1.74 gm/cm^3 were computed for Propellants A and B, respectively.

APPENDIX G

EXPERIMENTAL PRELIMINARIES

Nitrogen Considerations

Gaseous nitrogen was used as a side burning inhibitor, pressurizing gas, and diluent. As a side burning inhibitor it was necessary to know if the side flow velocity affected the burning rate. It seemed obvious that simple fluid flow considerations would hold in that if the inlet line pressure to the mixing chamber were increased, the flow velocity exiting the mixing chamber through the 1/16 inch diameter holes would increase. A crude measurement using a rotating vane to measure outlet flow velocity verified that this was the case.

Experiments were then performed using Propellants A and B where the burning rate was measured using the Optron with the inlet nitrogen pressure varied. The combustion pressure was one local atmosphere. The results of these experiments indicated the following.

1. For Propellant B, there was no measurable burning rate change with inlet nitrogen pressure.

2. For Propellant A, there was no measurable burning rate change with inlet pressure beyond an inlet pressure of 40 psig. At 20 psig, the lowest inlet pressure used, the measured burning rate was on the average approximately

5% higher than the burning rate at the higher supply pressures. At 30 psig inlet pressure, the average burning rate was between the values corresponding to the lower and higher supply pressures.

Thus, the effect of nitrogen side flow velocity on burning rate was, overall, very weak. For all other experiments, however, the side flow velocity was maintained beyond the value corresponding to an inlet pressure drop of 40 psig.

Nitrogen flow conditions inside the combustion bomb required consideration. Constant pressure burning was desired in the combustion bomb. At the same time, a suitable side flow velocity should be preserved plus combustion smoke had to be removed from the vicinity of the sample (Chapter IV). To accomplish all of this at one time ultimately required rather high nitrogen flow conditions. These flow provisions are given below.

Bomb exit volumetric flow as a function of bomb pressure for different sized exit valves was measured using a calibrated Brooks Rotometer. Mean side flow velocities inside the vessel were calculated from this data using mass conservation, correcting for pressure. The calculations from these cold flow tests enabled an exit valve to be selected and then preset before each experiment to provide an adequate side flow velocity at a specified combustion bomb pressure.

The nitrogen gas also served as a reaction quench and diluent for combustion gases exhausting from the combustion bomb. Figure 41 illustrates experimentally determined ratios of mass efflux of nitrogen to mass efflux of combustion gases for Prcpellants A and B as a

function of combustion pressure. For this figure, the nitrogen mass flow rate was based on measured cold flow data using a 1/2 inch diameter exit valve and the propellant mass flow rate was based upon Optron burning rate data (at no-voltage). From Figure 41 it is seen that the nitrogen strongly dilutes the combustion products.

Nonburning Equipotential Plots

As another preliminary experiment, a high voltage probe with a 20 mil diameter tip was attached to a vacuum tube voltmeter to determine equipotential lines for the electrode geometries of Figure 9. The propellant sample was set, unignited, in position. High voltage was applied. The nitrogen gaps, the propellant, and other apparatus in the vicinity of the applied voltage were then probed to record the local static potential. Precise locations in the gaps were determined with the aid of a small helium-neon alignment laser.

It was known that the potentials recorded would not represent the situation during burning since no conducting gases existed. The purpose of the experiment was mainly to gain some knowledge of the differences in static distribution of impressed voltage for the various electrode geometries. The results indicated the following.

1. For electrode geometries where the propellant served as an electrode, the distribution of potential in the vicinity of what would be the combustion zone was essentially one-

dimensional. Propellant A represented essentially an equipotential body and Propellant B represented a large resistor dropping the entire applied voltage across the propellant.

2. For electrode geometries where the propellant acted as part of the media between electrodes, the distribution of potential was distorted by the presence of the propellant from the case where the propellant was removed.

3. The potential distribution would not be distorted by physical boundaries located at a distance greater than 2 1/2 inches from the voltage source (for an applied voltage of 15 KV). At pressures higher than atmospheric pressure, this distance can be expected to decrease.

Other Preliminaries

All apparatus used for experiments was checked and calibrated before use. Additionally, a number of experiments were always conducted before earnest experiments began to develop working checklists and to disclose experimental peculiarities. For the most part, calibration steps are described in Chapters IV and V. The exception noted is for calibration of recording galvanometers. For each galvanometer used to measure a variable, a plot of the magnitude of that variable versus the deflection of the galvanometer was prepared. Recording circuits were adjusted, if necessary, so that deflections were linear with the variable in question.

APPENDIX H

OPTRON DETAILS

The Optron system utilizes an image dissector tube as an optical sensor which differentiates light contrast. A burning propellant sample ideally represents a light-over-dark target to the optical sensor. In operation, the light-to-dark target interface was focused upon the photocathode surface of the image dissector tube. Electrons, proportional to the intensity of projected light from the target interface, were emitted from the back side of the photocathode. These electrons were then accelerated, by supplying a voltage of approximately 2KV to the dissector tube, to a plate containing a 10 mil diameter aperture. As electrons passed through the aperture, their presence was amplified by a photomultiplier tube to yield an output current proportional to the number density of emitted electrons. As the target interface moved and traversed the aperture, a change in output current resulted. The servo-mechanism responded to this change to realign the target and aperture. Thus, the target interface was "locked on" the aperture.

In the orthogonal sweep mode, the target was effectively caused to sweep across the face of the aperture plate. Operationally, the moving electrons were deflected by supplying an alternating magnetic field from a deflection yoke in a direction parallel to the servo-tracking direction. The deflection coils were driven by a saw

tooth current producing a linear displacement measurement with an instantaneous return. The width of target to be repetitively sampled was adjusted by varying the amplitude of the saw tooth current.

Performance specifications for the Optron are given below. The percentages given are percentages of fullscale field-of-view.

1. Optical range - 0.02%

2. Output - ±5VDC fullscale, 100 ohms impedance

3. Noise level - ±0.025% at the 100 Hz bandwidth

4. Stability - less than ± 0.1% over 1 to 5 minutes operation
   - less than ± 0.5% over 8 hours operation

5. Linearity - less than ± 0.5%

6. Repeatability - ± 0.02%

7. Accuracy - ± 0.05% (1/2 of 8 hour drift and linearity)

The continuous burning rate provided by the Optron is given simply by

$$r = \frac{d\chi}{dt} = \frac{d\chi}{d\phi}\,\frac{d\phi}{dt} \qquad \text{(H-1)}$$

where $\frac{d\phi}{dt}$ is the slope of the Optron output voltage versus time plot. The term $\frac{dx}{d\phi}$ was determined by calibration of the instrument plus knowing the working distance L between the propellant sample and optical lens. Precisely,

$$\frac{dx}{d\phi} = WL \tag{H-2}$$

where $W = 4.86 \times 10^{-3}$ volts^{-1}. Combining Equations (H-1) and (H-2) results in the burning rate expression used for the Optron.

Error assessment using the Optron involved consideration of the following.

1. The effect of refraction through the Herculite plate glass wind w.

2. The effect of parallax.

3. The effect of light-to-dark fluctuations due to the heterogeneity of the burning propellant.

4. The effect of smoke or combustion debris in the combustion bomb.

5. The accuracy of the output recording equipment.

6. The accuracy of determining the output voltage versus time slope.

The first two factors involve working distance errors. The next two factors are more random error sources. The next factor involves equipment interfacing with the Optron. The last factor involves human judgment.

The working distance error contribution to burning rate was estimated to be less than ± 1% of the burning rate assuming a precise time base. This estimation was based upon a refraction correction to a working distance of 30 inches for the 3/4 inch thick Herculite window assuming a window with an index of refraction of 1.5 and an infinite focal length. Any parallax error was felt to be completely negligible since, for typical working distances, the total angle covering the entire propellant sample was less than 3°. Actually, the Optron critically viewed only the light-to-dark interface from this working distance.

During burning, the light-to-dark interface might be vague. However, irregularities of the interface should be random. Nonetheless, as a precaution, the Optron output was filtered. An error of perhaps one part in a thousand might occur due to target interface fluctuations. Any error introduced by the instrument inadvertently tracking properly contrasted smoke or debris was minimized by operating the instrument in the light-over-dark mode, thereby inhibiting the tracking of targets contrasted otherwise.

The repeatability of the time base of the X-Y Plotter was ± 1 5%. As noted (Chapter IV), the fullscale voltage was precisely adjusted before each experiment. The time base error seemed to be

the greatest error source involved in the system. The magnitude of this error could have been reduced by eliminating the X-Y Plotter and using the output current to drive a recording galvanometer. A circuit was designed and fabricated for this purpose but never used.

The human error associated with determining the output voltage versus time slope was minimized as much as possible by the construction of a template made of plexiglass to lay over the output data sheet. Etched into the template were lines of different slope. The best fit, over a consistent time interval, was selected.

The overall error involving the Optron as a burning rate measurement device was put at $\pm$ 3% of the true burning rate (based on the worst case of working distance error and time base error plus 0.5%). This percent error was felt to be conservative. Based on Table VI, this seems to be the case since data in Table VI includes the inherent variation in burning rate due to propellant ingredient irregularities.

VITA

Robert F. Bestgen was born on 19 June 1939 in Omaha, Nebraska, the son of Dr. Fred P. Bestgen M.D. and Barbara Kabourek Bestgen. He graduated from Kansas State University on the Dean's Honor List in 1962, receiving the degree of Bachelor of Science. He graduated from the Air Force Institute of Technology receiving the degree of Master of Science in 1963. He served with the Air Force Systems Command from 1963 until reentering the Air Force Institute of Technology in 1966. He is the father of two daughters.

Permanent address: 1011 N. Juliette
Manhattan, Kansas

This dissertation was typed by Mrs. Kathleen E. Licht.